4 - SEP 4
1962

REACTOR MATERIALS

A Quarterly Technical Progress Review

Prepared for DIVISION OF TECHNICAL INFORMATION, USAEC, by
R. W. DAYTON, E. M. SIMONS, and ASSOCIATES, BATTELLE MEMORIAL INSTITUTE

August 1962

● VOLUME 5

● NUMBER 3

TECHNICAL PROGRESS REVIEWS

To meet the needs of industry for concise summaries of current atomic developments, the Atomic Energy Commission is publishing this series, Technical Progress Reviews. Issued quarterly, each of the reviews digests and evaluates the latest findings in a specific area of nuclear technology and science.

The four journals published in this series are:

Nuclear Safety, Wm. B. Cottrell, W. H. Jordan, and associates, Oak Ridge National Laboratory

Power Reactor Technology, W. H. Zinn and J. R. Dietrich, General Nuclear Engineering Corporation

Reactor Materials, R. W. Dayton, E. M. Simons, and associates, Battelle Memorial Institute

Reactor Fuel Processing, Stephen Lawroski and associates, Chemical Engineering Division, Argonne National Laboratory

Each journal may be purchased ($2.00 per year for subscription and individual issues $0.55) from the Superintendent of Documents, U. S. Government Printing Office, Washington 25, D. C. See back cover for remittance instructions and foreign postage requirements.

The views expressed in this publication do not necessarily represent those of the United States Atomic Energy Commission, its divisions or offices, or of any Commission advisory committee or contractor.

Availability of Reports Cited in This Review

Unclassified AEC reports are available for inspection at AEC depository libraries and are sold by the Office of Technical Services, Department of Commerce, Washington 25, D. C. Some of the reports cited are not available owing to their preliminary nature; however, the information contained in them will eventually be made available in formal progress or topical reports.

Unclassified reports issued by other Government agencies or private organizations should be requested from the originator.

Unclassified British and Canadian reports may be inspected at AEC depository libraries. British reports are sold by the British Information Service, 45 Rockefeller Plaza, New York, N. Y.; Canadian reports (AECL series) are sold by the Scientific Document Distribution Office, Atomic Energy of Canada, Ltd., Chalk River, Ontario, Canada.

Classified U. S. and foreign reports identified in this journal as Classified may be purchased by properly cleared Access Permit Holders from the Division of Technical Information Extension, U. S. Atomic Energy Commission, P. O. Box 1001, Oak Ridge, Tenn. Such reports may be inspected at classified AEC depository libraries.

REACTOR MATERIALS

A REVIEW OF RECENT DEVELOPMENTS

Prepared for DIVISION OF TECHNICAL INFORMATION, USAEC,
by R. W. DAYTON, E. M. SIMONS, and ASSOCIATES,
BATTELLE MEMORIAL INSTITUTE

● AUG. 1962
● VOLUME 5
● NUMBER 3

Foreword

Reactor Materials is one of a series of four quarterly technical progress reviews broadly covering the field of nuclear science and technology. Under the auspices of the USAEC Division of Technical Information, *Reactor Materials* is prepared by Battelle personnel from worldwide literature. It covers properties, behavior, and fabrication processes of materials applicable to nuclear reactor components and associated equipment.

The reader will recognize that the scope of this Review is too broad to permit detailed coverage of every topic. Rather, the authors and editors attempt to combine the highlights of significant new developments into an informative summary of current research for both management and the technical specialist. As a rule, enough of the results are presented to define the research and summarize the findings. For readers desiring more information on any particular topic, a complete set of references is provided at the end of each section.

Each quarter, a number of bibliographies, monographs, and books appear on subjects within the scope of *Reactor Materials*. Although the main purpose of this Review is to call attention to findings that are new and significant, such publications are noted in the text because they often represent excellent compilations of available information on important materials topics.

R. W. DAYTON
E. M. SIMONS
R. W. ENDEBROCK
Battelle Memorial Institute

Contents

Foreword

I FUEL AND FERTILE MATERIALS . . . 1

Uranium Metal and Alloys 1
Plutonium 3
Thorium 7
Coated-Particle Fuel Materials 8
Refractory Fuel and Fertile Materials . . 14
Basic Studies of Irradiation Effects on Fuel Materials 17
References 18

II MODERATOR MATERIALS 22

Beryllium Metal and Alloys 22
Beryllium Compounds 27
Solid Hydrides 28
Graphite 31
References 31

III NUCLEAR POISONS 34

Metallic Poisons 34
Control and Burnable-Poison Composites 34
References 36

IV CLADDING AND STRUCTURAL MATERIALS 37

Corrosion 37
Metal-Water Reactions 43
Radiation Effects in Nonfuel Materials . . 45
Selected Mechanical Properties of Cladding and Structural Materials . . . 54
Selected Metallurgical Aspects of Cladding and Structural Materials . . . 56
Ceramic Technology 59
References 60

V SPECIAL FABRICATION TECHNIQUES 64

Melting and Casting 64
Fabrication and Heat-Treatment 65
Cladding 65
Welding and Brazing 70
Explosive Forming 71
Nondestructive Testing 74
References 75

Issued quarterly by the U. S. Atomic Energy Commission. Use of funds for printing this publication approved by the Director of the Bureau of the Budget on November 1, 1960.

Section

I

Reactor Materials

Fuel and Fertile Materials

Uranium Metal and Alloys

Unalloyed Uranium

Fisher and McSkimin[1] have reported a phase transformation in uranium at 42 ± 1°K, as indicated by measurements of the single-crystal elastic moduli using ultrasonic-pulse techniques. The indicated transformation coincides closely to anomalies noted in the thermal expansion, Hall coefficient, electrical resistivity, and thermoelectric power.

Investigators at Temple University[2] have determined the density of pure liquid uranium from its melting point, 1406°K, to about 1900°K, by use of the Archimedean method. The variation in the density of liquid uranium with temperature is given below.

$$D_{liq} = 19.356 - 10.328 \times 10^{-4}\, T$$

where D is the density in g/cm^3 and T is the temperature in °K.

The determination of the temperature dependence of the diffusion coefficient of chromium in gamma uranium is reported by Argonne.[3] The diffusion coefficient, D, is given by

$$D = 1.98 \times 10^{-3} \exp(-21{,}800/RT)\ \text{cm}^2/\text{sec}$$

where R is the gas constant and T is the temperature (°K). This equation is in poor agreement with the data of Mossé et al.[4] Possible reasons for the discrepancy are discussed, and it is concluded that the above data are to be preferred as a basis for theoretical studies of the diffusion of tracers in gamma uranium.

The self-diffusion of uranium in the alpha phase has been investigated by the French.[5] Their results for the variation of D, the diffusion coefficient, with temperature are shown below.

Temp., °C	D, cm^2/sec
580	1.1×10^{-13}
618	2.4×10^{-13}
625	3.8×10^{-13}
650	6.0×10^{-13}

The linear variation of the logarithm of the coefficient of diffusion as a function of the absolute temperature permitted the calculation of the activation energy, Q, which is 40 kcal/g-atom and the frequency factor, D_0, which is 2.1×10^{-3} cm^2/sec.

The recrystallization of deformed alpha-uranium single crystals was studied at Argonne.[6] It was found that the orientation relation between deformed and recrystallized alpha uranium can be expressed at 27.5° rotation about axes located 70.0° from the (1 0 0), 63.5° from the (0 1 0), and 34° from the (0 0 1). In deriving this relation it was necessary to consider the recrystallized grains found upon annealing deformed single crystals as originating from twins as well as from the parent crystal. Comparisons of deformation and recrystallization textures of polycrystalline uranium agree well with the finding.

Investigators at Battelle[7] have studied the corrosion behavior of bare and organic- or metal-coated uranium coupons and composite assemblies that are joined by soldering, welding, or machine screws. The corrosion during storage for at least one year in both uncovered and loosely covered metal containers in a water-

front building, an unheated warehouse, and on a rooftop was evaluated. The uranium samples generally darkened, and some were covered with black nodules. Although weight losses were relatively minor, random pits up to 1.6 mils deep were detected. Organic and aluminum coatings blistered under many of the exposure conditions. There was no indication of crevice- or galvanic-couple corrosion in any of the dissimilar-metal combinations studied. It was concluded that protective coatings would be required to ensure complete protection of uranium.

(M. S. Farkas)

Alpha-Phase Uranium Alloys

An investigation of uranium-titanium alloys performed at Knolls[8] has shown that small amounts of titanium were very effective in increasing the strength of martensitic uranium. The strengthening effect saturated at about 2 at.% titanium. It was not caused by the presence of a second phase but, on the basis of X-ray diffraction studies, was attributed to the presence of nonuniform microstresses.

The Japanese[9] have studied briefly the casting, rolling, transformation, thermal-cycling resistance, and the resistance to high-temperature oxidation and hot-water corrosion of alpha uranium–molybdenum alloys. Data from previous investigations are also presented for comparison purposes.

The French[10] have investigated heat-treatment of a uranium–0.1 wt.% chromium alloy with the aim of producing fine grain size and favorable properties. The physical and mechanical properties that govern the behavior under thermal cycling and irradiation between 20 and 600°C are described. After isothermal quenching, the alloy has clearly improved properties compared with unalloyed uranium.

Another study[11] on the recrystallization of uranium has shown that a substructure superimposed on the alpha structure forms after heat-treatment in the gamma phase. Conditions for the appearance of the substructure were studied for uranium and uranium–1.4 at.% chromium alloys. It is believed that the substructure represents the polygonization of the beta phase after the gamma-to-beta transformation, and the role of impurities in the substructure formation is discussed.

High-uranium alloys of the uranium-zirconium-silicon system were investigated at Battelle.[12] Thermal analysis, metallography, and X-ray diffraction were used to construct isothermal ternary sections at temperatures from 550 to 950°C. No new ternary phases were encountered; however, extensive solution of zirconium in U_3Si_2 gives $(U,Zr)_3Si_2$. Otherwise, the solubility of zirconium in uranium-zirconium alloys is less than 2 at.%. Similarly the solubility of silicon in uranium-zirconium alloys is below 2 at.%. The addition of silicon to uranium-zirconium alloys is accompanied by the formation of Zr_2Si, which alters the alloy constitution by removing zirconium from solution. Below 930°C, uranium-silicon rich alloys with small amounts of zirconium contain the suitable allotropic form of uranium plus Zr_5Si_3 and U_3Si. The region $(U,Zr)_3Si_2$ plus U_3Si plus Zr_5Si_3 is also found. If larger amounts of silicon are present, the region $(U,Zr)_3Si_2$ plus U_3Si is stable.

(M. S. Farkas)

Gamma-Phase Uranium Alloys

A study of uranium self-diffusion in the gamma phase with alloys containing 10 at.% additions of molybdenum, niobium, and zirconium is reported by the French.[13] Diffusion coefficients, activation energies, and frequency factors were determined. The results indicate that the mechanism for diffusion is the same in the alloys as in pure uranium. Measurements of electrical resistivity and metallography were employed in a study of gamma-phase transformation in the uranium–16 wt.% molybdenum alloy reported by Atomics International.[14] Transformation proceeds with appearance of alpha uranium, which reaches a maximum volume fraction at the time that ordering of the gamma phase begins. The alpha phase subsequently redissolves. Ordering of the gamma to form U_2Mo proceeds most rapidly at 500°C. Under microscopic observation, the ordered phase is detected after 12 hr at 500°C, but only after a period of 48 to 72 hr at 550°C.

The magnetic susceptibilities and electrical resistivities of a series of gamma-phase uranium-niobium alloys have been measured as a function of temperature by British investigators;[15] their results were presented in plotted form. No description of variations in these properties with temperature and composition in terms of electronic-band structure appears appropriate.

(A. A. Bauer)

Aluminum-Uranium Alloys

It is interesting to note that studies by Kraus[16] agree, at least qualitatively, with diffusion data obtained by other investigators. Essentially he annealed aluminum-uranium diffusion couples for various times at 272, 296, 348, 404, and 450°C. These times varied from 60 min at 450°C to 5720 min at 272°C. Kraus concluded from his data that (1) 75 per cent of the total diffusion-layer thickness penetrates into the aluminum, (2) 25 per cent of the total diffusion-layer thickness penetrates into the uranium, and (3) no UAl_4 was identified in any of the diffusion zones. It should be pointed out that these penetration values are higher than any previously reported.

Chalk River[17] has successfully produced good aluminum–28 wt.% uranium alloy by reducing UO_2 with excess aluminum under a flux of $3NaF\text{-}AlF_3$ (cryolite). The procedure consists essentially of covering an aluminum block with cryolite and adding the proper amount of UO_2 mixed in cryolite to a graphite crucible. After charging is complete, the temperature is brought to 1120°C and maintained for about 25 min. With this process, homogeneous alloys were produced with a uranium yield of 98 per cent. Brookhaven,[18] on the other hand, reported some difficulty in obtaining aluminum–8 wt.% uranium alloys by melting and casting. Segregation in the alloys gave uranium contents as high as 13 per cent in ingot centers. Lowering the pouring temperature and stirring just before the pouring helped correct the situation.

Studies have been in progress at Argonne[19] for the purpose of determining the swelling-temperature limitations of the aluminum–17 wt.% uranium alloy and the aluminum–39 wt.% U_3O_8 dispersion. The specimens were irradiated with aluminum cladding on both faces with all edges bare. Postirradiation annealing was used to provide the required temperature variation.

The data indicate that, for the aluminum–17 wt.% uranium alloy with burnups of less than 1.6×10^{20} fissions/cm^3, resistance to swelling is good up to and including 550°C. However, with a burnup of 5.5×10^{20} fissions/cm^3, swelling does occur at 550°C. The aluminum–39 wt.% U_3O_8 dispersion shows excellent resistance to swelling for burnups to 1.35×10^{20} fissions/cm^3 and temperatures to 500°C.

It must be emphasized that these data were obtained as a result of postirradiation annealing. Whether this duplicates actual in-pile heating is yet to be definitely resolved.

(R. F. Dickerson)

Mechanism of Oxidation of Uranium

British scientists have reported[20] on the oxidation of irradiated uranium in CO_2. Burnups ranged up to 2350 Mwd/ton. The uranium was heated out-of-pile to 600 or 800°C during exposure to flowing carbon dioxide. There was no difference in oxidation rates between irradiated and unirradiated uranium that was treated at 600°C. On the other hand, the irradiated uranium that was treated at 800°C exhibited self-heating, rapid oxidation, and severe swelling. It is believed that the swelling was caused by the release of fission gas within the uranium. This in turn increased the surface area exposed to CO_2 (presumably by surface cracking) and resulted in catastrophic oxidation.

Argonne[21] has studied the oxidation of uranium at 125 to 250°C and at oxygen pressures between 20 and 800 mm. The reaction rate was found to be divided into two stages: (1) an initial slow reaction and (2) a more rapid second stage. Both reaction rates appeared to be linear. Oxidation rates were found to increase with increasing oxygen pressure. The reaction product was identified as UO_2. On the basis of their results, the workers at Argonne conclude that the rate-controlling step during the first stage of oxidation occurs on the outer oxide surface rather than the rate being governed by diffusion of ions through an oxide film (diffusion barrier) of constant thickness. The increase in rate leading to the second stage was attributed to a net increase in surface area. (W. E. Berry)

Plutonium

Plutonium Metal and Alloys

The effects of impurity content, stresses, beta-heat-treating time and temperature, hydrostatic pressure, and thermal cycling on the beta-to-alpha transformation of plutonium have been investigated at Hanford.[22] Results were as follows:

1. Decreasing the impurity content increases the rate of transformation.

2. High tensile stress retards the beta-to-alpha transformation.

Table I-1 COMPARISON OF MECHANICAL PROPERTIES* OF VARIOUS COMPOSITIONS OF PLUTONIUM-ZIRCONIUM ALLOY AND UNALLOYED PLUTONIUM AT ELEVATED TEMPERATURES[24]

Alloy composition (balance Pu), at.%	Test temp., °C	Ultimate strength, psi	Elongation,† %	Reduction in area, %	Av. density at room temp., g/cm³	Remarks
3 Zr	180	18,000			17.41	Held at 180°C for 20 min and then tested
3 Zr	130	28,940				Held at 130°C for 30 min and then tested
2 Zr	180	16,105			17.55	Held at 180°C for 20 min and then tested
2 Zr	130	26,000				Held at 130°C for 30 min and then tested
1 Zr	180	12,000	100	100	19.21	Held at 180°C for 20 min and then tested
1 Zr	130	24,224				Held at 130°C for 30 min and then tested
0.5 Zr	180	6,448	450	75	19.45	Held at 180°C for 20 min and then tested
0.5 Zr	130	13,308	160	30		Held at 130°C for 30 min and then tested
Unalloyed Pu	180	3,580	503.2	100	19.59	Beta-phase Pu
Unalloyed Pu	130	12,100	294	100		Beta-phase Pu

*All tensile specimens were 0.250 in. in diameter.
†Gauge length was 1 in.; testing speed was 0.015 in./min.

3. Increasing the beta-heat-treating time and temperature markedly decreases the rate of transformation.

4. Hydrostatic pressing at 90,000 psi accelerates the beta and alpha transformation under pressure but decreases any subsequent beta-to-alpha transformations by as much as two orders of magnitude.

5. Specimen size has no effect on the start of transformation, but an increase in the specimen size from 0.010 to 0.37 in. decreases the rate of transformation by several orders of magnitude.

6. Thermal cycling less than 15 cycles does not affect the rate of transformation.

In an investigation of the Hall effect in plutonium, the British[23] report that three alpha-plutonium samples showed a continuous increase in R_H [up to $(-18.0 \pm 1.2) \times 10^{-5}$ cm³/coulomb] if held at 77°K up to 6 hr.

The effects of zirconium additions up to 3 at.% on the mechanical properties of beta plutonium at 130 and 180°C have been investigated at Hanford.[24] Data are presented in Table I-1. Thermal-expansion and -contraction curves for a plutonium–3 at.% zirconium alloy are shown in Fig. I-1. On heating, the alloy starts to transform to gamma at 270°C, transforms to delta at 295°C, and starts transforming, possibly going through delta prime, to epsilon at 485°C. On cooling, the sharp transition from delta to beta would suggest that gamma did not appear. The increase in length at the end of cooling is due to cracks that formed during volume changes accompanying phase transformations.

Aluminum-plutonium and aluminum–12 wt.% silicon–plutonium alloys that contained 1.65 to 20 wt.% plutonium all exhibited good irradiation behavior at temperatures from 650 to 850°F. As seen in Fig. I-2, the aluminum-plutonium alloys appear to be more resistant to deformation than the aluminum-silicon-plutonium alloys. Also, the resistance to deformation in both alloys tends to increase with increasing plutonium content.

The Zircaloy-4 cladding of an aluminum–2.3 wt.% plutonium–2 wt.% nickel alloy was intentionally ruptured after the element had been operating for 18 days at full power in the Engineering Test Reactor (ETR) high-temperature loop. Only small activity release rates were observed while the element operated for 47 hr after being ruptured.

Los Alamos[25] reports that no failures have been observed in tantalum crucibles that contain a molten plutonium-cerium-cobalt alloy after 1000 hr at 750°C and 600 hr at 850°C. The ceramics TaC, TiC, ZrC, HfC, TiB_2, and

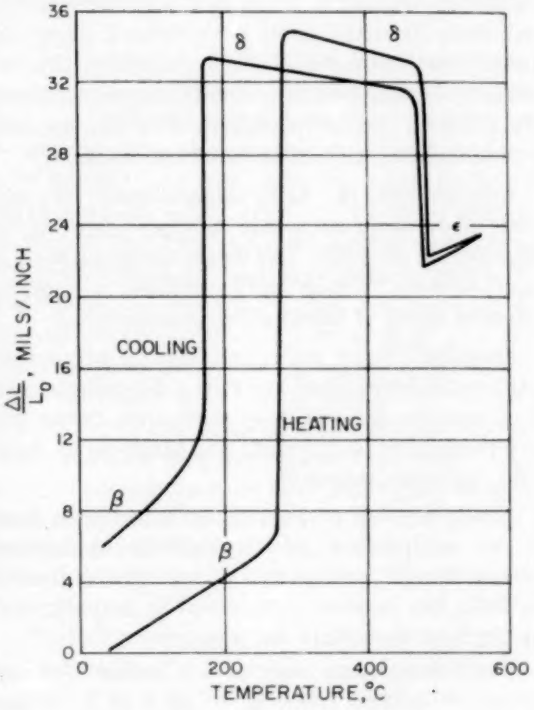

Fig. I-1 Expansion and contraction curves of plutonium–3 at.% zirconium alloy.[24] Heating and cooling rate was 25°/hr; L_0 = 1.0008 in.

ZrB_2 are also being tested as container materials for the alloy. Some incipient intergranular penetration along certain grain boundaries of ZrC was observed. The other ceramics exhibited little or no surface reaction with the alloy.

Preliminary tests of five ceramic crucibles, Al_2O_3, Y_2O_3, MgO, BeO, and CaO, as containers for a molten plutonium-uranium-manganese alloy indicate little or no reaction after 200 hr at 900°C.

Preliminary estimates at Mound Laboratory[26] indicate a viscosity of approximately 5 centipoises at 700°C for a cerium–24.2 at.% cobalt–19.6 at.% plutonium alloy.

A technique has been developed at Chalk River[27] for preparing plutonium-beryllium alloys by heating a mixture of plutonium fluoride and beryllium at 1000 to 1350°C in a vacuum to reduce the fluoride and alloy the reduced metal.

Battelle[28] reports that heat-treating iron–27.6 wt.% plutonium and iron–27.5 wt.% plutonium–2.1 wt.% molybdenum for periods up to 20 hr at 900°C results in increased coalescence of the $PuFe_2$ phase with increasing heat-treating time. Hardness of these alloys decreases slightly with increased heat-treating time. Similarly heat-treated iron–27.6 wt.% plutonium–11.9 wt.% chromium alloy specimens exhibited microstructures that showed little change as compared with the cast alloy (iron-chromium surrounded by a eutectic mixture of $PuFe_2$ and iron-chromium). The hardness of the heat-treated chromium-containing-alloy specimens was higher than that of cast specimens, possibly as a result of nitrogen pickup during heat-treating in a nitrogen glove-box atmosphere.. (V. W. Storhok)

Plutonium Compounds

Research on the stability of PuO_2 in various atmospheres at elevated temperatures has continued at Hanford.[29] Oxygen-to-plutonium ratios have been found to decrease as a function of both increased time and temperature of sintering. PuO_2 decomposes to $PuO_{1.85}$ after being heated[30] for 1 hr in vacuum at 1900°C. The tentative existence of a eutectoid has been

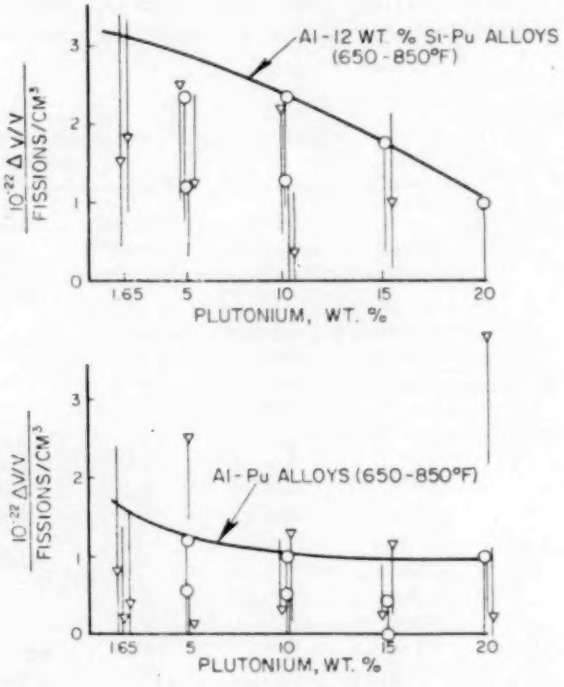

Fig. I-2 Ratio[24] of core volume change to fissions/cm^3 as a function of plutonium concentration for aluminum-plutonium and aluminum-silicon-plutonium in the temperature range 650 to 850°F. ○, from density change. ▽, from dimensional change. Vertical lines show range for value.

postulated at $PuO_{1.85}$ on the basis of metallographic studies of quenched compounds.[30,31] Attempts to produce the plutonium silicides, $PuSi_2$ and Pu_2Si_3, which were successful for the sesquisilicide are described. The process involved the reaction of PuO_2 and silicon, in the mole ratio of 40 : 60, at 1385°C in vacuum.

A report[32] has been issued concerning the PuO_2-ZrO_2 system which shows that single-phase, face-centered-cubic solid solution exists from 0 to 80 mole % ZrO_2. From 80 to 99.8 mole %, a two-phase region exists which consists of monoclinic ZrO_2 and the ZrO_2-PuO_2 solid solution. The entire system shows an experimental liquidus that is continuous from ZrO_2 to PuO_2.

PuN has been prepared by arc-melting metallic plutonium in 1 atm of nitrogen.[33,34] The material contained 5 wt.% alpha plutonium that was eliminated by subsequently remelting in nitrogen. The melting point of the stoichiometric compound is in excess of 2400°C, with a partial decomposition occurring at 1800°C.

In addition, Hanford continues experimental work on loading long tubes with UO_2 that is uniformly enriched with 0.5 wt.% PuO_2 for irradiation testing.[24] Work is also in progress to hot-roll, directly from the powders, strip material that consists of PuO_2 dispersed in a UO_2 matrix. Irradiation of graphite impregnated with PuO_2 shows lattice expansion of both components which is indicative of irradiation damage.[31]

Fabrication of molybdenum-PuO_2 cermets that have approximately 94 per cent of the theoretical density has been accomplished by Los Alamos.[35] This work includes a comprehensive study of fabrication parameters.

Battelle[36,37] is continuing to accumulate vapor-pressure data for PuO_2. No complete interpretation has yet been presented. Other data are presented on the sintering behavior of PuO_2-ThO_2 solid solutions.[38]

The moisture pickup of PuO_2 has been found to be independent of atmosphere at ambient temperatures, and plasma-torch spheroidization of PuO_2 has been accomplished by investigators at Nuclear Materials and Equipment Corp.[39]

The composition limit of arc-melted PuC appears to extend from 42 to 48.5 at.% carbon. For arc-melted and annealed alloys,[24] single-phase composition limits are narrower (44 to 47 at.% carbon). (W. M. Pardue)

Table I-2 ROOM- AND ELEVATED-TEMPERATURE TENSILE PROPERTIES OF IRRADIATED THORIUM[42]

Sample	Test temp., °C	Thermal nvt × 10^{-20}	Burnup, at.%	Strength, 1000 psi		Total elongation in 1 in., %
				0.2% yield	Ultimate	
			Battelle Material			
CT-1	RT	0		16.7	24.4	41
CT-2	RT	0		16.4	24.6	50
CT-6	RT	0		17.5	26.5	57
CT-8	815	0		~7	~17	~43
EX	RT	8.1	0.077	44.2	44.6	24
GX	RT	7.1	0.058	44.5	44.9	29
AX	590	7.3	0.060	~24	~27	~22
CX	815	7.6	0.065	~20	~21	~9
			Hanford Material			
CT-9	RT	0		21.0	31.7	55
CT-12	RT	0		22.3	29.9	*
CT-10	590	0		~9	~20	~92
CT-4	815	0		~8	~16	~26
DX	RT	7.7	0.070	50.5†	51.1	*
FX	RT	8.4	0.085	48.6†	49.5	*
9X	590	7.3	0.060	~22	~23	~24
BX	815	7.5	0.065	~19	~19	~16

*Sample broke outside of 1-in. gauge length.
†Lower yield strength.

Thorium

The solubility of ThO_2 in liquid thorium is reported by Atomics International[40] to be 3.5 wt.% at 2090°K and 8.2 wt.% at 2450°K. The predominant gaseous species over the mixture was found to be ThO with the vapor pressure being given by $\log P\ (\text{atm}) = -(22{,}200 \pm 700)/T + (4.70 \pm 0.31)$. The vapor-pressure equation for $ThO_2(s) \rightarrow ThO_2(g)$ was also determined and is $\log P\ (\text{atm}) = -(35{,}500 \pm 1100)/T + (8.16 \pm 0.47)$. Extrapolation of vaporization data for solid thorium gave the following equation for thorium (l) → thorium (g): $\log P\ (\text{atm}) = -27{,}960/T + 5.575$. Solubility studies indicated that the partial pressure of thorium and ThO_2 from a mixture of liquid thorium and solid ThO_2 would be less than that calculated from the pressure equations for thorium (g) and ThO_2(g).

Diffusivity of carbon in thorium as determined at Ames[41] is 7.4×10^{-9} cm²/sec at 1000°C, 2.8×10^{-8} cm²/sec at 1100°C, and 5.7×10^{-8} cm²/sec at 1200°C. Activation energy for diffusion is 38 kcal/mole. Evidence of a change in diffusivity with concentration was observed.

The effects of fast-neutron irradiation on the mechanical properties of unalloyed thorium at 590 and 815°C were investigated at Hanford.[42] Two lots of thorium were tested. The Battelle thorium contained 70 ppm iron, 370 ppm carbon, and 1125 ppm oxygen, and had a grain size of 3 grains/cm² at 100×; the Hanford thorium contained 155 to 315 ppm iron, 295 to 730 ppm carbon, and 850 ppm oxygen, and had a grain size of 23 grains/cm² at 100×. Neutron irradiation resulted in a slight increase in the ultimate strength and a large increase in the yield strength of the thorium at 590 and 815°C. The data are listed in Table I-2.

The effects of neutron irradiation on the room-temperature mechanical properties of Th–1, –4, and –5.4 wt.% uranium (93 per cent U^{235}) alloys have also been studied. Center temperatures of the specimens during irradiation were less than 250°C. Data given in Table I-3 indicate that irradiation increases the yield strength and decreases the ductility of the alloys tested.

The Bureau of Mines[43] is investigating the effects of additions of holmium, neodymium, and praseodymium on the properties of thorium. These alloy additions gave little increase in hardness over that of unalloyed thorium in the cast condition. The greatest change was from $60R_E$ for unalloyed thorium to $70R_E$ for a thorium-holmium alloy. An increase in the praseodymium or neodymium content lowers the alpha-to-beta transformation temperature of thorium, whereas an increase in holmium tends to raise the transformation temperature.

Brookhaven[44] reports that the thorium and uranium in a bismuth–5 wt.% thorium–5 wt.%

Table I-3 MECHANICAL PROPERTIES OF IRRADIATED AND NONIRRADIATED THORIUM-URANIUM ALLOYS[42]

Specimen	Composition (balance Th), wt.%	Accumulated exposure		Elastic modulus, 10^6 psi	Yield strength (0.2% offset), 1000 psi	Ultimate strength, 1000 psi	Total elongation, %
		10^{20} nvt	At.% burnup				
133	1.0	Unirradiated, swaged		8.6	49.5	51.7	25.4
121	1.0	4.9	0.19	10.6	70.9	71.7	9.6
425	4.0	Unirradiated, swaged		10.1	51.8	55.7	24.6
441	4.0	0.4	0.08	10.3	68.7	68.7	15.6
412	4.0	0.7	0.15	10.5	70.7	72.2	15.0
B1-Z	5.4	Unirradiated, annealed		13.1	25.5	41.8	22.3
A91	5.4	0.25	0.07	10.7	62.6	63.8	13.8

Table I-4 COMPRESSIVE-STRENGTH DATA ON THORIUM-URANIUM COMPOUNDS[28]

Compound	Temp., °F	Fracture strength, psi
$(Th_9U)B_4$	RT	45,000
	1200	48,800
$(Th_9U)C$	RT	23,300
	1200	16,700
$(Th_9U)C_2$	RT	58,500
	1200	14,600

Table I-5 MEAN THERMAL-EXPANSION COEFFICIENTS FOR THORIUM-URANIUM COMPOUNDS[28]

Temp. range, °F	Mean thermal-expansion coefficients, 10^{-6}/°C					
	$(Th_9U)B_4$		$(Th_9U)C$		$(Th_9U)C_2$	
	Heating	Cooling	Heating	Cooling	Heating	Cooling
68 to 200	3.5	3.3	3.5	3.7	4.1	4.3
68 to 400	3.7	3.6	3.6	3.7	4.2	4.3
68 to 600	3.8	3.7	3.6	3.7	4.3	4.4
68 to 800	4.0	3.8	3.8	3.8	4.4	4.5
68 to 1000	4.1	3.9	3.8	3.8	4.4	4.5
68 to 1200	4.2	4.1	3.9	3.9	4.6	4.6
68 to 1400	4.3	4.2	3.9	4.0	4.7	4.8
68 to 1600	4.4	4.3	4.1	4.1	4.8	5.0
68 to 1800	4.4	4.4	4.1	4.1	5.0	5.3

Table I-6 OXIDATION DATA FOR THORIUM-URANIUM COMPOUNDS IN DRY AIR[28]

Compound	Temp., °F	Total weight change at time shown, mg/cm²							
		1 hr	2 hr	4 hr	8 hr	24 hr	112 hr	160 hr	200 hr
$(Th_9U)B_4$	900		0.151		0.342	0.513			
	1300		0.171		0.684	1.196			
	1500		0.256	0.513	0.854	2.136			
	1700					6.8	18.17	22.98	27.77
	1900					12.2	24.89	30.57	35.84
$(Th_9U)C$	900	0.185	0.37	0.555	2.586	11.821			
	1100	1.77	7.086	17.27	33.8	77.78			
	1300	14.98	29.31	51.46	81.11				
	1500	20.61	35.42	60.42	100.1				
$(Th_9U)C_2$	700			0.16		0.6576			
	800	0.161	0.322	0.90		24.25			
	1500	13.23	21.48	35.5					
$(Th_9U)Be_{13}$	900				0.234	0.623			

uranium alloy contained in a stationary, horizontal, graphite tube under a ΔT of 530°C (800 to 270°C) migrates rapidly toward the cooler end of the container. Migration was caused by dissolution mass transfer rather than mass transfer of the solid $ThBi_2$ and UBi_2. Thermal-convection currents in the liquid phase accelerated the transfer.

Properties of the compounds $(Th_9U)B_4$, $(Th_9U)Be_{13}$, $(Th_9U)C$, and $(Th_9U)C_2$ are being investigated at Battelle.[28] The results of compression tests of the borides and carbides at room temperature and at 1200°F are shown in Table I-4, and thermal-expansion coefficients in temperature ranges up to 1800°F are listed in Table I-5. The oxidation resistance of $(Th_9U)B_4$ in dry air appears to be very good at temperatures up to at least 1900°F. Oxidation data for all the compounds are presented in Table I-6.

(V. W. Storhok)

Coated-Particle Fuel Materials

Preparation and Fabrication

Oxide-Base Fuel. The use of vacuum evaporation techniques to deposit iron, chromium, nickel, and molybdenum films on spherical UO_2 powder (Fig. I-3*) was reported at Plansee by representatives of Euratom and the Belgian Centre d'Étude de l'Énergie Nucléaire.[45] Coating rates of about 1 to 2 μ/hr were obtained, and source temperatures between 1370 and 1950°C were employed. Substrate temperatures

*Figure I-3 is reprinted here by permission from *Metal Progress*.[45]

Fig. I-3 Particles of UO_2 powder coated with about 2 μ of iron by vacuum evaporation.[45]

were kept below 300°C. Studies on electroless, electrolytic, and vapor coatings of nickel on UO_2 (Fig. I-4) are also being carried out by Martin-Marietta Corporation,[46] and Nuclear Materials and Equipment Corporation (NUMEC) has reported[47] on the preparation of copper- and nickel-coated PuO_2 powder (Fig. I-5). NUMEC has applied multistage "electroless" nickel from standard nickel chloride-hypophosphite baths at 80 to 85°C by use of manual agitation. Electrolytic copper was deposited over nickel-coated oxide, and attempts were made also to deposit electroless copper over vacuum-deposited copper-coated oxide. However, the thickness of the vacuum-deposited copper films (1 to 3 μ) was insufficient to protect the substrate against attack by the copper-cyanide plating solution. A number of patents on the chemical vapor deposition of metals in fluidized beds were recently awarded. The metals include niobium, tungsten, and tantalum,[48,49] and silicon [50,51] and chromium.[52]

NUMEC is studying barrel-plating techniques, Thermal Dynamics is investigating plasma reactions, and Battelle is continuing its fluidized-bed program.

Further progress on ceramic-coated fuel particles (Fig. I-6) has been reported by Battelle.[28,53] Major effort has been directed toward the preparation of composite coatings which are resistant to fission-recoil damage and which permit controlled substrate swelling and limit crack propagation. It has been found that carbon overcoating of Al_2O_3-coated particles seems to result in cracking of the Al_2O_3 undercoat despite considerable variations in the temperature of application of the two coatings. Heat-treatment for 48 hr at 1250°C in hydrogen of 1000°C Al_2O_3 coatings on porous UO_2 particles resulted in deterioration of the coating as indicated by xenon-release ratios (>92 ppm at 1300°C). Poor-quality Al_2O_3 coatings were also encountered in preparing thin, dense Al_2O_3 coatings over porous Al_2O_3 inner coatings despite initial heat-treatments to stabilize the porous layers. It is now becoming clear that the properties of the oxide substrate can have a considerable effect on the structure of the oxide coatings. Work is being continued on the deposition of BeO and MgO coatings by the hydrolysis of $BeCl_2$ and MgI_2, respectively. The quality of the MgO coatings has so far been considerably inferior to that of the Al_2O_3 coatings now undergoing irradiation, although the BeO coatings are beginning to look promising. Until recently, the major emphasis on the coating program

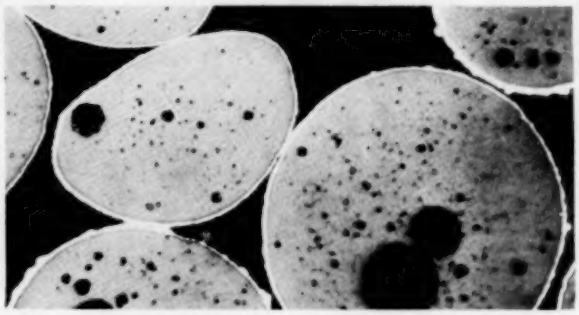

Fig. I-4 Spherical UO_2 particles coated with electroless nickel (1 to 3 μ).[46]

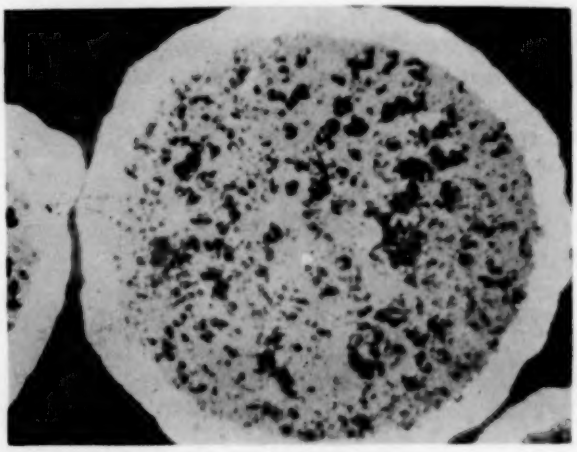

Fig. I-5 PuO_2 particles coated with electroless nickel (12 μ).[47]

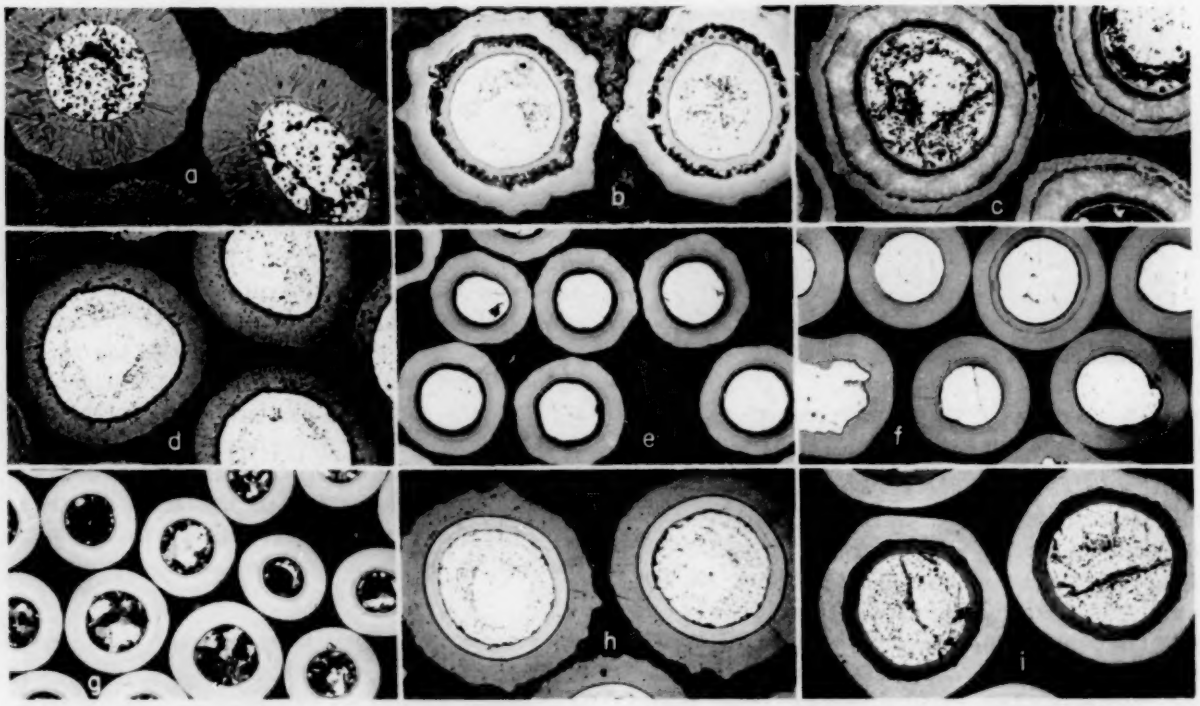

Fig. I-6 Various types of ceramic-coated nuclear-fuel particles. (*a*) 1400°C Al_2O_3 coating in UO_2. (*b*) 1000-700-1000°C Al_2O_3 coatings on UO_2. (*c*) 1000-700-1000°C Al_2O_3 coatings on UO_2 with void between porous and inner dense coatings. (*d*) 1400°C BeO coating on UO_2. (*e*) 1400°C, 5 μ/hr PyC coating on UC_2. (*f*) 1400°C, 37 μ/hr PyC coating on UC_2. (*g*) PyC-coated U shot after conversion of core to UC. (*h*) Al_2O_3-overcoated PyC-coated UO_2. (*i*) PyC-overcoated Al_2O_3-coated UO_2. The diameter of the fuel particles is approximately 125 μ. (Courtesy of J. M. Blocher, Jr., M. F. Browning, et al.)

was concentrated on Al_2O_3 and carbon studies. Eleven types of Al_2O_3, pyrolytic carbon (PyC), or composite coatings on uranium dioxide fuel have now passed neutron-activation tests (<5 ppm xenon release at 1300°C), and most are now being irradiated both as unsupported particles and in graphite matrices. Recently, matrix samples prepared by pelletizing procedures, whereby improved uniformity of the dispersed coated-particle fuels was obtained, passed neutron-activation tests (<1 ppm xenon release at 1150°C) and are candidates for the next irradiation experiments.

Preparation of Carbide-Base Fuel. General Atomic has scaled up its carbon-coating process to produce between 1 and 2 kg of coated $(U,Th)C_2$ per charge. Low-permeability graphite was used as the structural material and was designed so that warm unloading will be possible. Either resistance or induction heating can be employed.[54] Coating thicknesses averaged about 45 μ after a 5-hr run.[55] Basically the process entails jettisoning the carbide particles from a semifluid bed into the hot zone of a vertical tube by means of a high-speed stream of gas which contains a hydrocarbon, generally methane, as the coating medium. Coating temperatures between 1000 and 1400°C are used, and yields of about 50 per cent are obtained. Several minor system changes are being evaluated in an attempt to remedy the primary problem of excessive soot deposits that build up over the 5-hr run. Experience has indicated that the fraction of the material always present in the bed is quite possibly hot enough for coating to take place should sufficient contact with the gas be permitted. To explore this possibility, various designs are being tried in an attempt to bleed off a portion of the high-speed gas stream and allow it to pass very slowly through the dynamic bed.[56]

General Atomic has issued a summary report[57] on the development and evaluation of

graphite-matrix fuel compacts for the High-Temperature Gas-Cooled Reactor. The fuel compacts consist of PyC-coated $(Th,U)C_2$ particles dispersed in a high-density graphite matrix (Figs. I-7 and I-8) and are produced by a hot-pressing technique. Two compacts that contained carbon-coated $(Th,U)C_2$ particles were examined after a 3100-hr heat-treatment at 1700°C. Particles coated by the use of methane were in one compact; the other contained particles that were coated using acetylene as the source of carbon. Preliminary results indicate some reaction between particles and coatings in each case; however, the coating deposited from acetylene appeared to be more heavily attacked.[55]

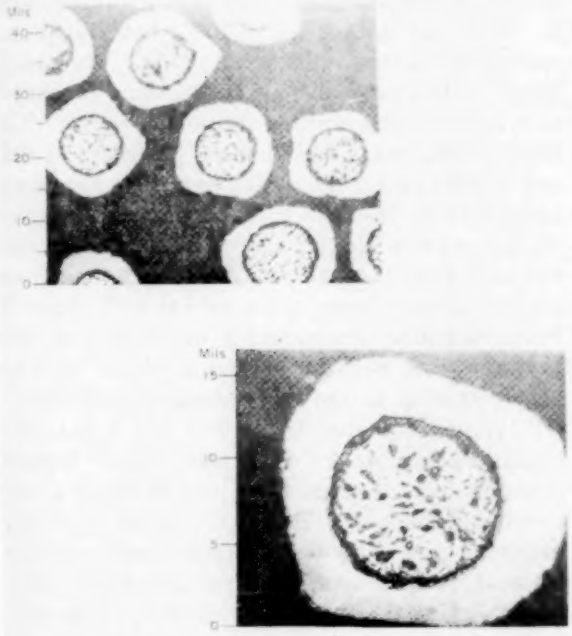

Fig. I-7 PyC-coated $(Th,U)C_2$ fuel particles[57] prepared for irradiation in capsule GA-309-9; coating was deposited from acetylene at 1400°C.

Oak Ridge[58,59] is currently evaluating PyC-coated fuel (Fig. I-9) supplied by Minnesota Mining and Manufacturing Company (3M), National Carbon Company (NCC), High Temperature Materials, Inc. (HTM), and General Atomic (GA). A diffusion coefficient of 1.41×10^{-10} cm^2/sec at 2180°C for Xe^{133} through HTM coatings on UC_2 was determined. There was no evidence of rupture of this material, as contrasted

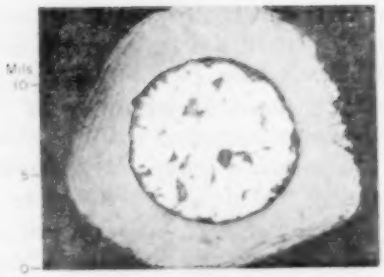

Fig. I-8 PyC-coated $(Th,U)C_2$ fuel particle[57] typical of those prepared for irradiation in capsule GA-309-8; coating was deposited from methane at 1400°C.

with previous experience, and the release appeared to be controlled by diffusion. Acid leaching of an early shipment of 3M pellets which contained PyC-coated UC_2 fuel revealed uranium losses of from 7 to 700 ppm for various samples. Neutron activation of 3M pellets showed Xe^{133}-release ratios of between 65 and 200 ppm at 1300°C. The 3M pellets fired at 1800°C showed considerably higher release ratios, presumably because of the high firing temperature. It was also reported that PyC-coated particles, heat-treated to 1600°C, after successfully passing neutron-activation tests were completely attacked by nitric acid.[25] Later analysis of PyC-coated particles supplied by GA, HTM, 3M, and NCC revealed surface-contamination levels between <0.9 and 116 ppm by alpha assay and between 1.9 and 1900 ppm by acid leaching.[59]

Four different types of PyC-coated UC_2 particles, prepared at Battelle, have exhibited xenon-release ratios of less than 3 ppm at 1300°C and are now being irradiated. Coating

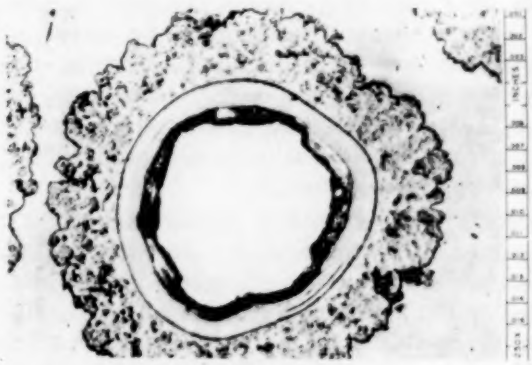

Fig. I-9 Typical microstructure of PyC-coated UC_2 particles[58] supplied by National Carbon Company illustrating polyphase structure of the coating.

temperatures of 1400°C were employed, and acetylene was used as the reactant hydrocarbon. A 950°C coating is now being prepared to investigate the possible advantage of the considerably higher densities that can be obtained in this temperature range. The development of pelletizing techniques to disperse coated-particle fuels uniformly has neared completion, and irradiation specimens are being prepared.[28,53]

Irradiation and Evaluation of Coated-Particle Fuels

Oxide-Base Fuel. Battelle has presented a summary of the irradiation performance of various types of coated UO_2 fuel particles in a series of nonsweep experiments.[28,53] The experiments were factorially designed to evaluate the effects of matrix support, low and high temperatures (60 and 1100°C), and two levels of burnup (3 and 6 at.%). The tentative results are presented in Table I-7 in terms of the fractional release of Xe^{133}, determined after irradiation by puncturing and evacuating the specimen containers after cooling to room temperature. At elevated temperatures the dense Al_2O_3 coating appears to have quite remarkable fission-product retention and is not affected by burnup over the ranges studied. A composite coating that consisted of PyC-overcoated Al_2O_3 also showed excellent fission-product retention despite the fact that the Al_2O_3 was cracked during the overcoating. At low temperatures a porous inner layer of Al_2O_3 seemed to give superior performance over fully dense coatings of Al_2O_3 or PyC. In general, xenon release was much more severe after low-temperature irradiation than after high-temperature exposure; support by matrix material appeared to be more important at low temperatures. Additional data are now being obtained on PyC-coated UO_2 and Al_2O_3 coatings containing porous interlayers on UO_2 after irradiation at temperatures of 1050°C to burnups of about 6 at.%.

Data[28] from a 1050°C sweep capsule that contained fully dense Al_2O_3 coatings on UO_2 particles supported by a graphite matrix indicated initial R/B values (rate of release of fission products divided by birth rate) of 10^{-8} to 10^{-9}. After 10 days of operation, heater failure and reduced power level resulted in a drop in the specimen temperature to 400°C; at this time the R/B values quickly rose to the 10^{-4} to 10^{-6} level. This low-temperature failure supports the earlier evidence that low-temperature irradiation is apparently the more severe environment for damage to ceramic-coated-particle fuels in the temperature range from 60 to 1100°C. Additional sweep capsules that contain Al_2O_3- and PyC-coated UO_2 are being planned for irradiation at both ambient and elevated temperatures. A number of static capsules are also attached to the sweep section. Seven different types of coated UO_2 are to be studied in these experiments.[28]

Irradiation of Carbide-Base Fuel. Additional data were reported by Oak Ridge[58] on the sweep experiment at the Materials Testing Reactor (MTR). PyC-coated UC_2 particles with a 175- to 250-μ fuel diameter (coated with 80 to 100 μ of PyC by 3M and then fabricated into elements by NCC) had R/B ratios of 10^{-2} to 10^{-3} at temperatures between 950 and 1370°C. As mentioned previously, the elements were prepared at a baking temperature in excess of 2000°C. Matrix specimens which were prepared by 3M and which contain 3M coated particles are being irradiated in the Oak Ridge Research Reactor (ORR) poolside facility at temperatures between 940 and 1240°C. After 48 days the R/B values for this sample were in the 10^{-3} to 10^{-5} range.[59] Postirradiation examination of HTM and 3M particles that were irradiated at 1100°C to 4 to 5 at.% burnup in the Low-Intensity Test Reactor facility revealed between 1 and 5 per cent cracked particles for both materials.[59] Future plans include irradiation in the MTR of a GA specimen which contains PyC-coated $(U,Th)C_2$ particles and which has a 9-ppm xenon-release ratio at 1000°C after neutron activation. Also scheduled is irradiation in the ORR-C1 facility of unsupported PyC-coated UC_2 particles supplied by 3M.

General Atomic[55] has indicated that, except for the initial 1000- to 2000-Mwd burnup, compacts containing PyC-coated $(Th,U)C_2$ particles showed very little, if any, further deterioration when temperatures remained less than 1850°C. Compacts with temperatures that have risen above this level appear to release inversely with abrupt changes in temperature; that is, the release corrected for temperature in the usual way (using activation energies of 29 and 34 kcal/mole for krypton and xenon, respectively) seems to peak when the temperature drops and fall when the temperature rises.

Table I-7 FRACTIONAL RELEASE OF Xe^{133} FROM COATED-PARTICLE MATERIALS[53]

Specimen lot	Fuel core		Coating*		Matrix support	Fractional Xe^{133} release,† ppm			
						3% burnup		6% burnup	
	Material	Diam., μ	Material	Thickness, μ		Capsules CFP-4 and CFP-1D (irradiated at 60 to 120°C)	Capsule CFP-1C (irradiated at 1100°C)	Capsule CFP-1B (irradiated at 60°C)	Capsule CFP-1A (irradiated at 1100°C)
4E	UO_2E0	127	Dense Al_2O_3	8	None	9.7			
			Porous Al_2O_3	6					
			Dense Al_2O_3	28					
721C	UO_2-E3	127	Dense Al_2O_3	8	None	31			
			Porous Al_2O_3	18	None	2.1	2.1	17	26
			Dense Al_2O_3	28	Graphite	18	23	3.0	120‡
					Carbon	2.0	1.2	61	55§
715A	UO_2-E2	127	Dense Al_2O_3	42	None	130			
					None	120	0.043	140	0.009
					Graphite	2.2	¶	0.12	2.9§
921	UO_2E2	127	Dense Al_2O_3**	48	None	56	0.065	15	0.009
			Mixed PyC	32					
920A	UO_2E3	127	Laminar PyC	45	None	290			

*Thickness of layers is given in order from that adjacent to the fuel particle to that at the outside of the particle.

†Fractional release values for specimens irradiated in capsules CFP-1A, CFP-1B, and CFP-1C are approximate.

‡Gas initially collected while specimen was at ambient temperature. Release under these conditions was 110 ppm. Specimens were subsequently heated to 400°C. Additional gas released under this condition was equivalent to a release fraction of 13 ppm.

§Gas collected while specimen was at 400°C.

¶No data. Specimen was damaged during capsule-opening operations.

**Inner Al_2O_3 layer was cracked during carbon overcoating.

There was a much greater rate of release of Kr^{85}, Xe^{133}, and Xe^{135} evident in the case of capsule 309-9 after shutdown. This was taken to indicate that cracks had developed in the coatings of some of the PyC-coated particles and that they tended to open up when the temperature dropped to ambient levels.

Metallographic examination[60,61] revealed only 4 per cent broken-particle coatings in capsule 309-8 and 15 per cent in capsule 309-9. The fission-product-release data indicated 15 per cent and 75 to 100 per cent coating failure. Hence there is a difference by a factor of 5 in the two results. To check the possibility of increased permeability of the coatings due to microcracks generated during irradiation, several apparently undamaged particles will be separated from the matrix of each compact and tested for fission-gas release. The following contributing factors were postulated to lead to tensile stresses in the carbon coatings during high-temperature irradiation:

1. Neutron- and fission-recoil exposure leading to shrinkage
2. Annealing or graphitizing of the coating from purely thermal effects leading to coating shrinkage
3. Differential thermal expansion between the coating and the particle
4. Fission-gas pressure
5. Expansion of the carbide particle during irradiation

The damaged coatings appear to have failed in tension, and, if longer than 3-year lives are to be obtained, it was suggested that a more graphitized coating would be desirable to minimize the first two effects which were thought to be the major factors in generating stresses in the coating.

No new data are available from Battelle on coated-carbide fuel particles although PyC-coated UC_2 particles are being irradiated at 1050°C to 6 at.% burnup. Previous data on PyC-coated UC_2 fuel after irradiation at 120°C to 3 at.% burnup suggested that a laminar structure was more desirable than a columnar structure on the basis of xenon-release measurements (18 vs. 250 ppm). The laminar structure (37 μ/hr deposition rate) is less dense than the columnar material (6 μ/hr deposition rate) although both were prepared at 1400°C using acetylene as the reactant hydrocarbon. However, there are not yet sufficient data to indicate whether this is a significant difference.

(J. H. Oxley)

Refractory Fuel and Fertile Materials

Properties and Behavior of Uranium Oxide Fuels

The Russians[62] have reported studies of chemical interactions between oxides of uranium and tungsten. In the UO_3-WO_3 system, UO_2WO_4 was found to exist as a stable compound. Thermal decomposition of UO_2WO_4 in vacuum at 800°C resulted in the formation of $UWO_{5.5}$, whereas at 900°C $UWO_{5.01}$ was formed. Above 1250°C, UWO_{5+x} was found to disproportionate. Combination of UO_2 and WO_3 by sintering under vacuum at 900 and 1250°C produced a distorted tetragonal cubic structure for UO_2 to WO_3 ratios of 1 to 25 and 1 to 50. At ratios of 15 to 1, 25 to 1, and 50 to 1, no cubic phase was observed, and the unit cell was a distorted rhombic structure. No reactions were observed between UO_2 and WO_2 at temperatures up to 1250°C.

Results of experimental studies of the kinetics of various reduction processes involving uranium oxides are presented in a series of Russian papers. One paper[63] covers studies of UO_3 reduction by hydrogen at temperatures ranging from 300 to 500°C and hydrogen pressures of 50 to 400 tons; a second paper[64] deals with the reduction of UO_3 by CO; and the reduction of U_3O_8 by hydrogen is the topic of a third paper.[65]

A Polish article[66] describes some phase relations of the BaO-UO_2 system. X-ray studies showed that, up to 50 mole % BaO, only the UO_2 and $BaUO_3$ phases exist. At 50 mole % BaO, $BaUO_3$ formed with a pseudocubic perovskite structure. At higher BaO contents, a marked solubility of BaO in $BaUO_3$, which persisted up to 75 mole % BaO, was observed. Above 75 mole % BaO, there was evidence of the presence of free BaO.

Melting-point studies on irradiated UO_2 have continued at Hanford.[42] The melting point of UO_2 was found to increase from 2790°C for unirradiated material to a maximum of 2910 ± 15°C at a burnup of 0.09 at.%. Irradiations in excess of 0.09 at.% burnup resulted in pro-

gressively lower melting points. UO_2 irradiated to a burnup of 1.2 at.% melted at 2790°C. Burnups of 8.5 and 11.5 at.% yielded melting points of 2760 ± 15°C and 2660 ± 15°C, respectively. It is proposed that the increase in the melting point is caused by the agglomeration of vacancies at fission-fragment sites in the lattice. The vacancy agglomeration is thought to lower the net lattice strain and decrease the equilibrium concentration of thermal vacancies that are free to move through the lattice; thus the melting point is increased.

Investigators at Atomics International[67] have determined lattice parameters as a function of oxygen content for nonstoichiometric uranium oxides quenched from 100°C in the composition range UO_2-U_4O_9. The lattice parameters in this range can be represented by two linear relations, which are characteristic of UO_{2+x} and U_4O_{9-y}. The relations are $a_0 = 5.4705 - 0.094x$ (A) for $0 \leq x \leq 0.125$ and $a_0 = 5.4423 + 0.029y$ (A) for $0 \leq y \leq 0.31$. Helium displacement densities gave results which are consistent with an oxygen-interstitial model for UO_{2+x} and an oxygen-vacancy model for U_4O_{9-y}.

(R. H. Barnes)

Investigators in the Nuclear Division of Combustion Engineering, Inc.,[68] have attempted to simulate internal power generation in tubular UO_2 specimens. They heated the tubular specimens with a coaxial tungsten-resistance heater and measured the quantity K_{eff}, or total thermal conductance. K_{eff} is defined by

$$\frac{Q \ln (R_2/R_1)}{2\pi L\ (T_2 - T_1)} \text{ Btu/(hr)(ft)(°F)}$$

where Q = total heat input, Btu/hr
R_2 = outer radius of specimen, ft
R_1 = inner radius of specimen, ft
T_2 = inner temperature, °F
T_1 = outer temperature, °F
L = specimen length, ft

The temperature gradient along the specimen radius was determined by measuring (by optical pyrometer) the temperatures at the bottoms of holes of various depths. Total heat input was calculated from the power dissipation per unit length of the resistor. The following conclusions were drawn from the work on UO_2:

1. K_{eff} increased with temperature at temperatures exceeding 1200°C.

2. K_{eff} was increased by thermal cycling at high temperature.

3. The UO_2 exhibited considerable volatility at about 1800°C.

4. The microstructure of the specimens after axial heating was similar to that of UO_2 specimens that had been heated by fission. The UO_2 grains close to the inner diameter of the specimen were large and columnar. Grains in the interior of the specimen were large and equiaxial, and those near the outer surface were unchanged.

A process for flame-spraying UO_2 onto stainless steel and Zircaloy-2 has been reported.[69] Weare and associates found that $UO_{2.00}$ of up to 90 per cent of theoretical density could be deposited with about 40 per cent efficiency. The coatings were quite adherent to both substrates and have been deposited in thicknesses up to 0.100 in. The investigators stated that the process appears to be technically and economically feasible. (A. K. Smalley)

Fabrication of UO_2-Containing Ceramics

Observers at Oak Ridge[70] report that swaged fuel-element cans ruptured during brazing of the can at 1010°C in hydrogen. The cans contained fused UO_2, and outgassing of the UO_2 was suspected. In order to explore this, 16 samples of fused-and-ground UO_2 were heated in vacuum at up to 1010°C and the evolved gases were measured and analyzed. Total evolution at 1010°C ranged from 0.025 to 0.4 cm^3 (standard temperature and pressure) per gram of UO_2. Nitrogen was the major constituent, although substantial quantities of CO_2, H_2, and H_2O also were found. The bulk of the evolution occurred at temperatures exceeding 500°C. The investigators felt that the gases either were adsorbed on the UO_2 or were decomposition products of organic contaminants. In any case, swelling of the cans was prevented by outgassing the UO_2 for 24 hr at 1000°C in a vacuum prior to loading the cans. (A. K. Smalley)

Properties of Uranium Carbides and Sulfides

Buckley[71] has interpreted lattice-parameter data on quenched samples of a uranium–4.7 wt.% carbon alloy to indicate that the solubility of uranium in uranium monocarbide may be as high as 1.5 at.% at 2000°C. This suggests that the existence range of UC extends to 4.5 wt.% carbon at 2000°C. This is considerably below the limit of existence that has been suggested

by other investigators, although there is general agreement that UC will dissolve some excess uranium at high temperatures.

Hudson et al. are investigating mixed carbides based on uranium carbides as thermionic emitters.[72,73] Vaporization losses from surfaces of UC-ZrC alloys were studied at temperatures near 2300°K. A 90 mole % UC–10 mole % ZrC alloy suffered prohibitive losses of UC at this temperature, and the surface concentration dropped to 35 mole % UC. At this concentration the vapor phase contained 76 wt.% uranium. However, no significant surface losses of uranium were detected from a 10 mole % UC–90 mole % ZrC alloy. Weight losses from this alloy were found to be a linear function of reciprocal temperature from 2120 to 2320°K. The resistivities of several alloys were determined and are shown in Table I-8. A diffusion couple of UC and niobium which had been annealed for 5 min at 1875°C produced a zone identified as liquid plus UC-NbC. A similar reaction was noted in a UC-Ta diffusion couple which had been annealed for 90 min at 1925°C. On the other hand, after 10 to 50 hr at 1800°C, no liquid metal was produced in diffusion couples of UC_2 with tantalum, niobium, tungsten, or molybdenum. The compounds UC_2, U_2C_3, UC, and (U,M)C were detected on the UC_2 side of the original interface after these tests. TaC, Ta_2C, WC, W_2C, NbC, Nb_2C, Mo_2C, and other phases were found on the respective metal sides of the original interface. In units of microns and hours, the reaction rates at 1800°C may be expressed as follows:

For UC_2 vs. tantalum: $X = 8.2t^{1/2}$
UC_2 vs. niobium: $X = 43.8t^{1/2}$
UC_2 vs. tungsten: $X = 49.2t^{1/2}$
UC_2 vs. molybdenum: $X = 225t^{1/2}$

It is argued that, if the reaction $UC_2 + M \rightarrow UC + MC$ were controlling, then the most powerful carbide formers would show the largest rate constants. If diffusion in UC were controlling, all the rate constants would be similar. It is concluded that (1) the rate of diffusion in MC is controlling and (2) all rates are too fast for use of these combinations at 1800°C.

Gordon reports data[74] which suggest that in hypostoichiometric UC the uranium metal phase is oxidized in preference to the UC. A uranium–4.4 wt.% carbon alloy was heated for 260 hr at 1500°F in sodium in a sealed niobium bottle. Examination showed that the uranium metal in the carbide grain boundaries was converted to UO_2 to a depth of 1 mil. The carbide itself was apparently unaffected. The oxygen which caused this effect is presumed to have come from gas adsorbed on the system surfaces. A uranium–5.2 wt.% carbon alloy tested at the same time showed cracking and chipping of the surface to a depth of 2 mils. This effect was also attributed to oxidation. A 0.1-mil-thick unidentified layer was detected on the inner surface of the niobium bottle after this test.

Table I-8 RESISTIVITIES OF AS-CAST URANIUM-CARBON-ZIRCONIUM[72,73]

Actual composition, mole %	Resistivity, μohm-cm
UC + 5 UC_2	15.4 + 0.112T (°K)
UC + 7 UC_2	29.2 + 0.112T
ZrC + 2 C	41.2 + 0.0781T
64 UC_2 + 36(35 UC–65 ZrC)	75.2 + 0.104T
80 UC_2 + 20(40 UC–60 ZrC)	75.9 + 0.113T
70 UC_2 + 30 UC	31.0 + 0.136T
43 Zr + 10 U + 47 C	171 + 0.0507T
90 ZrC + 10 UC	147 + 0.0668T

Accary and Lucas have made a study[75] of grain growth in UC and UC-U cermets at temperatures from 1100 to 1700°C. Grain growth in stoichiometric UC is very slow at 1100°C and rapid at 1700°C. The process apparently occurs in two stages: one stage has an activation energy of 57 kcal/mole and the other, 61 kcal/mole.

According to a report from Brookhaven,[44] diffusion of Xe^{133} from UC powder (100 to 140 mesh) occurs with an activation energy of approximately 32 kcal/mole. At 680 and 1150°C, diffusion coefficients of 8×10^{-22} and 2.5×10^{-19} cm^2/sec, respectively, were calculated.

Cater et al. have summarized[76] some physical properties of US which were obtained during an investigation of the vaporization of this compound. The lattice parameter of US is 5.4903 A; the melting point is 2460°C; the free energy of formation of solid US is $-268{,}000 + 64.0T$ (°K) cal/mole; the composition US evaporates congruently and produces a mixture of uranium, sulfur, and US molecules in the vapor; and the effective vapor pressure of this vapor over US is given by the expression

$$\log P\ (\text{atm}) = -1.7382 + 3.127 \times 10^4/T - 1.3181 \times 10^8/T^2 + 0.093776 \times 10^{12}/T^3$$

(W. Chubb)

Fabrication of Uranium Carbide Fuels

Several sites have attested to the difficulties involved in fabricating dense UC bodies by sintering. The densification is complicated by such factors as particle size, stoichiometry, oxygen content, and sintering conditions. To ease the fabrication problems, a liquid-phase sintering technique has been investigated. Increased sintered densities are obtained with additions of nickel. Union Carbide[77] reports that 1 to 2 vol.% nickel is ideal with sintering times greater than 2 hr at 1600°C. Carborundum[78] indicates that optimum conditions are 0.1 to 0.5 wt.% (0.2 to 0.8 vol.%) nickel addition with a 4-hr sinter at 1525°C. According to Union Carbide, a solution of carbon in the nickel eliminates UC_2. Carborundum states that as much as 0.5 per cent free carbon detrimentally affects densification. Union Carbide experienced cracking of specimens in the final stages of densification which is believed to be due to formation of metal-vapor pockets. The report[77] includes a microstructure showing large grains of cubic symmetry in a light-etching matrix which resulted from a large addition of nickel. Carborundum reported that the addition of 0.1 wt.% nickel generated 10 vol.% or more of a second phase which they tentatively identified as UC-nickel solid solution. Annealing at 1850°C decreased the amount of this phase, which disappeared at 2150°C and reportedly left UC plus uranium metal at the grain boundaries. Some studies of UC-metal systems at the University of Sheffield,[79–83] in England, may be helpful in interpreting the above results. These investigators contend that cobalt and nickel are incompatible with UC. Uranium-nickel intermetallic compounds were formed from mixtures on the UC-nickel tie line. UC-iron, UC-copper, and UC-chromium behaved as binary systems with eutectics.

Researchers at Oak Ridge[84] used UAl_2 as the liquid-promoting agent and indicated that densities as high as 94 per cent of theoretical were achieved at sintering temperatures as low as 1350°C (which is below the melting points of both UC and UAl_2) with as little as 3 per cent of the original aluminum remaining. Presumably the aluminum was volatilized, whereas the uranium was combined with carbon according to the reaction $12UC_{(1+x)} + UAl_2 \rightarrow (12-y)UC + (1 + y)$ liq (U, Al, C) $\rightarrow 2Al\uparrow + 13UC$. Two ternary aluminum-uranium-carbon compounds have been previously reported.[85]

Cold-compacting and sintering of uranium-graphite mixtures have been studied by the British.[86] Expansion at 800°C indicated initiation of the reaction. The optimum temperature for "plunge sintering" was 1125°C, and densities of about 12.4 g/cm^3 were achieved. The development of porosity was thought to be associated with the different diffusion rates of the two elements. The addition of 10 wt.% UFe_2 increased the sintered density[87] to about 13.1 g/cm^3. Other British investigators[3–7] have reported a binary type eutectic at 93 wt.% UFe_2 in the UC-UFe_2 system.

In the last issue of this Review, it was reported that UC compacts made from powder precipitated from liquid zinc-magnesium solutions "exploded" during sintering attempts. Argonne[19,88] has found that this was caused by Carbowax 4000 binder instead of the powder. Because dry-pressed specimens had internal cracks after sintering, 1.5 per cent naphthalene, which made a good binder but not a good lubricant, was used. Vacuum-sintered products with 88 per cent of theoretical density were obtained at 1750 to 1800°C. Metallographic examination showed traces of uranium metal but no UC_2. Additives appear to have increased the yield of UC in the precipitation process.

(E. O. Speidel)

Basic Studies of Irradiation Effects on Fuel Materials

Metallic Fuels

The special effects that occur during irradiation in fissile materials by transmutation and in materials that are in contact with fissile materials are considered by Barnes.[89] He discusses the process of growth, swelling, and changes in mechanical properties in relation to the formation, behavior, and effect of displaced atoms and impurities produced. These can be described in terms of interaction of vacancies, interstitials, and impurity atoms and are illustrated by the behavior of inert-gas atoms, which

are usually an appreciable proportion of the products. Workers at Knolls have derived an anisotropic migration model of point defects for zirconium-uranium alloys. They have compared the behavior predicted by other growth models with this derived model. A critical evaluation of the anisotropic migration model as made with existing data showed that samples irradiated at the same burnup rate to the same burnup showed a decrease in growth rate with an increase in irradiation temperature. This type of behavior is not in agreement with the prediction of the anisotropic migration or anisotropic atomic-displacement models. It was concluded that the anisotropic condensation model appears to be the most plausible of those currently proposed.

A summary of an investigation carried out at Hanford[90] has been prepared on the basis of engineering data from two types of swelling experiments: (1) annealing of irradiated uranium which was not restrained but which had been restrained during irradiation and (2) irradiation of uranium that was clad with Zircaloy-2 for low external restraint. The volume of uranium increased with the increase in irradiation temperature or postirradiation-annealing temperature. It was found that Zircaloy-2 cladding does not provide much restraint to in-reactor swelling of uranium in the rod geometry used. It was also found that, for a given burnup and an equivalent in-reactor and ex-reactor temperature, final estimates of unrestrained swelling are the same. These data also indicate that postirradiation-annealing experiments may provide reasonably accurate predictions of swelling in a fuel material irradiated under particular conditions of temperature and low restraint. The Swedish[92] have published an appendix containing 42 abstracts to articles on radiation effects in solid-uranium-based nuclear fuel materials.

Irradiation Effects in Ceramic Fuels

The low-temperature release of fission products from UO_2 has been studied by workers at Oak Ridge.[58] This has been part of a program in materials investigations for advanced fuel-element design. These studies have been made at temperatures of 500 and 800°C in vacuum and at 400°C in hydrogen. Calculations of the activation energies for release in this temperature range have been made from the experimental data. The value obtained for the 400 to 800°C temperature range was 14.7 kcal/mole in contrast to the accepted value of 70 to 80 kcal/mole at higher temperatures (greater than 1200°C).

Recent studies at Brookhaven[18] on the release of fission-product Xe^{133} from UBi_2 platelets in the 600 to 700°C temperature range indicate that diffusion of the xenon is occurring along the [0 0 1] crystallographic direction of the material. The activation energy for diffusion was found to be 45.64 kcal/mole. The diffusion coefficient follows the relation $D = 1.43 \times 10^{-2} \exp(-22{,}970/RT)$. If one extrapolates using this relation, this yields a diffusion coefficient of 7.23×10^{-12} cm²/sec at 800°C. This value compares with that obtained experimentally in the early stages of the 800°C experiment. It does not, however, conform to that of the simple diffusion phenomenon. Explanation of this behavior is not readily apparent from the information at hand.

Diffusion studies are being continued at Battelle[36] to determine the diffusion coefficient of Kr^{85} in UO_2. The diffusion-coefficient values ranged between 2×10^{-18} at 1900°F and 2×10^{-15} cm²/sec at 3000°F, with an activation energy of 76 kcal/mole. These values are about the same as the coefficients for Xe^{135} and Xe^{133} diffusion into UO_2 after corrections to account for the precursor I^{135} and I^{133} diffusion. The diffusion coefficients for Xe^{135} (5.4×10^{-15} and 8×10^{-14} at 2700 and 3000°F, respectively) as well as those for I^{135} (5.7×10^{-15} and 8×10^{-14} at the same temperatures) give, after first-approximation correction, 90 kcal/mole for the activation energies for their diffusion. (F. A. Rough)

References

1. E. S. Fisher and H. J. McSkimin, Low-Temperature Phase Transition in Alpha Uranium, *Phys. Rev.*, 124: 67–70 (Oct. 1, 1961).

2. A. V. Grosse et al., Density of Liquid Uranium, *J. Am. Chem. Soc.*, 83: 4665–4666 (Nov. 20, 1961).
3. S. J. Rothman, The Diffusion of Chromium in Gamma Uranium, USAEC Report ANL-6320, Argonne National Laboratory, June 1961.
4. M. Mossé et al., Diffusion de quelques metaux en solution diluee dans l'uranium, *Compt. rend.*, 250: 3171 (1960).
5. Y. Adda et al., Metallography—Study of Self-Diffusion of Uranium in the Alpha Phase, USAEC Translation HW-TR-30 [translated from *Compt. rend.*, 253: 445–447 (July 17, 1961)], Dec. 1, 1961.
6. L. T. Lloyd, Recrystallization of Deformed Alpha-Uranium Single Crystals, *J. Nuclear Materials*, 2: 141–146 (June 1960).
7. E. F. Stephan et al., Corrosion of Thorium and Uranium During Long-Term Storage, USAEC Report BMI-1563, Battelle Memorial Institute, Jan. 24, 1962.
8. D. L. Douglass, The Structure and Mechanical Properties of Uranium-Titanium Martensites, *Trans. Am. Soc. Metals*, 53: 307–319 (1961).
9. M. Kawasaki et al., Studies on Uranium-Molybdenum Alloy, USAEC Translation AEC-tr-4468 [translated from *J. At. Energy Soc. Japan*, 2: 136–140 (1960)].
10. H. Aubert, Uranium–0.1% Chromium Alloy, *Mém. sci. rev. mét.*, 58: 276–284 (April 1961) (in French).
11. A. Robillard et al., The Effect of Heat Treatment in the Gamma Phase on the Appearance of Substructure in Uranium and in Low Content Uranium-Chromium Alloys, Report NP-tr-828 [translated from *Rev. mét.*, 55: 815–828 (1958)].
12. M. S. Farkas et al., The Solid State Constitution of High Uranium Alloys of the Uranium-Zirconium-Silicon System, *Trans. Am. Soc. Metals*, 53: 511–521 (1961).
13. Y. Adda et al., Effect of Additions of Molybdenum, Zirconium, and Niobium on the Self-Diffusion of Uranium in the Gamma Phase, *Compt. rend.*, 253: 653–655 (July 24, 1961).
14. D. Kramer and C. G. Rhodes, The Gamma to Gamma Prime Transformation in the Uranium-Molybdenum System, USAEC Report NAA-SR-6617, Atomics International, Dec. 30, 1961.
15. L. F. Bates and R. D. Barnard, The Electrical and Magnetic Properties of the Uranium-Niobium System, *Proc. Phys. Soc. (London)*, 78: 361–369 (Sept. 1, 1961).
16. V. Kraus, Growth Kinetics and Properties of the Diffusion Layer on the Phase Boundary Behavior of Uranium and Aluminum, *Jaderná energie*, (2): 48–53 (1961).
17. J. Baird and O. J. C. Runnalls, The Preparation of Aluminum-Uranium Alloys by the Aluminum Reduction of Uranium Dioxide, Canadian Report CRRM-1065, December 1961.
18. J. H. Reynolds (Ed.), Nuclear Engineering Department Progress Report, May 1–August 31, 1961, USAEC Report BNL-696, Brookhaven National Laboratory, January 1962.
19. Argonne National Laboratory, Reactor Development Program Progress Report, December 1961, USAEC Report ANL-6485, Jan. 15, 1962.
20. H. R. D. Diffey and D. T. King, The Oxidation of Irradiated Uranium in Carbon Dioxide, British Report AERE-R-3699, September 1961.
21. L. Leibowitz et al., The Kinetics of Oxidation of Uranium Between 125 and 250°C, *J. Electrochem. Soc.*, 108(12): 1155–1160 (December 1961).
22. R. D. Nelson, Transformation Kinetics of Plutonium, Part III, USAEC Report HW-70859, Hanford Atomic Products Operation, December 1961.
23. R. G. Loasly and J. C. Taylor, Hall Effect in Plutonium, *Proc. Phys. Soc. (London)*, 78: 776–777 (Nov. 1, 1961).
24. Hanford Atomic Products Operation, Plutonium Metallurgy Operation Quarterly Progress Report, April, May, June 1961, USAEC Report HW-70312, July 14, 1961. (Classified)
25. Los Alamos Scientific Laboratory, Quarterly Status Report on LAMPRE Program for Period Ending November 20, 1961, USAEC Report LAMS-2647, Dec. 27, 1961.
26. J. F. Eichelberger, Mound Laboratory Monthly Progress Report [on Chemistry] for September 1961, USAEC Report MLM-1119, Mound Laboratory, Sept. 29, 1961.
27. O. J. C. Runnalls, Alloys of Beryllium with Plutonium and the Like, Canadian Patent 615,734, Mar. 7, 1961.
28. R. W. Dayton and C. R. Tipton, Jr., Progress Relating to Civilian Applications During January 1962, USAEC Report BMI-1565(Del.), Battelle Memorial Institute, Feb. 1, 1962.
29. O. J. Wick, Plutonium Metallurgy Operation Quarterly Progress Report, July, August, September 1960, USAEC Report HW-66985, Hanford Atomic Products Operation, Oct. 15, 1960. (Classified)
30. F. W. Albaugh, Reactor and Fuels Research and Development Operation Monthly Report, October 1961, USAEC Report HW-71535A, Hanford Atomic Products Operation, Nov. 15, 1961. (Classified)
31. F. W. Albaugh, Reactor and Fuels Research and Development Operation Monthly Report, September 1961, USAEC Report HW-71222A, Hanford Atomic Products Operation, Oct. 15, 1961. (Classified)
32. D. F. Carroll, The System PuO_2-ZrO_2, USAEC Report HW-69305, Hanford Atomic Products Operation, April 1961.
33. F. W. Albaugh, Reactor Fuels Research and Development Operation Monthly Report, December 1961, USAEC Report HW-72142A, Hanford Atomic Products Operation, Jan. 15, 1962. (Classified)

34. F. W. Albaugh, Reactor and Fuels Research and Development Operation Monthly Report, January 1962, USAEC Report HW-72590A, Hanford Atomic Products Operation, Feb. 15, 1962. (Classified)
35. W. C. Pritchard et al., Compaction and Sintering of PuO_2-Mo Powder Mixtures, USAEC Report LA-2621, Los Alamos Scientific Laboratory, Aug. 23, 1961.
36. R. W. Dayton and C. R. Tipton, Jr., Progress Relating to Civilian Applications During December 1961, USAEC Report BMI-1561, Battelle Memorial Institute, Jan. 1, 1962. (Classified)
37. R. W. Dayton and C. R. Tipton, Jr., Progress Relating to Civilian Applications During January 1962, USAEC Report BMI-1565, Battelle Memorial Institute, Feb. 1, 1962. (Classified)
38. S. J. Paprocki et al., Properties of PuO_2 and PuO_2-ThO_2 Ceramics, USAEC Report APEX-696, General Electric Co., Flight Propulsion Laboratory Dept., July 28, 1961. (Classified)
39. K. H. Puechl, Development of Plutonium-Bearing Fuel Materials, Monthly Progress Letter for January 1962, USAEC Report NUMEC-P-37, Nuclear Materials and Equipment Corp., Feb. 5, 1962.
40. A. J. Darnell and W. A. McCollum, High Temperature Reactions of Thorium and Thoria and the Vapor Pressure of Thoria, USAEC Report NAA-SR-6498, Atomics International, Sept. 15, 1961.
41. D. T. Peterson, Diffusion of Carbon in Thorium, *Trans. Am. Soc. Metals*, 53: 765–773 (1961).
42. Hanford Atomic Products Operation, Fuels Development Operation, Quarterly Progress Report, October, November, December 1960, USAEC Report HW-70355, Jan. 13, 1961. (Classified)
43. Bureau of Mines, Quarterly Metallurgical Progress Report No. 13, October 1, 1961, to December 31, 1961, USAEC Report USBM-U-887.
44. Brookhaven National Laboratory, Annual Report [on Physical Sciences, Engineering, and Life Sciences], USAEC Report BNL-682, July 1, 1961.
45. T. Bishop, Powder Metallurgy in the Nuclear Age, *Metal Progr.*, 81(2): 136–154 (February 1962).
46. R. L. Baer, PM Research and Development Program, Quarterly Progress Report No. 1, April 15–June 30, 1961, USAEC Report MND-MD-2560-1, Martin Co., June 30, 1962.
47. Nuclear Materials and Equipment Corp., Development of Plutonium-Bearing Fuel Materials, Progress Report, October 1–December 31, 1961, USAEC Report NUMEC-P-90.
48. W. A. Jenkins II and H. W. Jacobson, Metal Preparation, Canadian Patent 610,592, Dec. 13, 1960.
49. W. A. Jenkins II and H. W. Jacobson, Production of Refractory Metals, U. S. Patent 3,020,148, Feb. 6, 1962.
50. H. W. Ling, Production of Silicon, U. S. Patent 3,012,861, Dec. 12, 1961.
51. L. Bertrand and C. M. Olson, Silicon Production, U. S. Patent 3,012,867, Dec. 12, 1961.
52. I. E. Campbell and J. H. Oxley, Improvements in or Relating to Chromium Production, British Patent 880,130, Oct. 18, 1961.
53. R. W. Dayton and C. R. Tipton, Jr., Progress Relating to Civilian Applications During December 1961, USAEC Report BMI-1561(Del.), Battelle Memorial Institute, Jan. 1, 1962.
54. General Atomic Div., General Dynamics Corp., 40-Mw(e) Prototype High-Temperature Gas-Cooled Reactor Research and Development Program, Quarterly Progress Report for the Period Ending September 30, 1961, USAEC Report GA-2747, March 1962.
55. General Atomic Div., General Dynamics Corp., Coated Fuel Particle Newsletter, January 1962, USAEC Report GAMD-2646(Pt. 7), February 1962.
56. General Atomic Div., General Dynamics Corp., 40-Mw(e) Prototype High-Temperature Gas-Cooled Reactor Research and Development Program, Quarterly Progress Report for Period Ending June 30, 1961, USAEC Report GA-2493, February 1962.
57. W. V. Goeddel, The Development and Evaluation of Graphite-Matrix Fuel Compacts for the HTGR, USAEC Report GA-2289, General Atomic Div., General Dynamics Corp., Aug. 8, 1961.
58. Oak Ridge National Laboratory, Gas-Cooled Reactor Program Quarterly Progress Report for Period Ending September 30, 1961, USAEC Report ORNL-3210, Feb. 5, 1962.
59. Oak Ridge National Laboratory, Coated Particle Fuel Element Development, Monthly Activity Letter for Period Ending December 15, 1961.
60. General Atomic Div., General Dynamics Corp., Coated Fuel Particle Newsletter, November 1961, USAEC Report GAMD-2646(Pt. 5), December 1961.
61. General Atomic Div., General Dynamics Corp., Coated Fuel Particle Newsletter, October–December 1961, USAEC Report GAMD-2646 (Pt. 6), January 1962.
62. V. K. Trunov et al., Double Oxides in the System Uranium-Tungsten-Oxygen, *Doklady Akad. Nauk S.S.S.R.*, 141(1): 114–116 (1961).
63. V. N. Strekalovskiy and V. G. Vlasov, Kinetics of Reduction of Uranium Trioxide by Hydrogen, *Zhur. Priklad. Khim.*, 34(1): 32–38 (1961).
64. V. G. Vlasov and V. N. Shalaginov, Reduction of Uranium Trioxide by Carbon Monoxide, *Zhur. Priklad. Khim.*, 34(1): 20–27 (1961).
65. V. N. Strekalovskiy and V. G. Vlasov, Reduction of U_3O_8 by Hydrogen, *Zhur. Priklad. Khim.*, 34(1): 38–43 (1961).
66. W. Trzebiatowski and A. Jablonski, Some Phase Relations of BaO-UO_2-O_2 System, *Nukleonika*, 5(10): 588–595 (1960).
67. W. A. Young et al., An X-Ray and Density Study of Nonstoichiometry in Uranium Oxides, USAEC

Report NAA-SR-6765, Atomics International, Mar. 30, 1962.

68. B. E. Murtha and W. P. Chernock, The Development and Testing of the UO_2 Fuel Element System, USAEC Report CEND-141, Combustion Engineering, Inc., June 1961.
69. N. E. Weare et al., Development of Clad Ceramic Fuel Plates by Spray-Coating Techniques, USAEC Report ATL-A-121, Advanced Technology Laboratories, Div. of American-Standard, June 1961.
70. Oak Ridge National Laboratory, Maritime Reactor Program Annual Progress Report for Period Ending November 30, 1961, USAEC Report ORNL-3238, Mar. 9, 1962.
71. S. N. Buckley, The Formation and Properties of Sub-Stoichiometric Uranium Monocarbide, British Report AERE-R-3872, November 1961; to be published in *J. Nuclear Materials.*
72. A. F. Weinberg et al., Investigations of Carbides as Cathodes for Thermionic Space Reactors, Quarterly Progress Report for Period Ending August 31, 1961, Report GA-2548, General Atomic Div., General Dynamics Corp.
73. A. F. Weinberg, Investigations of Carbides as Cathodes for Thermionic Space Reactors, Quarterly Progress Report for Period Ending November 30, 1961, Report GA-2670, General Atomic Div., General Dynamics Corp.
74. E. Gordon, Nuclear Fuel Research Fuel Cycle Development Program Quarterly Progress Report, October 1–December 31, 1961, USAEC Report UNC-3001, United Nuclear Corp., Feb. 1, 1962.
75. A. Accary and R. Lucas, The Effect of Heat Treatment on Uranium Monocarbide and U-UC Cermets, *Mém. sci. rev. mét.*, 58: 383–387 (May 1961).
76. E. D. Cater et al., Uranium Monosulfide, Vaporization, Thermodynamics, and Phase Behavior, *J. Chem. Physics*, 35: 608–618 (August 1961).
77. M. Korchynsky et al., Columbium Alloy Clad Uranium Carbide Fuel Element, USAEC Report ORO-501, Union Carbide Metals Co., Sept. 15, 1961.
78. K. M. Taylor and C. H. Murtry, Synthesis and Fabrication of Refractory Uranium Compounds, Second Quarterly Report for June 1 through August 31, 1961, USAEC Report ORO-477, Carborundum Co., Sept. 15, 1961.
79. Binary Carbide-Metal Systems, Progress Report No. 1, British Report AERE/EMR/PR-1084/1.
80. Binary Carbide-Metal Systems, Progress Report No. 2, British Report AERE/EMR/PR-1084/2.
81. Binary Carbide-Metal Systems, Progress Report No. 3, British Report AERE/EMR/PR-1084/3.
82. Binary Carbide-Metal Systems, Progress Report No. 4, British Report AERE/EMR/PR-1084/4.
83. Binary Carbide-Metal Systems, Progress Report No. 5, British Report AERE/EMR/PR-1084/5.
84. Oak Ridge National Laboratory, Oak Ridge National Laboratory Status and Progress Report, January 1962, USAEC Report ORNL-3256, Feb. 13, 1962.
85. *Reactor Core Materials*, 4(2): 8 (May 1961).
86. M. C. Regan and H. J. Hedger, The Properties of Uranium Monocarbide Fabricated by Direct Reaction of the Elemental Powders, British Report AERE-R-3802, August 1961.
87. M. C. Regan and J. Williams, The Sintering of Uranium-Carbon-Iron Alloys in the Presence of a Liquid Phase, *Powder Met.*, (8): 128–144 (1961).
88. Argonne National Laboratory, Reactor Development Program Progress Report, January 1962, USAEC Report ANL-6509, Feb. 15, 1962.
89. R. S. Barnes, Atomic Displacement and Impurity Effects in Fissile Metals, British Report AERE-R-3821, September 1961; to be published in *Nuovo cimento.*
90. T. K. Bierlein et al., Swelling in Uranium: A Comparison of the Effects of Irradiation and Postirradiation Annealing, USAEC Report HW-69393, Hanford Atomic Products Operation, April 1961.
91. Reference canceled.
92. W. Uhlmann, Radiation Effects on Solid, Uranium Based Nuclear Fuel Materials. Appendix to Part VDIT-16.1, A Bibliography, Swedish Report VDIT-16.1a, November 1961.

Section II

Reactor Materials

Moderator Materials

Beryllium Metal and Alloys

Although the not wholly unexpected announcement was made that stainless steel will replace beryllium as a canning material in the British AGR reactor,[1-3] research on beryllium continues apace on both sides of the Atlantic. Strenuous efforts are being made toward the solution of the following problems:[3]

1. Unsatisfactory mechanical properties, particularly the lack of ductility at room temperature, resulting in elongations of less than 2 per cent
2. Possible lack of corrosion resistance to conventional reactor coolants
3. Susceptibility to radiation damage
4. High cost and toxicity
5. Lack of satisfactory fabrication methods

Production

Industrial development of a method for producing beryllium by chlorination of beryllium oxide with CCl_4, followed by electrolysis of the resulting $BeCl_2$ with NaCl, was reported in a Russian article.[4] After chlorination at 650 to 700°C and electrolysis in a nickel crucible with a graphite anode, large crystals which contained 99.966 per cent beryllium and smaller crystals which contained 99.937 per cent beryllium were produced. The yield, including treatment of the residues, was 96 per cent, and the current efficiency was more than 80 per cent. Several tons of high-purity material for nuclear applications was produced.

An Italian patent[5] claims beryllium or alloys of beryllium can be reduced from BeF_2 (free of oxide) or alkaline fluoberyllates (e.g., $2NaF \cdot BeF_2$, also free of oxide) quantitatively by reduction with magnesium or an alkaline-earth metal in the presence of calcium fluoride. The calcium fluoride prevents the formation of metallic sodium. The process can be carried out in a high-frequency induction furnace or other melting furnace. No excess of reactants is used. Numerous economic advantages are pointed out.

Beryllium Casting and Purification

Sound, crack-free beryllium ingots with a nominal diameter of 3 in. have been produced by the use of a thermal-gradient casting technique.[6] The beryllium was melted under vacuum and bottom poured into a graphite mold with a hot top and cold bottom. During solidification the dendrites form at the mold wall and grow inward and upward toward the hot top.

Beryllium (from the Beryllium Corporation), zone refined five passes at the Franklin Institute, was analyzed by a double-focusing mass spectrometer. The analyses indicate relatively large amounts (approximately 200 ppm) of carbon and oxygen, about 50 ppm of iron, nickel, and BeH, 10 ppm of copper, and less than 10 ppm of silicon, calcium, sulfur, and nitrogen in the zone-refined metal. For most impurities in beryllium, the detection limit at optimum exposure is about 10 ppb. The mass-spectrographic technique[7a] also indicates the presence of compounds such as BeH, BeO, and Be_2O.

Beryllium Fabrication

Recent work by the British[8] has shown that sound, crack-free beryllium ingots can be cast in sizes up to 6 in. square by 3 in. thick, consistently. These can be jacketed and rolled directly to sheet, which is claimed to have a markedly superior formability to that produced from powder. Texture measurements indicate that the basal-plane population is between 2

and 4 times random at the maximum point, compared with 12 and 20 normally exhibited by powder sheet. A large economic advantage is claimed for the casting route.

Meanwhile, Wyman-Gordon Company reports[7b,9] that improved properties result from direct forging of beryllium powder in metal cans. Pressures ranging from 20,000 to 100,000 psi and sintering times of 1 sec to 1 min were used. Properties of forgings made at 1600°F were always superior to those made at 1900°F. In the past two years, cost reductions for finished beryllium parts of 50 per cent were claimed to have been effected by forging.

Ladish[7c] reported that beryllium forged from hot-pressed block or shaped powder-metallurgy preforms has 100 per cent of theoretical density and complete leaktightness against helium. Properties are shown in Table II-1. Preliminary creep-rupture results showed 0.240 per cent total creep, without failure, at a stress level of 2500 psi at 1200°F over a 75-hr period. Forging now is second only to machining from hot-pressed blocks as a method of making beryllium parts.

Table II-1 HOT-PRESSED AND UPSET-FORGED BERYLLIUM[7c]

Forging temp., °F	Test temp., °F	Yield strength, psi	Ultimate strength, psi	Elongation in 1 in., %	Reduction of area, %
1300	80	48,500	78,600	13.5	14.2
1375	80	50,500	81,700	9.7	13.7
1450	80	42,500	77,000	16.0	14.0
1300	800	30,800	32,300	21.6	48.4
1375	800	31,400	31,400	13.7	56.1
1450	800	27,700	31,200	30.8	63.1

Northrop[10] reports success in the extrusion of channels up to 39 ft long and 0.06 in. thick, using the process developed by Nuclear Metals, Inc., to extrude finned beryllium tubing. Tolerance on channels 24 ft long by 0.125 in. thick was held to 0.003 in. After extrusion and heat-treatment at 750°F for 1 hr, the tensile strength was 100,700 psi and the elongation was 7 per cent.

A British patent[11] claims that good ductility at right angles to the extrusion direction can be obtained in beryllium tubing reextruded from extruded beryllium rod. A hole is drilled in the rod, which is then reextruded with a reduction in area of not more than 15 : 1.

The feasibility of using the isostatic-forming process to fabricate beryllium parts was demonstrated by Sylcor.[12] A cylindrical tube with a closed hemispherical end and another with a funnel section were produced with properties equivalent to those of conventional hot-pressed material. This process is believed to offer economic advantages for complex shapes, although it probably could not compete for simpler ones.

Stevens Institute reported[13] on the production of beryllium military components by slip casting. The techniques used are commonly employed in the ceramic industry. Minus-325-mesh beryllium powder was slip cast, using a 0.5 per cent solution of Kelcosol (an alginate) in distilled water as the binder. It is possible to sinter slip-cast parts to 98 per cent or better of theoretical density. The sintered parts can be hot-extruded or used as preforms for hot or warm forging. High shrinkage on drying makes control of as-sintered dimensions difficult.

Brush Beryllium Company[14,15] has made high-strength beryllium wire with diameters down to 0.0047 in. by drawing at about 800°F; diamond dies and solid-film lubricants were used. This wire had a tensile strength of 190,000 psi, a yield strength of 160,000 psi, an elongation of 0.5 to 1.5 per cent, and a reduction in area of 10 per cent. It was suggested that it may prove useful for making wrapped, high-strength structures or for electrical applications where weight is the prime consideration.

Oak Ridge reported[16] preliminary test results which indicate that the tungsten-arc-welding process yields stronger joints than the electron-beam process. Tubes that were arc-welded at one end remained leaktight to helium after 500 cycles between 380 and 1380°F.

MacPherson and Beaver[17] found that the major factor in attaining quality fusion welds in beryllium by the TIG process appears to be the maintenance of a proper thermal equilibrium in the weld zone. The most critical variable is the amperage, which should be as low as possible. Uncoated, drawn beryllium wire was the best filler material found.

Lawrence Radiation Laboratory continues to prefer braze-welding techniques where the temperature of application permits. Marcellin[18] noted that braze welding by either the MIG or

TIG process avoids the brittle weld structure which is characteristic of fusion welding. The MIG process is faster and more economical, but the TIG process can provide crack-free weldments on difficult jobs where the former fails. Procedures are described for using 12 or 5 per cent silicon-aluminum alloys and 99.9 per cent pure silver as the braze material. When the TIG process is used, the joints are "prebuttered." Joint strengths of 18,000 to 24,000 psi are attained on metal-arc and manual tungsten-arc braze welds. Direct-current, tungsten-arc, prebuttered lap, or T-section joints reach an ultimate shear strength of 25,000 psi, whereas 29,500 psi is typical when alternating current is used.

Physical Metallurgy of Beryllium

Bennett,[19] on the basis of the narrow temperature range for the ductile-to-brittle transition and the double yield point that is often noted (both interpreted in terms of Cottrell locking theories), predicted that the ductile range for beryllium may be extended to room temperature by a combination of grain refinement, increased purity, and reduction of the strain rate.

The solubility of hydrogen in beryllium is found to be negligibly small. Therefore hydrogen does not affect the ductile-to-brittle transition temperatures.[7d]

Bastien and Pointu[20] were able to determine the glide elements responsible for the asterisms in Laue photographs of hexagonal metals. Two new modes of deformation, active at high temperatures, were found in beryllium that had a component of glide along the hexagonal axis. These were $(10\bar{1}1)$ $[\bar{1}101]$ and $(10\bar{1}0)$ $[\bar{1}2\bar{1}3]$, active at 800 and 1000°C.

Hill[21] reported that basal-plane alignment in an extruded finned tube is nearly the same regardless of whether it was extruded from a randomly oriented hot-pressed beryllium billet or from a highly oriented hot-extruded beryllium rod. The final texture depends only on the amount of reduction during the final extrusion.

The second year's work at Nuclear Metals, Inc., on beta-phase beryllium alloys disclosed no alloy in which the beta could be retained at as low a temperature as the beryllium–8 at.% nickel alloy discovered earlier. With cooling rates of up to 60,000°C/sec, the transformation temperature in this alloy was lowered to 242°C. The nickel alloy is extremely brittle at room temperature but showed 20 per cent reduction of area at 1070°C (compared with 0 per cent for unalloyed beryllium).[22]

Fine-grained, equiaxed beryllium sheet has been produced by warm-rolling (at 200 to 500°C) cast billets of Pechiney flake beryllium which had previously been hot rolled to 0.070-in.-thick sheet with a uniform grain size of 85 μ. The rerolled specimens could be completely recrystallized by thrusting them into a hot vacuum furnace for 30 sec. Best results were obtained on a material that had been reduced 54 per cent at 400°C, recrystallized to 40-μ grain size, rerolled 40 per cent at 400°C to 0.22 in., and again recrystallized. The relation between grain size and tensile properties[7e] is shown in Table II-2.

Table II-2 RELATION BETWEEN THE GRAIN SIZE OF SHEET ROLLED FROM VACUUM-CAST ELECTROLYTIC FLAKE BERYLLIUM AND ITS TENSILE PROPERTIES[7e]

Grain size, μ	Ultimate tensile strength, psi	Limit of proportionality, psi	1% proof stress, psi	Elongation, %
30	64,200	28,300	45,700	12.5
42	64,900	35,900	54,700	5.3
60	49,300	33,100	47,500	2.3

Properties of Beryllium

The enthalpy and specific heat of beryllium were determined by Kantor et al.[23] at temperatures said to be higher than any reported previously. They reported the following equations:

1. From 600 to 1560°K

$$H_T - H_{298.16} = 4.322T + 1.09 \times 10^{-3}T^2 - 1490 \text{ cal/g-atom}$$

$$C_p = 4.322 + 2.18 \times 10^{-3}T \text{ cal/(°C)(g-atom)}$$

2. From 1560 to 2200°K

$$H_T - H_{298.16} = 6.079T + 2.569 \times 10^{-4}T^2 + 1327 \text{ cal/g-atom}$$

$$C_p = 6.079 + 5.138 \times 10^{-4}T \text{ cal/(°C)(g-atom)}$$

The melting point of beryllium was found to be 1560 ± 5°K, which agrees well with Losana's 1557 ± 5°K. The heat of fusion was determined to be about 3520 cal/g-atom.

The stress-rupture behavior of beryllium was investigated in the range 400 to 650°C with test durations up to 10,000 hr. Virtually no difference was found in the second-stage creep rates of specimens taken longitudinally and transverse to the pressing direction. Some test results[7f] are shown in Table II-3.

Table II-3 CREEP RUPTURE OF HOT-PRESSED BERYLLIUM[7f] AT 600°C

Stress, psi	Specimen orientation	Time to rupture, hr	Ductility at failure, %	Secondary creep rate, %/hr
2000	Longitudinal	2077	0.67	1.9×10^{-4}
2000	Transverse	2193	1.52	3.2×10^{-4}
2185	Longitudinal	567	0.67	7.1×10^{-4}
2185	Transverse	2058	1.90	6.7×10^{-4}
2470	Longitudinal	228	1.24	2.2×10^{-3}
2470	Transverse	287	0.83	2.1×10^{-3}
2280	Longitudinal	410	1.42	10.9×10^{-4}
2280	Transverse	844	1.16	9.5×10^{-4}

Corrosion and Irradiation Behavior of Beryllium

Although the British do not consider the behavior of beryllium in CO_2 at 600°C and above satisfactory at the present time, since they have decided to use stainless-steel-clad fuel elements in the Advanced Gas-Cooled Reactor (AGR),[24] research in this field continues to be active. The results obtained by different laboratories (references 7*g*, 7*h*, 16, 25, and 26) vary in detail but agree that a "breakaway" type of rapidly accelerating reaction does occur at some temperature above 600°C after an inhibition period of varying length. Smith et al.[7g] reported that the reaction could be effectively inhibited by oxidizing the beryllium powder in oxygen at elevated temperatures before consolidating it to form tube or sheet. Werner and Inouye[7h] found that the breakaway reaction occurred in wet CO_2 after 60 to 70 hr at 725°C. The products of reaction with water vapor are BeO, H_2, and CH_4 [from reaction of the water vapor with Be_2C (the latter being formed by the reaction of wet CO_2 with beryllium)]. Werner[16] noted a breakaway reaction on Brush tubing in wet helium and wet CO_2 at 650°C after about 50 hr but found none on Pechiney-flake tubing after exposures up to 200 hr. Gregg et al.[25] reported that, in the reaction of beryllium in moist CO_2, the reaction with water vapor predominates over that with CO_2 in proportion of approximately 4:1. They found the oxidation protective to 600°C and nonprotective at 650°C and above. In mixtures of moist CO and CO_2, the CO has little effect on the reactions. Higgins and Antill[26] found that protective films were formed on beryllium in dry CO_2 at temperatures up to 850°C and times up to 10,000 hr, but the breakaway reaction occurred at 1000°C after a 15-hr exposure. In CO_2 that contained 3 per cent water vapor, the breakaway reaction occurred at 700°C.

Higgins and Antill probably pointed to the reason for these widely varying results. They found that the linear rate of attack, after the breakaway, could vary by as much as a factor of 1000 between different batches of metal. The differences in linear rates of attack for wet gas seemed to be related, not to impurity content but to an intergranular network of oxide in certain batches. The behavior of beryllium in dry CO_2 also varied with the method of fabrication. Their most and least corrosion-resistant specimens were both French-flake material.

Steele[27] reported that of six vacuum-deposited coatings on beryllium, including silver, titanium, aluminum, zirconium, nickel, and silicon monoxide, tested in accordance with MIL-E-5272B, Section 4·4·1 Humidity Test, Procedure 1, the only samples resisting corrosion were hot-pressed and sheet specimens coated with silicon monoxide and sheet coated with zirconium. Similar specimens were held at 1600°F in an oxidizing (air) atmosphere for 20 hr. The lowest weight gains (less than one-fifth of those of unprotected beryllium) were found on the specimens coated with silicon monoxide and with titanium.

Vickers[7i] reported on the compatibility of beryllium with various metals and refractories that could be found in a reactor; he used annealing times of up to 2000 hr. A condensation of some of his results is shown in Tables II-4 and II-5. Chromium plate, Al_2O_3 spray, ZrO spray, SiC spray, or WC spray on either mild or stainless steel made these materials compatible with beryllium at 600°C in CO_2.

Levy[28] determined the anodic and cathodic behavior of beryllium in a number of unstirred aqueous electrolytes at 22°C with current densities in the range of 10^{-7} to 10^{-2} amp/cm^2. CrO_4 and PO_4 ions induced considerable anodic po-

larization. Na_2CrO_4 was an effective cathodic polarizer over a broad range of current densities. Beryllium was activated and attacked preferentially in the presence of chlorine, ClO_3, fluorine, and SO_4 ions.

Weir[16] obtained swelling data for beryllium irradiated to a neutron dose of 3.6×10^{20} neutrons/cm^2 (<1-Mev); he used specimens of various compositions, manufactured by various techniques. His results are summarized in Fig. II-1.

Beryllium is a reactor material that forms gas within the metal lattice under irradiation. The volume of helium formed is sufficient to destroy the structural properties under certain conditions. At low temperatures (500°C or below) the problem is not serious, but in the 700°C range and above, larger bubbles accumulate by diffusion, and swelling will take place up to a 30 vol.% increase[3,29] at 1000°C. The threshold for damage[30] is around 10^{19} nvt (fast). Oak

Table II-4 COMPATIBILITY OF BERYLLIUM WITH METALS[71]

	Condition			
	In vacuum		In dry CO_2	
Material	At 600°C	At 550°C	At 600°C	At 550°C
Alumel	Incompatible	Incompatible	Incompatible	Incompatible
Chromel	Incompatible	Incompatible	Incompatible	Incompatible
Copper	Incompatible			
Mild steel	Incompatible	Incompatible	Incompatible	Incompatible
Molybdenum	Compatible		Probably compatible	
Nickel	Incompatible		Incompatible	
Niobium	Compatible			
Stainless steel	Incompatible	Incompatible	Incompatible	Incompatible
Tantalum	Compatible			
Titanium	Compatible		Compatible	
Tungsten	Compatible		Compatible	
Uranium	Incompatible			
Zirconium	Incompatible			
Zirconium alloy	Compatible	Compatible		Compatible
Nimonic 75		Incompatible	Incompatible	Incompatible

Table II-5 COMPATIBILITY OF BERYLLIUM WITH REFRACTORY OXIDES[71]

Oxide	Temp., °C	Atmosphere	Remarks
Sintered alumina	550	Vacuum	Compatible
Sintered alumina	600	Vacuum	Compatible
Alumina powder	550	Vacuum	Incompatible
Alumina powder	600	Vacuum	Incompatible
Sintered magnesia	550	Vacuum	Compatible
Sintered magnesia	600	Vacuum	Compatible
Fused silica	600	Vacuum	Incompatible
Sintered zirconia	550	Vacuum	Compatible
Sintered zirconia	600	Vacuum	Incompatible
Powdered zirconia	550	Vacuum	Incompatible
Powdered zirconia	600	Vacuum	Incompatible
Thermoflex on clean beryllium, no pressure	600	CO_2	Compatible
Thermoflex on clean beryllium, heavy pressure	600	CO_2	Incompatible
Thermoflex on preoxidized beryllium, heavy pressure	600	CO_2	Compatible

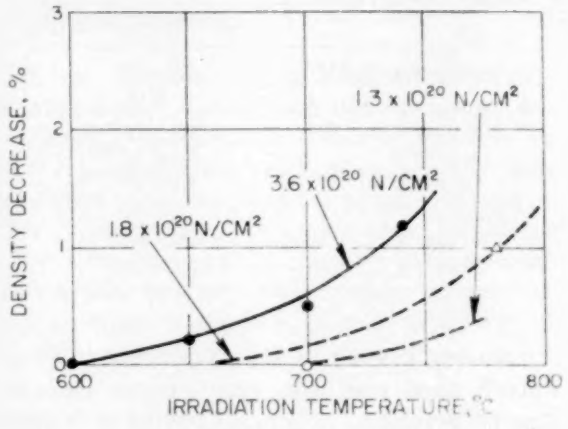

Fig. II-1 Swelling of beryllium under irradiation at elevated temperatures.[16]

Ridge[16,31] has reported that strengths of beryllium are reduced by about 2000 psi at 600°C by irradiation to 3.6×10^{20} nvt. (W. Hodge)

Beryllium Compounds

Beryllium Oxide

Investigators at Harwell,[32] who are studying BeO with a high-temperature X-ray diffractometer, report evidence of a new phase appearing at 2080 ± 50°C. The transformation was reversible, and the structure of the BeO reverted to the usual hexagonal on cooling to the range of 1980 ± 50°C. The new phase was reported to have pronounced cubic characteristics. Similar observations have been made at Atomics International and at Livermore. Detailed structural analyses of the high-temperature phase are being pursued at Harwell, Atomics International, and Livermore.

An Oak Ridge report[33] describes attempts to synthesize a stable, cubic modification of BeO. The impetus for this work appears to be the desire to combine the nuclear and thermal properties of BeO with the radiation stability of a cubic lattice. Binary mixtures of BeO with Al_2O_3, CaO, Li_2O, MgO, Sc_2O_3, TiO_2, or ZrO_2 were heated at temperatures exceeding 2050°C in an attempt to induce a phase transformation in the BeO. No evidence of cubic material was observed by microscopic and X-ray diffraction analyses.

Work on BeO single crystals is continuing at Atomics International. Studies of impurities in the crystals showed that ions of magnesium, calcium, and the transition elements in limited concentrations have little effect on the quality of the crystals. Small cations such as silicon and boron seemed actually beneficial in minimizing macroinclusions in the BeO crystals. The investigators speculated that the character of the original nucleus or seed crystal may control the character of the final crystal; exploratory experiments are being made in this area. Russian investigators Budnikov and Shishkov[34] have reported BeO single crystals that were apparently grown by a vaporization-condensation mechanism. The author heated "semicrystalline" BeO for 10 hr at temperatures of 1600 to 1900°C. The BeO was contained in closed graphite crucibles, and the ambient atmosphere was argon of unspecified moisture content. The crystals, which were about 5 mm, were reported to have formed as platelets, rods, and whiskers on the underside of the graphite lid, which was cooler than the sample by 10 to 50°C. The observers speculated some on the mechanism of crystal growth, the crystal habit, and axial orientation. It was concluded that the method described could be very promising if means of accelerating and regulating the growth could be found.

Investigators at General Electric[35] have described a process for making readily sinterable BeO powder and have written specifications on both the process and the product. The process consists of treating high-purity $Be(OH)_2$ with acetic acid to form beryllium basic acetate. This is then hydrolyzed to re-form $Be(OH)_2$. The hydroxide is calcined on a rather complex schedule to yield BeO. The BeO particles are reported to be spherical and very closely sized in the range of 0.1 μ. Typical analyses indicated less than 500 ppm of total impurities. Few sintered-density data were given.

Reprocessing of sintered $BeO-UO_2$ fuel-element bodies is often a problem owing to the chemically stable nature of BeO. Studies by Union Carbide[36] on fluxing and dissolution of $BeO-UO_2$ specimens were reported. Bodies of unspecified density and composition were fused for 1 hr at 650°C in seven times their weight of Na_2O_2. The residue from this treatment was completely soluble in dilute HNO_3. The effectiveness of the Na_2O_2 flux was extremely sensitive to temperature of fusion. Temperature deviations in either direction from 650°C less-

ened appreciably the solubility of the residue in HNO_3. An alternative flux is potassium pyrosulfate ($K_2S_2O_7$). Pellets treated at 800°C for 2 hr in 20 times their weight of $K_2S_2O_7$ also produced HNO_3-soluble residues.

Investigators at Atomics International[37] report that single-crystal tungsten can be machined very readily to form crucibles. BeO melts in these crucibles showed no signs of reaction with or adherence to the crucibles at temperatures up to 2350°C. Single-crystal tungsten was reported to be far superior to TaC in this respect. Fused-cast BeO, uncontaminated by the container, is suggested as another form of BeO for study.

Clarke,[38] at Harwell, has reviewed the literature through 1961 on the behavior of BeO under neutron irradiation. The following facts have emerged: The property changes in BeO irradiated at less than 100°C are remarkably consistent, regardless of the starting materials and conditions of fabrication and irradiation. A temperature increase of a few hundred degrees reduces the magnitude of the property changes. The nature of the radiation effects probably depends on the total exposure of the specimen. Point defects appear to predominate at exposures less than 5×10^{19} nvt (>1 Mev). These defects tend to agglomerate at higher exposures. Disintegration of a specimen may occur either by cracking or by powdering. Powdering is associated with high specimen density and low irradiation temperature. Cracking is much more complex and seems to involve thermal stresses, anisotropic growth, specimen density, gas production by nuclear transmutation, etc. BeO specimens have withstood exposures up to 3×10^{21} nvt (>1 Mev). However, the factors that allow one specimen to remain intact while another cracks up have not yet been defined.

(A. K. Smalley)

Other Beryllium Compounds

Brush Beryllium Company[39] conducted oxidation tests on Ta_2Be_{17} in dry, CO_2-free air. The following results were obtained:

1. 100 hr at 1300°F gave 0.01-mil penetration.
2. 100 hr at 1600°F gave 0.05-mil penetration.
3. 10 hr at 3000°F gave 3.05-mil penetration.

The following vapor-pressure measurements were obtained for beryllium, Ta_2Be_{17}, and Zr_2Be_{17}:

	Vapor pressure, mm
Beryllium at 2300°F	7.5×10^{-3}
Ta_2Be_{17}:	
At 2300°F	1.7×10^{-3}
At 2400°F	5.6×10^{-3}
At 2500°F	5.2×10^{-3}
Zr_2Be_{17}:	
At 2300°F	1.4×10^{-3}
At 2500°F	11.3×10^{-3}

Sintering studies of $(Th_{19}U)O_2$-$ThBe_{13}$ at Oak Ridge[40] have met with only limited success. Cracks developed in compacts of 40 wt.% oxide due to gas evolution from the as-received powders when they were fired at 1550°C. Microstructures show voids around the oxide particles as well as microcracks. Gas evolution from as-received powders has cropped up in studies of the niobium and zirconium beryllides at several sites.

(R. W. Getz)

Solid Hydrides

Studies of several metal hydrides at General Electric[41] have demonstrated the superior hydrogen retention of yttrium hydride at high temperature. The hydrogen content of yttrium, cerium, calcium, and zirconium hydrides as a function of temperature is shown in Fig. II-2.

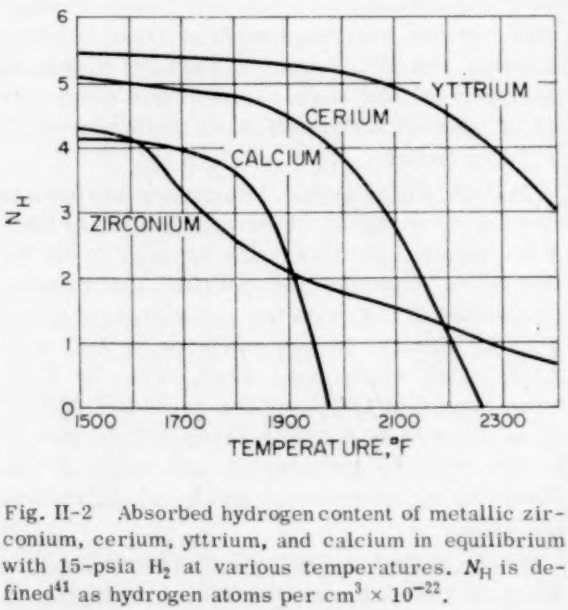

Fig. II-2 Absorbed hydrogen content of metallic zirconium, cerium, yttrium, and calcium in equilibrium with 15-psia H_2 at various temperatures. N_H is defined[41] as hydrogen atoms per $cm^3 \times 10^{-22}$.

Zirconium Hydride

X-ray diffraction data obtained at Atomics International[42] have shown that, at room temperature, the range of coexistence of the face-centered cubic delta phase and the face-centered tetragonal epsilon phase lies between $ZrH_{1.64}$ and $ZrH_{1.73}$ compositions. An earlier report,[43] based on less-complete data, had indicated that the two-phase region covered the composition range $ZrH_{1.57}$ to $ZrH_{1.76}$, but apparently the region is not that broad.

Yttrium Hydride

Physical-property data on yttrium hydride have been reported by General Electric[41] from studies made in several laboratories. The solubility relations in the yttrium-hydrogen system are shown in Fig. II-3, which was established

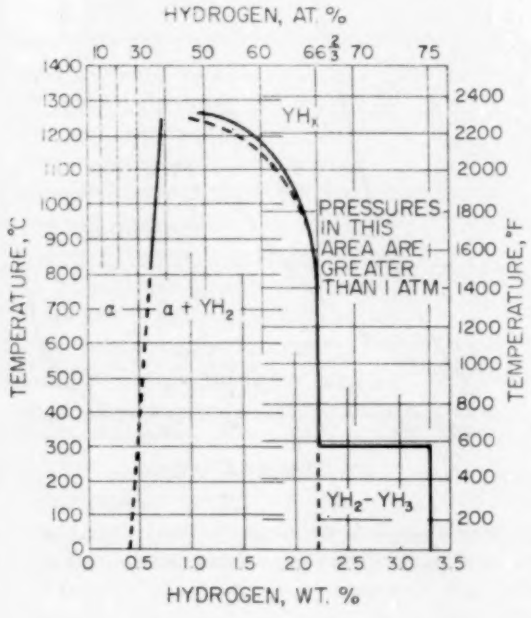

Fig. II-3 Schematic diagram of solubility relations in yttrium-hydrogen system (pressure is not constant).[41]

from equilibrium hydriding isotherms, metallography, and X-ray diffraction data. The pressure-composition isotherms for the system from 1475 to 2375°F are presented in Fig. II-4. Measurements of electrical resistivity for yttrium hydride show that the initial absorption of hydrogen increases the resistance sharply, as indicated in Fig. II-5. The dotted line in the figure is drawn because of the uncertainty of the maxima. An earlier publication[44] showed that the resistivity decreased gradually from that of the metal to about 20 μohm-cm at YH_2, an error that resulted from incomplete data at low hydrogen concentrations. The dynamic modulus of elasticity of yttrium metal is compared

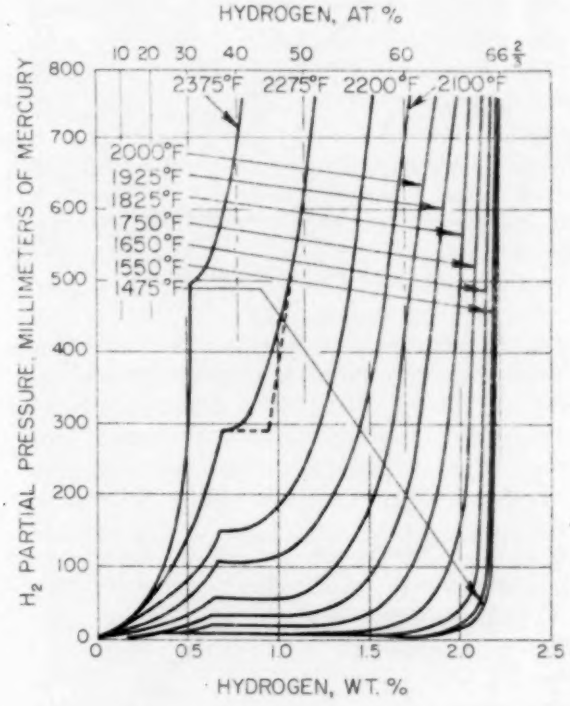

Fig. II-4 Tentative equilibrium pressure-composition isotherms in the yttrium-hydrogen system.[41]

with that of $YH_{1.5}$ in Fig. II-6. Some loss of hydrogen occurred above 1200°F, and the dotted line is an empirical correction for this loss. The hardness of yttrium hydride at room temperature as a function of hydrogen content is shown in Fig. II-7. The inflection point in the curve occurs at a composition approximating the solubility limit of hydrogen in yttrium. There was a good deal of scatter in the data, and the curve shown represents an average. The exceptional compressive strength of yttrium hydride at high temperature is shown in Fig. II-8, where it is compared with two types of stainless steel over the temperature range 1500 to 2100°F.

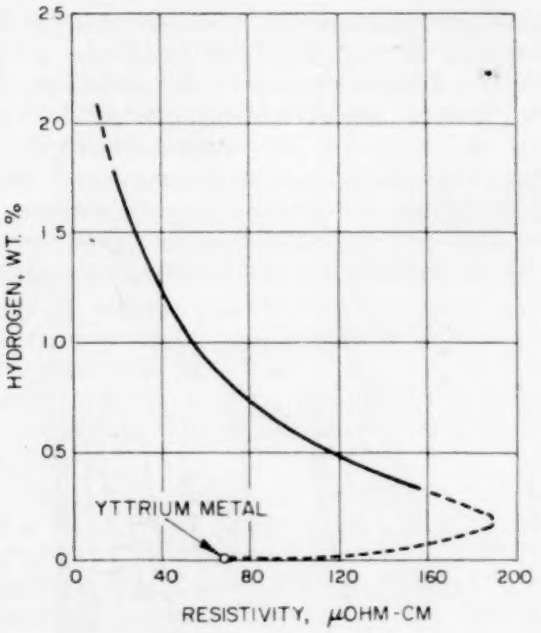

Fig. II-5 Electrical resistivity of yttrium at room temperature as a function of hydrogen content.[41]

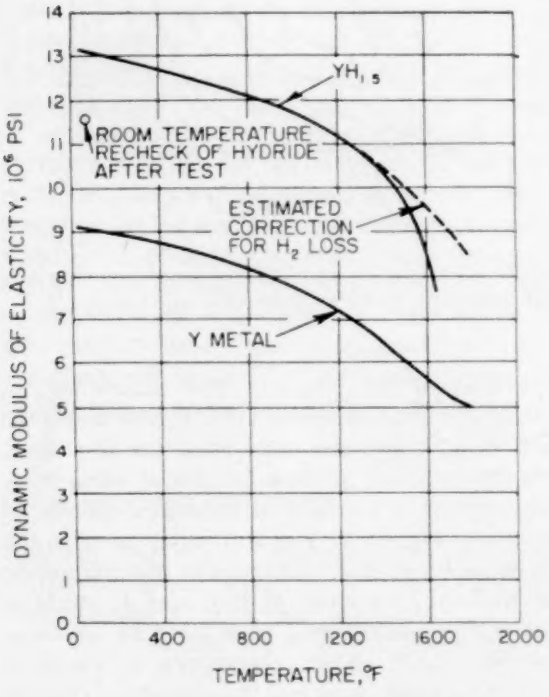

Fig. II-6 Dynamic modulus of elasticity of yttrium and a massive hydrided yttrium as a function of temperature.[41]

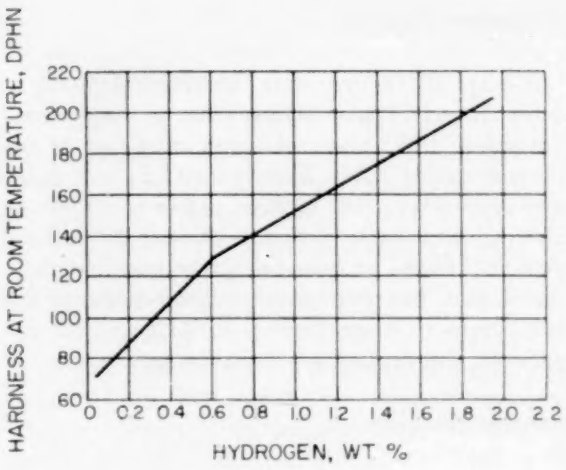

Fig. II-7 Hardness of hydrided yttrium vs. hydrogen content.[41]

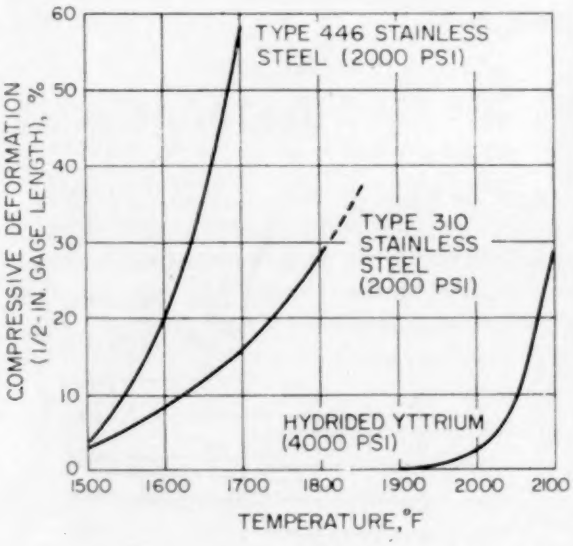
COMPRESSIVE DEFORMATION (1/2-IN. GAGE LENGTH), %
TEMPERATURE, °F
TYPE 446 STAINLESS STEEL (2000 PSI)
TYPE 310 STAINLESS STEEL (2000 PSI)
HYDRIDED YTTRIUM (4000 PSI)

Fig. II-8 Compressive strength of hydrided yttrium[41] as a function of temperature under load for 100 hr.

Alloy Hydrides

Investigation of moderator materials at General Electric[45,46] has shown that hydrided 95 wt.% yttrium–5 wt.% chromium alloy, clad with 75.5 wt.% iron–20 wt.% chromium–4.5 wt.% aluminum, will withstand exposure to air at 1000°C for long periods with no measurable loss of hydrogen. A nondestructive method of testing for hydrogen content, based on neutron scattering, has been developed. Testing in both static and dynamic air of the clad moderator

assemblies showed good thermal-mechanical stability for periods in excess of 1000 hr.

(H. H. Krause)

Graphite

The oxidation of reactor-grade graphites in air, in the temperature range 450 to 750°C, differs considerably with their source of manufacture and the treatment they have received. Recently published research[47] has provided additional information as to the role of impurities in such oxidation behavior, particularly with respect to pitting susceptibility.

The relation between pitting oxidation and impurity localization in graphite was clarified by autoradiography. After neutron activation, a definite coincidence was observed between the position of sodium, as indicated by the autoradiographs, and pits developed by subsequent oxidation. Although the rate of loss was not directly related to the concentration of sodium, there was a strict relation between sodium concentration and tendency to form pits. To clarify the possibility that sodium might behave as a "tracer" associated with various impurities at certain positions in graphite, micro samples of graphite were taken both in and outside the areas of spots shown by autoradiographs. Spectrographic analysis showed that practically all the impurities found were concentrated in the areas of the radiographic spots.

To study their effects on oxidation, these specific impurities were added by aqueous impregnation to graphite samples previously purified by heating to temperatures greater than 3000°C in inert atmospheres, which reduced impurities to traces of iron, copper, or silica detectable by spectrography. Among the impurity elements examined, copper, vanadium, iron, and sodium markedly increased the rate of oxidation of the treated samples. Sodium had a great effect only when present with vanadium, either alone or associated with other elements. Magnesium, calcium, and titanium had little effect.

Limited efforts were made to determine why impurities which are originally diffused in the base coke become localized in the graphite and at what point in the manufacture they become localized. The results indicate that localization appears in synthetic mixtures of pitch, coal, and petroleum after they have been heated to 2000°C. When graphite that was free of sodium but contained vanadium was placed in an atmosphere of NaF at 1000°C, the sodium seemed to become fixed. It therefore appears that this element might collect at positions already containing vanadium during the manufacturing stage; at this stage the temperature drops to 1000°C.

It has been long recognized that the strength of graphites increases significantly with increasing temperature to a maximum at about 2400°C, but the mechanisms of this strength behavior are not clearly understood. Limited data have previously been published which showed that absorbed gases can have a significant effect on graphite strength. Recently published data[48] provide additional evidence to support the belief that gas desorption at elevated temperatures is an important factor affecting high-temperature strength of graphites. Experiments were performed in a vacuum furnace which was capable of maintaining a vacuum of 10^{-5} mm Hg when cold and 10^{-4} mm Hg at 2100°C. When specimens were maintained in vacuum throughout the steps of heating to elevated temperature, cooling to room temperature, and testing, they were nearly as strong as if they had been tested at the elevated temperature. If the experiment was repeated except that air was admitted to the outgassed- and -cooled specimen before final testing, the strength was reduced to roughly the same value as was originally observed before heating the graphite.

Because graphite behaves predominantly as a brittle material, it has been impossible with available test equipment to obtain truly uniaxial-tensile-strength data even at room temperature and particularly at elevated temperatures. Now, Southern Research Institute[49] has developed test equipment that promises to resolve this problem, thus providing more precise tensile data for structural design with graphite. Through the use of "frictionless" gas bearings, these researchers claim to achieve almost perfect uniaxial tension in test specimens. Limited test data have been obtained up to 5000°F using these test facilities, and the data indicate significant reduction in data scatter and higher strengths than previously reported for the particular graphites tested. (M. C. Brockway)

References

1. Stainless Steel Will Replace Beryllium, *Metalworking Production*, 106(5): 5 (Jan. 31, 1962).

2. Beryllium Out, D_2O In, *Nuclear Eng.*, 7(70): 83 (March 1962).
3. *Power Reactor Technol.*, 5(2): 48–50 (March 1962).
4. L. Ye. Vil'komirskiy et al., Production of High Purity Beryllium by the Chloride Method, *At. Energy (U. S. S. R.)*, 11(3): 233–239 (September 1961) (in Russian).
5. Fabrication Procedure for Beryllium or Beryllium Alloys (in French), French Translation CEA-tr-X-258 (translated from Italian Patent 350,669), Dec. 12, 1960.
6. B. H. Hessler and J. P. Denny, Beryllium Casting, Report NP-11072, Beryllium Corp., July 5, 1961, to Nov. 10, 1961.
7. Preprints of papers presented at the Institute of Metals Conference on the Metallurgy of Beryllium, London, Oct. 16–18, 1961.
   a. G. D. Perkins and R. K. Willardson, Impurities in Zone-Refined Beryllium.
   b. M. E. Cieslicki, Beryllium Forging.
   c. A. F. Hayes and J. A. Yoblin, New Concepts for Fabricating Beryllium Through Advanced Forging and Powder Metallurgy Techniques.
   d. P. Cotterill et al., An Evaluation of the Hydrogen Content of Commercially Pure Beryllium and Its Effect upon the Ductile-to-Brittle Transition Temperature.
   e. C. I. Bort and A. Moore, Grain Refinement of Ingot Sheet Beryllium by Warm Working and Annealing.
   f. W. D. G. Bennett and G. Sumner, Some Creep and Stress Rupture Properties of Sintered and Extruded Beryllium.
   g. R. Smith et al., Inhibition of Breakaway Oxidation of Beryllium in Carbon Dioxide.
   h. W. J. Werner and H. Inouye, The Reactions of Beryllium with Wet Carbon Dioxide.
   i. W. Vickers, Compatibility of Beryllium with Various Reactor Materials.
8. Advances in Forming Beryllium Sheet, *Nuclear Power*, 7(71): 46 (March 1962).
9. M. E. Cieslicki, Forging Beryllium Powder, *J. Metals*, 14(2): 149–153 (February 1962).
10. Extrude Longer Beryllium Shapes, *Iron Age*, 189(8): 99 (Feb. 22, 1962).
11. W. Munro and N. A. Hill, Improvements in or Relating to the Fabrication of Beryllium, British Patent 884,108, Dec. 6, 1961.
12. J. Fugardi and I. Sheinhartz, Isostatic Forming of Beryllium, Report SCNC-322, Sylcor Div., Sylvania Electric Products, Inc., February 1961.
13. Stevens Institute of Technology, Development of Military Components from Beryllium by Slip Casting and Powder Metallurgy Techniques, USAEC Report SCR-306, December 1961.
14. R. Schmidt, New Developments Improve Ductility of Beryllium, *Metal Progr.*, 81(2): 78–82 (February 1962).
15. A. G. Gross, Jr., et al., Fabrication of Beryllium Fine Wire, Report AD-243448, Brush Beryllium Co., April 1961.
16. Oak Ridge National Laboratory, Gas-Cooled Reactor Program Quarterly Progress Report for Period Ending September 30, 1961, USAEC Report ORNL-3210, Feb. 5, 1962.
17. B. M. MacPherson and W. W. Beaver, Fusion Welding of Beryllium, USAEC Report WADD-TR-60-917, Brush Beryllium Co., April 1961.
18. W. J. Marcellin, Automatic and Manual Braze-Welding Techniques for Beryllium, paper presented at Beryllium Metallurgy Conference, New York University, New York, December 1961.
19. W. D. Bennett, Some Fracture Characteristics of Beryllium and Their Theoretical Implications, Canadian Report CW-R&DL-5, September 1960.
20. P. Bastien and P. Pointu, Determination of the Elements of Glide of the Hexagonal Metals by the Asterism of Laue Spots and by a Study of the Deformation Modes of Beryllium at High Temperatures, *J. Nuclear Materials*, 5(1): 101–108 (1962) (in French).
21. N. A. Hill, Textures in Beryllium Tubes Produced from Hot Extruded Rod, British Report AERE-R-3701, May 1961, in Proceedings of Institute of Metals Conference on Beryllium Metallurgy, London, October 1961, to be published.
22. J. J. Pickett et al., Fundamental and Applied Research and Development in Metallurgy: Stability of the High Temperature Beta Phase in Beryllium and Beryllium Alloys, USAEC Report NMI-1252, Nuclear Metals, Inc., Sept. 11, 1961.
23. P. B. Kantor et al., Determining the Enthalpy and Specific Heat of Beryllium in the Interval 600-2200°K, *Fiz. Metal. i Metalloved.*, 10(6): 835–837 (1960) (in Russian).
24. The Advanced Gas-Cooled Reactor, *Nuclear Eng.*, 6(59): 151 (April 1961).
25. S. J. Gregg et al., The High Temperature Oxidation of Beryllium. Part V. In Moist Carbon Dioxide and Moist Carbon Monoxide, *J. Nuclear Materials*, 4(1): 46–48 (1961).
26. J. K. Higgins and J. E. Antill, Oxidation of Beryllium in Carbon Dioxide and Oxygen, *J. Nuclear Materials*, 5(1): 67–80 (January 1962).
27. J. R. Steele, General Problems in the Corrosion of Beryllium, paper presented at 13th Annual Northeast Regional Conference, National Association of Corrosion Engineers, New York, October 30–November 2, 1961.
28. D. J. Levy, The Electrolytic Polarization of Beryllium, Report NP-11154, Lockheed Aircraft Corp., November 1961.
29. R. S. Barnes, The Effect of Neutron Irradiation on Beryllium, *Nuclear Eng.*, 6(59): 149 (April 1961).
30. R. S. Barnes, The Behaviour of Irradiated Beryllium, British Report AERE-R-3769, July 1961.

31. General Nuclear Engineering Corp., Gas-Cooled Reactor Project Terminal Report, USAEC Report GNEC-176(Del.), June 10, 1961.
32. T. W. Baker and P. J. Baldock, A High Temperature Phase Transformation in Beryllia, British Report AERE-M-1017, February 1962; *Nature*, 193: 1172 (March 1962).
33. R. E. Thoma et al., Experimental Attempts to Stabilize a Cubic Form of BeO, USAEC Report ORNL-TM-94, Oak Ridge National Laboratory, Dec. 22, 1961.
34. P. P. Budnikov and N. V. Shishkov, Observations of the Crystallization of Beryllium Oxide from the Gaseous Phase, *Doklady Akad. Nauk S.S.S.R.*, 138(5): 1093–1094 (1961).
35. W. J. Kirkpatrick et al., Basic Material Studies Sinterable High Purity BeO, Final Report, USAEC Report APEX-684, General Electric Co., Flight Propulsion Laboratory Dept., June 30, 1961.
36. F. W. Postma, Jr., and R. E. Barringer, A Dissolution Study of High-Fired BeO-UO_2 Ceramics by Fusion, USAEC Report Y-1377, Union Carbide Nuclear Co., Y-12 Plant, Dec. 26, 1961.
37. Atomics International, 1961. (Unpublished)
38. F. J. P. Clarke, Irradiation Damage in Beryllium Oxide, British Report AERE-R-3971, February 1962; to be published in *Progress in Nuclear Energy*, Series IV, Vol. 5.
39. J. Booker et al., Investigation of Refractory Metal Beryllides and Silicides as Very High Temperature Materials, Report NP-11178, Brush Beryllium Co., Nov. 10, 1961.
40. Oak Ridge National Laboratory, January 1962. (Unpublished)
41. The Metallurgical Society, American Institute of Mining, Metallurgical, and Petroleum Engineers, A Symposium on Metallic Moderators and Cladding Materials, Held at Philadelphia, Pa., Oct. 19, 1960, *Nuclear Metallurgy (Vol. VII), IMD Special Report Series No. 10.*
42. W. L. Korst, X-ray Studies of δ and ϵ Zirconium Hydrides, USAEC Report NAA-SR-6880, Atomics International, Mar. 30, 1962.
43. R. L. Wallerstedt, SNAP-2 Nuclear Auxiliary Power Unit Development Progress Report, December 1960–March 1961, USAEC Report NAA-SR-6292, Atomics International, June 15, 1961. (Classified)
44. D. S. Parker, Properties of Hydrided Yttrium, USAEC Report APEX-558, General Electric Co., Aircraft Nuclear Propulsion Dept., July 20, 1960.
45. General Electric Co., Flight Propulsion Laboratory Dept., High-Temperature Materials Program Progress Report No. 7, Part A, USAEC Report GEMP-7A, Jan. 15, 1962.
46. General Electric Co., Flight Propulsion Laboratory Dept., High-Temperature Materials and Reactor Component Development Programs, First Annual Report, Vol. I. Materials, USAEC Report GEMP-106A, Feb. 28, 1962.
47. S. Keraudy et al., The Effect of Impurities on the Rate of Oxidation of Reactor Grade Graphite, British Report DPC.CPh/59-711, July 1, 1959.
48. R. W. Rowe, High Temperature Strength of Clean Graphite, *Nuclear Eng.*, 7(70): 102–103 (March 1962).
49. Southern Research Inst., The True Stress-Strain Properties of Brittle Materials to Very High Temperatures, USAEC Report ORO-461(Rev.), Oct. 28, 1961.

Section

III

Reactor Materials

Nuclear Poisons

Metallic Poisons

Knolls[1] is corrosion testing synthetic hafnium alloys that contain tantalum, lutetium, and tungsten (transmuted products) in 550 and 680°F deionized and deoxygenated water, as well as in 680 and 750°F steam. Small additions of tantalum and lutetium produced measurable decreases in corrosion resistance of hafnium alloys in 550°F water. Small additions of iron to hafnium that contained 0.4 wt.% tantalum produced improved corrosion resistance in 750°F steam.

Results of tests performed at Bettis on hafnium alloys in 600 and 680°F water and 680, 750, 800, and 850°F steam show that the materials possess good corrosion resistance at all temperatures up to and including 750°F. However, early spalling of the oxide occurs at 800 and 850°F corrosion-test temperatures.

The Russians[2] have reported data for hafnium-beryllium alloys (62.5, 70.0, 80.0, 84.0, 91.0, and 95.5 wt.% hafnium). The properties that are reported for a few of the alloys include melting point, hardness, microstructure, and microhardness. Beryllium-base alloys that contained up to 33.0 wt.% hafnium were also prepared and examined. (W. E. Murr)

Control and Burnable-Poison Composites

Irradiation behavior of bulk B_4C burnable-poison elements has been studied at Bettis,[3] and the following conclusions were reported: (1) the unit cell size of B_4C continually contracts with increased irradiation, and the resulting strains produce microcracking in the core; (2) this microcracking gives a linear swelling rate of 0.15 per cent $\Delta V/10^{20}$ depletions/cm^3 up to 90×10^{20} depletions/cm^3, and then a breakaway occurs; and (3) the microcracking catastrophically reduces the in-pile corrosion resistance of the B_4C, and its use in pressurized-water reactors is not recommended.

Bettis[4] has issued a report on the release of helium from slightly irradiated boron carbide and boron carbide–silicon carbide plates. The data for boron carbide were represented as $D = 1.4 \times 10^{-8} \exp(-29{,}000/RT)$. The release from the B_4C-SiC plates was less but could not be related by a simple equation since the D values did not show a temperature dependence. Average values for D were 2×10^{-14} and 5×10^{-15} cm^2/sec for 30 vol.% B_4C–SiC and 50 vol.% B_4C–SiC, respectively.

A comprehensive study of the irradiation behavior of B^{10} iron-base alloys has been completed at Bettis.[5] The following conclusions were reached:

Irradiation testing, at 80 to 310°C, of iron, ferritic stainless-steel, and austenitic stainless-steel alloys with 2 wt.% boron (enriched 92 per cent B^{10} in total boron) revealed gross swelling and cracking of these alloys when irradiated in excess of 90 per cent B^{10} depletion. Postirradiation corrosion testing of the stainless-steel alloys in 343°C water indicated that these alloys still retained their good corrosion resistance but that exposure to the elevated temperature caused further swelling and cracking. This same temperature effect was also observed in postirradiation annealing. Austenitic stainless-steel alloys exposed to 300, 400, and 500°C showed swelling and cracking, and, in addition, 40 to 50 per cent of the helium produced during irradiation was released from these samples during the annealing. The gross damage suffered by these alloys at high-percentage depletions indicates that the B^{10}

content in stainless-steel alloys should be limited to a maximum of 1 wt.%.

To explain these experimental results, a submicrocrack mechanism of irradiation damage was postulated. In this model the irradiation damage occurs in three distinct stages:

1. At low neutron exposures (low per cent B^{10} depletions) the alloys increase in hardness and strength and remain crack-free.
2. At some higher exposure the alloys are embrittled and internally stressed, and submicrocracks form within the matrix.
3. At still higher exposures the submicrocracks grow and connect to form microcracks and macrocracks.

Submicrocrack formation, the start of the second stage, was estimated to commence at about 4 to 15 per cent B^{10} depletion in these alloys and is accompanied by an increase in swelling rate and by a decrease in tensile strength. The end of the submicrocrack stage was noted by observable microcracks and gross swelling and was estimated to occur at 26 to 49 per cent B^{10} depletion in the iron alloys, at 71 to 92 per cent B^{10} depletion in the ferritic stainless-steel alloys, and at 76 to 96 per cent B^{10} depletion in the austenitic stainless-steel alloys. An estimate of the alloy-swelling rate in the submicrocrack stage was obtained for the ferritic stainless-steel alloys (0.30 to 0.40 per cent ΔV/per cent B^{10} depleted) and for the austenitic stainless-steel alloys (0.20 to 0.42 per cent ΔV/per cent B^{10} depleted). The swelling rate of the iron alloy was estimated as two to three times greater than the swelling rates of the stainless-steel alloys.

The submicrocrack formation in these alloys was attributed to the high boron content in solid solution, approximately 0.5 at.% boron, which transforms to lithium and helium during irradiation. These impurities are postulated to cause hardening and embrittlement of the matrix. The swelling of the boride particles in the embrittled matrix is believed to initiate the submicrocrack formation.

The lithium-boron-carbon system has been studied at Knolls.[6] The only ternary composition studied was obtained by reacting lithium with B_4C. The results indicated that Li_xB_y and Li_2C_2 were reaction products, with the boride reaction being predominant.

General Electric[7] has continued development work on europium oxide dispersions as high-temperature control materials. Iron-chromium-aluminum and iron-chromium-yttrium alloys were found to be unstable in the presence of Eu_2O_3 because both aluminum and yttrium reduce Eu_2O_3 to a lower oxidation state. Diffusion barriers or coated-particle techniques were considered necessary to protect Eu_2O_3 in the presence of these alloys. The Eu_2O_3 combined with palladium exhibits short-time thermal stability in air at 1400°C, and dispersions of the oxide in platinum and iridium are stable in air to 1600°C.

Aerojet-General[8] is considering the use of a thin foil of Eu_2O_3 dispersed in stainless steel as a burnable poison for the 10,000-hr operation of the ML-1 (Army gas-cooled) Reactor. Foil, prepared at Battelle, which was 0.010 in. thick by 4 in. wide and which contained 5.8 wt.% Eu_2O_3, was tested in 200°F water. After two weeks in a static capsule, the water contained 15 mg of europium. A similar foil, electroless nickel plated with a 0.002-in. coating, was run for two weeks, and no europium could be detected in the water.

Table III-1 TENSILE STRENGTH FROM DISK-CRUSHING TEST FOR B_4C-CARBON DISKS[10]

Irradiation conditions	Tensile strength, psi						Exposure, nvt (thermal)
	20 wt.% boron compacts		30 wt.% boron compacts		40 wt.% boron compacts		
	Pre-irradiation	Post-irradiation	Pre-irradiation	Post-irradiation	Pre-irradiation	Post-irradiation	
350°C:							
2 cycles	1450	1900	1350	1800	1225	1400	9.8×10^{20}
5 cycles	1450	1400	1350	600*	1225	†	2.4×10^{21}
700°C:							
2 cycles	1450	1675	1350	1325	1225	1300	9.8×10^{20}
5 cycles	1450	1725	1350	1100	1225	1425	2.4×10^{21}

*Sample crushed. †Sample broken.

Oak Ridge[9] has continued work in several areas in support of the Army reactor program. Studies are in progress to determine the mechanism of the detrimental swelling that occurs when dispersions of 30 and 40 wt.% Eu_2O_3 in stainless steel are exposed to high-temperature pressurized water. Work to date has suggested that the europium oxide contains a compound such as europium hydroxycarbonate; this compound decomposes to a cubic Eu_2O_3 structure during sintering of the dispersions, resulting in a two-phase (cubic and monoclinic) structure. The possibility of improving the corrosion resistance of Eu_2O_3 by stabilizing the cubic modification of the oxide is now being studied.

Study was continued on a control-rod concept that involves preparing a core structure with a boron content lower at the core-cladding interface than at the center of the core. This design was conceived to eliminate the excessively high burnup of boron which occurs at the core surface due to the self-shielding of boron. A full-sized absorber has been prepared for radiation testing in the SM-1 Reactor. Glass beads that contain 4 wt.% B_2O_3 are being considered for use as a burnable poison in UO_2–stainless steel dispersion fuel plates. It is reported that the glass beads do not stringer at temperatures up to 1050°C, do not react with UO_2 at 1100°C, and do not react with the stainless steel at 1100°C.

General Atomic[10] has tested compacts of B_4C and graphite after irradiation at temperatures of about 350 and 700°C. Diameter changes were small and did not appear to be either exposure- or temperature-dependent. Length changes were large (up to 4.5 per cent) and appeared to be dependent upon exposure. Strength tests indicated a general increase in the strength of the irradiated samples that contained 20 per cent boron. The results of the strength tests are shown in Table III-1. (G. W. Cunningham)

References

1. B. E. Dearing and A. M. Andrako, The Corrosion Behavior of Hafnium and Hafnium Alloys in High Temperature Water and Steam, USAEC Report KAPL-M-BED-4, Knolls Atomic Power Laboratory, Aug. 14, 1961.
2. P. I. Kripyakevich et al., Hafnium-Beryllium Compounds, Their Crystal Structure and Properties, *Zhur. Strukt. Khim.*, 2(4): 424–433 (1961).
3. Westinghouse Electric Corp., Bettis Atomic Power Laboratory, Pressurized Water Reactor (PWR) Project Technical Progress Report for the Period October 24, 1961, to December 23, 1961, USAEC Report WAPD-MRP-95.
4. J. C. Clayton et al., The Release of Helium from Slightly Irradiated Boron Carbide and Boron Carbide–Silicon Carbide Plates, USAEC Report WAPD-255, Westinghouse Electric Corp., Bettis Atomic Power Laboratory, January 1962.
5. Westinghouse Electric Corp., Bettis Atomic Power Laboratory, Bettis Technical Review, USAEC Report WAPD-BT-24, December 1961.
6. D. R. Secrist, A Study of the Lithium-Boron-Carbon System, USAEC Report KAPL-2182, Knolls Atomic Power Laboratory, Jan. 17, 1962.
7. General Electric Co., Flight Propulsion Laboratory Dept., High-Temperature Materials and Reactor Component Development Programs. Volume I. Materials, USAEC Report GEMP-106A, Feb. 28, 1962.
8. Aerojet-General Nucleonics, The Army Gas-Cooled Reactor Systems Program, Semiannual Progress Report for July 1 Through December 31, 1961, USAEC Report IDO-28581, Feb. 28, 1962.
9. Oak Ridge National Laboratory, Army Reactors Program Progress Report, USAEC Report ORNL-3231, Feb. 14, 1962.
10. General Atomic Div., General Dynamics Corp., 40-Mw(e) Prototype High-Temperature Gas-Cooled Reactor Research and Development Program. Quarterly Progress Report for Period Ending December 31, 1961, USAEC Report GA-2861.

Section

IV

Reactor Materials

Cladding and Structural Materials

Corrosion

Zirconium Corrosion

General Electric has summarized[1] studies on the effect of heat-treatment on the corrosion behavior of zirconium–1 to 3.5 wt.% niobium alloys. The results of short-time tests in 680°F water and 900°F steam have shown that an alpha anneal gives optimum corrosion resistance with no serious embrittlement from hydrogen. Beta-treated alloys were less resistant. Hydrogen pickup, as total amount or percentage of that theoretically available from corrosion, increased with increasing niobium content. It ranged from 7 to 27 per cent of theoretical in alpha-annealed material. Heat-treatment played a role in embrittlement — at the same hydrogen level, alpha-annealed alloys were much less embrittled than those which were beta treated.

Additional results have been reported by Bettis[2] on hydrogen pickup by Zircaloy in high-temperature water. It has been found that, at temperatures to 750°F, Zircaloy-2 and nickel-free Zircaloy-2 have comparable corrosion resistance, but the latter absorbs less hydrogen. At 850°F and above, Zircaloy-2 exhibits optimum corrosion behavior in the as-fabricated or alpha-treated condition, whereas the nickel-free Zircaloy-2 is best in the beta-quenched condition. The presence of approximately 9000 ml of hydrogen per kilogram of water at 650°F resulted in increased hydrogen pickup in both alloys, but the nickel-free Zircaloy-2 absorbed the smaller quantity. Additions of silicon to the alloys appeared to reduce hydrogen pickup, the effect being more pronounced in Zircaloy-2.

Hanford[3] has studied hydriding of purposely defected Zircaloy-clad UO_2 fuel rods during irradiation in the Materials Testing Reactor (MTR). Defects were 0.005 to 0.007 in. in diameter. Zircaloy-2 hydrided after relatively short exposure to the 75 to 120°F water. The hydride platelets migrated rapidly from the defect area to relatively cool sections of the cladding, and the concentration of platelets increased as exposure time and surface heat flux increased. Nickel-free Zircaloy-2 showed a dramatically lower hydride formation rate than did Zircaloy-2.

A statistical analysis of the effect of five impurities on the corrosion resistance of Zircaloy-2 in 680°F water and 750°F steam has been reported[4] by Bettis. Aluminum, copper, manganese, nitrogen, and silicon additions in Zircaloy-2 were studied at the upper portion of the specification range and at values in excess of this range. Aluminum, at the 172-ppm level, was found to be detrimental to corrosion resistance, whereas manganese (440 ppm) slightly increased the corrosion rate in 750°F steam. Copper (155 and 319 ppm) and nitrogen (48 and 123 ppm) did not affect corrosion rates, although higher weight gains were experienced at the high-nitrogen level. Silicon, at the 200- to 300-ppm level, improved the corrosion behavior of Zircaloy-2 that had been furnace-cooled from the beta phase.

Australian scientists have investigated[5] the reaction of zirconium with CO_2 at 550 to 750°C. A cubic reaction rate was observed, and breakaway occurred at much shorter times in CO_2 than in oxygen at the same temperature. Ninety-eight per cent of the weight gain was found to be represented by the reaction $Zr + 2CO_2 = ZrO_2 + 2CO$, whereas the other 2 per cent was represented by the reaction $Zr + CO_2 = ZrO_2 + C$. It was believed that the oxygen ions migrated inward through the oxide film via lattice vacancies, but the zirconium ions did not migrate outward. It was also believed that some carbon

diffused inward through the oxide film, thus accounting for the ZrC that was found.

(W. E. Berry)

Aluminum Corrosion

The corrosion of 6068 aluminum flow orifices on fuel-element clusters by D_2O has been described[6] by Chalk River. Coolant temperature was about 110°F, and flow velocity was 50 to 60 ft/sec. Pitting to the extent of complete penetration was observed over part of the circumference of the orifice. It was concluded that coolant velocities were too high — impingement erosion occurred on the upstream edge and cavitation erosion on the downstream edge of the orifice. Degassing of the coolant and vibration were also believed to contribute to the pitting. A new orifice has been designed, and other recommendations have been made to eliminate the corrosion. (W. E. Berry)

Stainless-Steel Corrosion

Hanford's examination[7] of a type 316 stainless-steel valve that failed after 1 month's exposure to *p*H 10 water (LiOH) at 300°C has revealed severe transgranular cracks. Cracking occurred in a region where concentration of the LiOH could take place from leakage. On the other hand, tests on type 316 stainless-steel tubing that was stressed to 5000 to 6000 psi have revealed no cracking after exposure for four months at 260°C where LiOH was deposited on the surface by flashing *p*H 10 water (LiOH). Stressed, type 304 stainless-steel specimens have not cracked after exposure for two months to 290°C water that contains 1 g of LiOH per liter.

General Electric has experienced[8] stress-corrosion cracking of type 304 stainless-steel cladding on UO_2 during irradiation exposure to superheated steam. The cladding was exposed to steam that contained about 20 ppm oxygen for 617 hr at a maximum temperature of 900°F. Maximum cladding temperature was 1150°F. Cracking was mainly intergranular in the sensitized material. The cracking was believed to have been caused by leakage into the steam loop of reactor water that had been contaminated with chlorides. The boiling-water-reactor water was known to have been contaminated with a maximum of 1 to 3 ppm chlorides for about 8 hr.

Also summarized[9] are the results of stress-corrosion tests of hardenable grades of stainless steel, and the 17-4 PH tube failure in the control-rod drive of the Dresden reactor is described. Stressed specimens were exposed to water that contained 0.2 to 1.2 ppm oxygen in loop tests at 536°F and were exposed to deoxygenated water in autoclave tests at 200, 400, and 550°F. It was concluded that 17-4 PH steel in the H900 heat-treated condition is subject to cracking in high-purity water at temperatures from 200 to 550°F. The H1100-condition material was more resistant; the only instances of cracking occurred at stresses approaching 1 per cent strain. The following alloys were less susceptible to cracking than the 17-4 PH steel in the H900 condition: 17-7 PH (1050°F treatment), A-286 (1325°F treatment), and AM-350 (850 and 1000°F treatments).

Oak Ridge has reviewed[10] the conditions that lead to catastrophic oxidation of iron-chromium-nickel alloys. Catastrophic oxidation has been observed with alloys that contain molybdenum, tungsten, or vanadium, or whose surfaces have been contaminated with compounds of these elements or such compounds as KF, Bi_2O_3, Na_2O, or lead. Also reviewed were the mechanism of failure, service failures, and recommendations for avoiding attack. Of pertinent interest were the observations that (1) types 316 or 317 stainless steel should not be used above 1200°F unless the surfaces are scrupulously clean and not above 1400°F in a stagnant atmosphere; (2) high-temperature insulation and cements should not be used in contact with stainless steel above 1200°F; and (3) clean iron-chromium-molybdenum and chromium-nickel-molybdenum alloy surfaces are not subject to catastrophic oxidation if the nickel content is greater than 25 per cent. (W. E. Berry)

Corrosion of Base-Metal Alloys

Aqueous Corrosion. Chalk River has investigated[11] corrosion and crud release in carbon steel out-of-pile loops circulating water at 150 to 205°C. At low oxygen levels, corrosion rates were the same as those at 260 to 315°C, adherent magnetite formed on the steel, and crud-release rates were low. The crud-release rate was always less than 1 ppm in the coolant and declined to less than 0.1 ppm after initial exposure, even without purification. Dissolved oxygen in the water increased corrosion and the

amount of crud release. On the basis of these experiments, it was concluded that carbon-steel systems can be conditioned by operation for several weeks at 150°C with oxygen-free *p*H 10 water.

Russian scientists have studied[12] the corrosion behavior of a low-alloy steel in 300°C water with air, hydrogen, or hydrazine. Corrosion rates were found to diminish with time. Uniform attack occurred with hydrogen and hydrazine, whereas pitting was observed with oxygen. It was concluded that (1) corrosion of the alloy steel in 300°C water was electrochemical in nature, (2) the rate of the cathode process was determined by the diffusion of oxygen to the surface of the metal, and (3) the rate of dissolution of the steel in the various media was expressed by one anodic polarization curve.

The Martin Company has recently reported[13] results of stress-corrosion tests of 2000-hr duration on Inconel, Monel, and nickel in 450°F water. The water contained 1 and 15 ppm oxygen and up to 1000 ppm chlorides and was adjusted to *p*H 10 with Na_3PO_4 and NaOH. No cracking was found in any of the alloys. Pitting up to 4 mils deep was observed, mostly in the high-oxygen, high-chloride conditions. Corrosion rates for the Monel, nickel, and Inconel were 15, 12, and 6 mg/(dm^2)(month), respectively.

Gaseous Corrosion. Aerojet-General has studied[14] the effect of lubricating-oil leakage on the corrosion behavior of Hastelloy X in nitrogen gas that contained no oxygen. Exposures up to 100 hr in 1750°F nitrogen, which had previously been bubbled through 300°F lubricating oil, resulted in intergranular attack and embrittlement. It was concluded that Hastelloy X would embrittle in a reactor coolant gas from which oxygen was removed.

Results of heating platinum, palladium, iridium, rhodium, and platinum–30 wt.% rhodium in air and argon have been reported[15] by General Electric. In static air, iridium oxidized rapidly at 1200 to 1600°C, whereas platinum and the platinum–30 wt.% rhodium alloy were the most resistant. Calculated times to produce 1-mil metal loss in the platinum ranged from 10,000 hr at 1200°C to 233 hr at 1600°C. Corrosion attack was attributed to sublimation of the oxides. Oxidation rates increased in flowing air. Iridium, platinum, and rhodium were little affected by temperature or flow rate in argon. On the other hand, palladium lost metal in argon at 1300 to 1400°C almost as fast as in air. This was believed to be related to metal sublimation. Palladium had excellent stability at 1000 to 1200°C.

The Australians have studied[16] the oxidation of 1 wt.% chromium–0.5 wt.% molybdenum steel in carbon dioxide in the temperature range 450 to 525°C. They found no effect on the oxidation rate of carbon dioxide pressure, up to 20,000 ppm moisture, or specimen surface preparation. Weight gains in carbon dioxide were greater than those in oxygen at the same temperature. They conclude that it is not safe to use this steel in carbon dioxide above 450°C.

(F. W. Fink)

Corrosion of Refractory Metals

Recent studies concerning the corrosion of refractory metals (niobium, molybdenum, tantalum, and tungsten) have been concentrated in two broad areas of investigation: (1) studies concerned with the corrosion (primarily oxidation) behavior of refractory metals and alloys and (2) studies involving the performance of coated refractory metals and alloys. Further, because of the relatively low cross section inherent in niobium and its alloys, AEC-related efforts in the field of refractory metals have been concentrated upon systems involving niobium.

Corrosion of Uncoated Refractory Metals. In a fundamental study of the oxidation behavior of unalloyed niobium, workers at Oak Ridge conducted oxidation experiments on niobium single crystals.[17] They found that, at oxidation temperatures of 400 to 425°C, crystals with a surface orientation that was 25° from the (1 0 0) plane oxidized at substantially lower rates during the initial stages than did those with other orientations. This behavior probably results from improved epitaxial fit between the substrate in this orientation and the resulting oxide.

The effects of stress upon the oxidation of tantalum were studied in an Air Force–Ohio State University program.[18] It was found that a stress of 24,000 psi about doubled the parabolic rate constant from rates of about 10^{-2} (no stress) to about 2×10^{-2} mil^2/hr (24,000 psi) during oxidation at 510 to 538°C. Parabolic activation energy, induction time for transition from parabolic- to linear-reaction kinetics, and

linear-reaction rates were not significantly affected in the temperature range studied.

Samsonov et al.[19] investigated the chemical compatibility at temperatures to 2100°C among BeO, MgO, and ZrO_2, or carbides of zirconium, hafnium, niobium, and tantalum and the refractory metals niobium, molybdenum, and tungsten. At higher temperatures, niobium reacted appreciably with all materials. The least reactive oxide : metal couples over the temperature range studied were BeO : W, MgO : W or Mo, and ZrO_2 : Mo. Regarding carbide compatibility, molybdenum versus TaC was stable to 2100°C, but molybdenum reacted with the other carbides at temperatures of 1800°C and higher.

Workers at Knolls have reported[20] that vanadium additions to niobium stabilize the NbO_2 oxide form, resulting in much-improved resistance to oxidation in steam at 360 to 482°C. At a concentration of 3.6 at.% vanadium, NbO_2 stabilization was incomplete, but in the niobium–8.9 at.% vanadium alloy, the NbO_2 form completely replaced the nonoxidation-resistant Nb_2O_5 oxide.

Battelle investigations[21] showed superiority, for binary additions to niobium, of titanium and zirconium, as well as vanadium, relative to hot-water (315 to 360°C) and steam (400°C) oxidation resistance. A niobium–28 at.% titanium–6 at.% chromium alloy was found to be particularly attractive, exhibiting parabolic weight gain at a rate of 1.96 $(mg/cm^2)^2$/day in 360°C water. This is markedly superior to the behavior exhibited by Zircaloy-2.

Efforts were continued at General Electric to understand the oxidation behavior of spall-resistant niobium–33 wt.% titanium–31 wt.% aluminum and niobium–30 wt.% titanium–24 wt.% aluminum–5 wt.% chromium alloys.[22,23] Less-attractive oxidation resistance in the chromium-free alloy at 1200 and 1315°C, compared with performance at 1425°C, was related to inability of the alloy to form continuous Al_2O_3 and the occurrence of Nb_3Al at the surface of the alloy at the lower temperatures. In the chromium-containing alloy, a continuous Al_2O_3 barrier formed at all temperatures, and the Nb_3Al layer contained chromium in solution, which apparently rendered this layer oxidation resistant. Because of incipient fusion of $NbCr_2$ at 1315°C, the chromium-containing alloy is restricted in potential, however, and investigations of niobium-titanium-aluminum base alloys have been terminated.

Ignition of the refractory metals has been investigated. In studies at General Electric,[24] the ignition temperature for niobium in dynamic [2000 to 8000 lb/(sq ft)(hr)] air was determined to be 1470 ± 10°C. During ignition, linear weight-change rates of 30 $mg/(cm^2)(sec)$ were observed. This represents on the order of 300 to 400 times the preignition-oxidation rate of niobium at an equivalent temperature. Ignition was postulated to be closely related to the occurrence of a molten oxide. In this regard, molybdenum-containing niobium alloys were observed to ignite at temperatures as low as 1398°C. The ignition temperature for F-48 (niobium–15 wt.% tungsten–5 wt.% molybdenum–1 wt.% zirconium) was determined to be 1450°C. The rate of air flow is highly important to ignition—at rates of less than about 2000 lb/(sq ft)(hr), the amount of oxygen was insufficient to support the ignition reaction, and ignition was not observed. The effects of air-flow rate on the normal oxidation kinetics were also investigated. Increased rates of air flow up to about 2000 lb/(sq ft)(hr) nearly doubled the scaling rate at a given temperature, but additional increases up to 8000 lb/(sq ft)(hr) exhibited relatively little effect.

Tungsten has been observed to be responsible for catastrophic oxidation failure of type 304 stainless steel. When using a stainless-steel protection tube for tungsten-rhenium thermocouples, investigators[10] at Oak Ridge were able to attribute the rapid failure of the tube to attack by WO_3. This phenomenon is well known in conjunction with V_2O_5 or MoO_3 attack, and the Oak Ridge report confirms suspicions that volatile WO_3 may result in similar effects.

Corrosion of Coated Refractory Metals. Activity in the field of coated refractory metals and performance of coated refractory-metal systems is extensive. Rather than attempt a comprehensive review of all recent activities, this section will highlight information on important developments not readily available elsewhere. The Defense Metals Information Center is making strenuous efforts to stay abreast of the field and report significant developments as they occur. Several reports and papers have recently been presented in this regard.[25–27]

General Electric[24] studies of ignition phenomena demonstrated that, for defected coated refractory metals, ignition does not result when small areas of refractory metals are exposed to

conditions that would result in ignition of the uncoated metals. This emphasizes the importance of available reaction surface relative to volume. In the presence of a massive heat reservoir to absorb the heat of reaction, ignition does not occur.

Researchers at Denver Research Institute[28] are investigating additions of titanium, vanadium, zirconium, silicon, and tin to $NbAl_3$ (a potential coating material for niobium) in attempts to eliminate the low-temperature (700°C) rapid-oxidation problem with this compound. (Similar problems exist for many high-temperature potential coating compounds — $MoSi_2$, WSi_2, etc.) $NbAl_3$ + 10 wt.% titanium has resisted failure for at least 1000 hr in air at 760°C. Similarly tin and silicon additions permit $NbAl_3$ to endure more than 100 hr at 760°C without failure. (E. S. Bartlett)

Corrosion by Liquid Metals and Fused Salts

Experiments were conducted at Atomics International[29] to assess the oxidation of zirconium and several zirconium alloys in 400 to 635°C sodium. It was found that unalloyed zirconium and Zircaloy-2 specimens exhibited similar weight gains. In the case of Zircaloy-2, the weight gain was about 0.45 mg/cm^2 for a 145-hr exposure at 595°C; this was not sensitive to oxygen concentration, which in individual experiments was varied from 10 to 500 ppm. Higher weight losses, by a factor of 2 to 4, were noted for zirconium-base specimens alloyed with 1.5 to 3 wt.% aluminum, 1.0 to 3 wt.% tin, and 1 to 1.5 wt.% molybdenum. Using the parabolic rate equation to describe the kinetics of oxidation, activation energies of 52.9 ± 0.5 kcal/mole for zirconium and 45.3 ± 1.5 kcal/mole for zirconium alloys were indicated. A transition from parabolic to linear rate of oxidation was observed in the temperature range 400 to 500°C for all the zirconium alloys except Zircaloy-2. Above 500°C the transition was not observed, and a protective film continued to form.

Corrosion-loop systems are being operated at Brookhaven[30] to evaluate the resistance to attack of potentially useful containment materials over long periods of exposure to boiling mercury with additions of magnesium, titanium, and zirconium (magnesium is used for wetting and deoxidation, and titanium and zirconium are used for corrosion inhibition). A preliminary assessment of the condition of a carbon steel system after 6015 hr of operation with 1000°F mercury (with magnesium and titanium additives) at the boiler section and 1150°F vapor at the superheater section indicated very slight (<1 mil) intergranular attack in the boiler and vapor-condensing zones; no attack was noted in the superheater or condenser liquid zones. Several other loop systems are either operating or being assembled; construction materials include 2.25 wt.% chromium–1 wt.% molybdenum steel, Haynes 25, carbon steel clad with Inconel, niobium–1 wt.% zirconium, and tantalum. Boiling-sodium experiments in the 2000 to 2400°F range are in the planning stage.

Research at General Electric demonstrated that molten LiH at temperatures from 1325 to 1425°F attacked 19-9 DL alloy sheet (Universal Cyclops) only very sparsely. In an extension of this investigation,[31] stressed specimens of 19-9 DL alloy were exposed to molten LiH to ascertain the effects of the combined stress-corrosion condition. Experiments employing parameters over the ranges listed below indicated virtually no influence of stess on factors such as surface attack, rupture strength, and notch sensitivity.

Temp., °F	1175, 1325, and 1425
Form of material	Unwelded and welded sheet
Stress level, psi	11,000 to 52,000
Time of exposure, hr	To 825

The over-all conclusion is that 19-9 DL alloy has the necessary qualifications for a structural material in contact with LiH to 1425°F.

Table IV-1 presents a summary of final information from the long series of forced-convection loops operated at Oak Ridge to investigate fluoride-salt compatibility with INOR-8 and Inconel.[32] The consistent superiority of INOR-8 as regards resistance to corrosion attack is apparent for all combinations of temperature, flow rate, and salt-mixture composition evaluated.

Certain basic differences in the 1500°F behavior of the niobium-oxygen-potassium, the (niobium–1 wt.% zirconium)-oxygen-potassium, and the niobium-oxygen-lithium systems are also being demonstrated. After 500 hr of exposure to 1500°F potassium containing 400, 1400, and 2400 ppm oxygen, the niobium–1 wt.% zirconium alloy showed significant pickups of oxygen, whereas niobium did not.[33] Neither material exhibited evidence of corrosion attack.

Table IV-1 SUMMARY OF DATA ON LONG-TERM FUSED-SALT LOOPS AT OAK RIDGE[32]

Loop	Material	Duration of test, hr	Salt mixture*	Maximum fluid-metal interface temp., °F	ΔT, °F	Reynolds number	Flow rate, gal/min	Results of metallographic examination
9075-1	Inconel	8,801	122	1250	100	5000	2.0	Intergranular penetrations to 1½ mils
9344-1	Inconel	8,892	123	1300	200	3250	2.0	Heavy intergranular voids to 38 mils
9344-2	Inconel	8,735	12	1200	100	8200	2.5	Intergranular voids to 8 mils
9354-1	INOR-8	14,563	126	1300	200	2000	2.5	Heavy surface roughening and pitting to 1½ mils
9354-3	INOR-8	19,942	84	1200	100	3000	2.0	No attack, slight trace of metallic deposit in cooler coil
9354-4	INOR-8	15,140	130	1300	200	3000	2.5	No attack
9354-5	INOR-8	14,503	130	1300	200	3000	2.5	No attack
9377-1	Inconel	3,390	126	1300	200	1600	2.0	Intergranular voids to 7 mils
9377-2	Inconel	3,046	130	1300	200	3000	2.0	Intergranular voids to 8 mils
9377-3	Inconel	8,764	131	1300	200	3400	2.0	Intergranular and general voids to 14 mils
9377-4	Inconel	9,574	130	1300	200	2600	1.75	Intergranular and general voids to 14 mils
9377-5	Inconel	15,038	134	1300	200	2300	1.8	Intergranular voids to 24 mils
9377-6	Inconel	13,155	133	1300	200	3100	1.8	Intergranular voids to 13 mils
MSRP-6	INOR-8	20,000	134	1300	200	2300	1.5	Pitted surface layer to 2 mils
MSRP-7	INOR-8	20,000	133	1300	200	3100	1.8	Pitted surface layer to 1 mil
MSRP-8	INOR-8	9,633	124	1300	200	4000	2.0	No attack
MSRP-9	INOR-8	9,687	134	1300	200	2300	1.8	No attack
MSRP-10	INOR-8	20,000	135	1300	200	3400	2.0	Pitted surface layer to ½ mil
MSRP-11	INOR-8	20,000	123	1300	200	3200	2.0	Pitted surface layer to 1 mil
MSRP-12	INOR-8	14,498	134	1300	200	2300	1.8	No attack
MSRP-13	INOR-8	8,085	136	1300	200	3900	2.0	Heavy surface roughening and pitting
MSRP-14	INOR-8	9,800	Bult 14 + 0.5 U	1300	200			Pitted surface layer to ½ mil
MSRP-15	INOR-8	10,200	Bult 14 + 0.5 U	1400	200			Pitted surface layer to ⅔ mil
MSRP-16	INOR-8	6,500	Bult 14 + 0.5 U	1500	200			Moderate subsurface void formation to 4 mils

*Salt compositions, mole%:

12 NaF-LiF-KF, 11.5-46.5-42
84 NaF-LiF-BeF_2, 27-35-38
122 NaF-ZrF_4-UF_4, 57-42-1
123 NaF-BeF_2-UF_4, 53-46-1
124 NaF-BeF_2-ThF_4, 58-35-7
126 LiF-BeF_2-UF_4, 53-46-1
130 LiF-BeF_2-UF_4, 62-37-1
131 LiF-BeF_2-UF_4, 60-36-4
133 LiF-BeF_2-ThF_4, 71-16-13
134 LiF-BeF_2-UF_4-ThF_4, 62-36.5-0.5-1
135 NaF-BeF_2-UF_4-ThF_4, 53-45.5-0.5-1
136 LiF-BeF_2-UF_4, 70-10-20
Bult 14 + 0.5 U LiF-BeF_2-ThF_4-UF_4, 67-18.5-14-0.5

Leading results thus far obtained for the niobium-oxygen-lithium system are as follows:

1. Corrosion of niobium by lithium increases with increasing oxygen concentration in the solid material.
2. At 1500°F the critical oxygen concentration for occurrence of corrosion is 500 ppm.
3. Oxygen concentration in the lithium does not affect the corrosion resistance of uncontaminated niobium.
4. Grain-boundary attack is favored, but as grain size increases, transgranular penetration increases.
5. Transfer of oxygen from the solid metal to the liquid metal has been observed.
6. Rapid attack can occur; for example, heavy attack has been observed after 0.1 hr at 1500°F. (J. H. Stang)

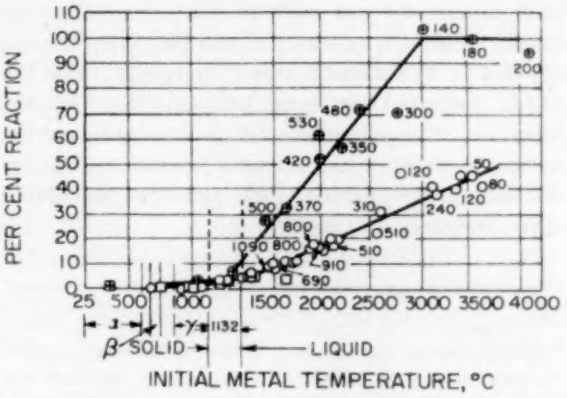

Fig. IV-1 Results of condenser-discharge runs with uranium wires.[34] ○, 30-mil wires. □, 60-mil wires. +, runs in heated water. Numbers indicate mean particle size in microns.

Metal-Water Reactions

The experimental program at Argonne[34,35] to determine rates of reaction of molten reactor fuel and cladding metals with water is continuing. One method involves the rapid melting and dispersion of metal wires in a water environment by a surge current from a bank of condensers. A series of runs[34] with 30-mil uranium wires in the high-pressure reaction cell has been completed. Water temperature ranged from 100 to 125°C (water-vapor pressure 15 to 33 psia) in these runs. The new results in heated water are compared with previous results of runs in room-temperature water in Fig. IV-1. The results show that considerably more reaction occurred in heated water than in room-temperature water. The uranium results are consistent with previous results with zirconium.

The more extensive reaction obtained in heated water was explained on the basis of a more rapid rate of gaseous diffusion of water vapor through the steam-hydrogen film in the case of zirconium. The same reasoning should apply to the uranium case. The fact that greater reaction in heated water also occurred with uranium further verifies the theoretical account of the zirconium-water reaction.

Transient-pressure traces from uranium indicated that the progression of slow reaction rates to explosive rates occurred over the temperature range from 1600 to 2500°C. Results were consistent with the findings for zirconium that particles smaller than 1000 μ in heated water and 500 μ in room-temperature water could undergo the explosive reaction. Analyses of the hydrogen that was retained by the residue from uranium runs indicated that, at most, a few per cent of the hydrogen generated during a run is retained by the partly oxidized metal.

A study is being conducted at Argonne[35] on the behavior of nuclear fuel materials subjected to neutron bursts of sufficient energy to achieve a meltdown in a water environment. The metals of main interest in water-cooled-reactor technology, namely, aluminum, type 304 stainless steel, uranium, and Zircaloy-2, are being investigated in this in-pile, fuel-meltdown program.

The data obtained with uranium wires and pins indicated that both the reactor period and the integrated power are of importance in determining the amount of metal-water reaction that occurs. For 64-mil-diameter uranium wires in water, the extent of uranium-water reaction (with 216 cal of energy input per gram of uranium) increased from 0.4 to 7.5 to 17.2 per cent as the reactor period changed from 515 to 267 to 96 msec, respectively. Peak uranium-wire temperatures up to 1500°C were recorded.

Meltdown results from uranium wires and uranium pins (20 per cent enriched, 0.2-in. diameter) indicated an increase in the metal-water reaction as the reactor burst became more energetic. At reactor periods of about 100 msec, bursts less energetic than 50 cal/g

of uranium did not melt the fuel pin. At bursts of 50 to 100 cal/g, the pin was partially melted (1133°C). Transients more energetic than 100 cal/g resulted in complete melting of the uranium. The correlated data on extent of the uranium-water reaction as a function of energy showed the following (for reactor periods of approximately 100 msec):

Fission energy input, cal/g of U	U-H_2O reaction, %	Chemical energy, cal/g of U	Energy ratio (chemical/nuclear)
50	0.4	2.4	0.048
100	2.4	14	0.104
150	5.0	30	0.200
200	8.9	53	0.265
300	23.8	142	0.473
450	50.0	298	0.662

The data obtained from the in-pile experiments on mixed-oxide- and cermet-core fuel pins were correlated as a function of the energy of the reactor burst in calories per gram of core in the fuel pin. The following tabulation summarizes the correlated results at three different energy bursts in the reactor for reactor periods of approximately 100 msec.

Type of fuel pin	Metal-water reaction,% At 300 cal/g of core	At 400 cal/g of core	At 500 cal/g of core	Reaction
Zircaloy-2-clad, mixed-oxide core	3.6	9.4	15.5	Zr-H_2O
90 wt.% 304 S.S.–10 wt.% UO_2 cermet	4.2	8.1	12.0	S.S.-H_2O
90 wt.% Al–10 wt.% U_3O_8 cermet	1.3	2.9	4.5	Al-H_2O
304 S.S.-clad, mixed-oxide core	0.0	0.1	0.6	S.S.-H_2O
Al-clad, mixed-oxide core	0.2	0.4	0.7	Al-H_2O

The uranium in these mixed-oxide- and cermet-core pins was 93 per cent enriched with U^{235}. The mixed-oxide core had the following composition: 81.5 wt.% zirconia, 9.1 wt.% calcia, 8.7 wt.% urania, and 0.7 wt.% alumina. The core pellets were 0.33 in. in diameter and were 0.50 in. long. The metal jackets had a 20-mil wall thickness.

From these comparisons on the high-temperature reactions of cladding metals with water, it appears that zirconium is the most reactive. Stainless-steel-cermet pins give more metal-water reaction than aluminum-cermet pins. For each of the three metals, the amount of reaction goes up as the burst becomes more energetic. It was also observed that the energy of the reactor burst which was required to cause failure (such as rupture or melting) of the oxide-core, metal-clad fuel pins depended on the metal used for the cladding. For example, a burst of 273 cal/g of core or more was needed, at a reactor period of 60 msec, to rupture an aluminum jacket; 301 cal/g of core caused the Zircaloy-2-clad, oxide-core pin to rupture and partially melt, whereas more than 395 cal/g of core was required to achieve partial destruction of the type 304 stainless-steel jacket. The peak adiabatic temperature at the center of the mixed-oxide core corresponds to 2550°C for an energy input of 395 cal/g of core with the fuel pin initially at 25°C.

Figure IV-2 summarizes the data that have been obtained to date on the in-pile studies of

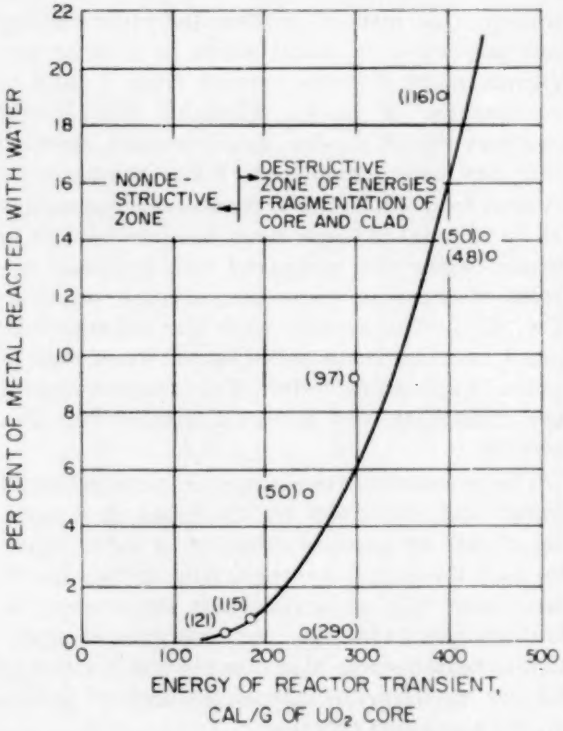

Fig. IV-2 Extent of stainless steel–water reaction resulting from in-pile meltdowns of urania-core fuel pins.[34] The UO_2 core was 20 per cent enriched, was clad with type 304 stainless steel, and had an 18-mil wall thickness. Numbers in parentheses near data points give the reactor period in milliseconds.

metal-water reactions for oxide-core, type 304 stainless-steel-clad fuel pins.

(A. W. Lemmon, Jr.)

Radiation Effects in Nonfuel Materials

Defects: Structure and Properties

Metals. Workers at Hanford[36] in extending their studies of fission tracks in various materials have succeeded in observing tracks in bulk aluminum. A high-purity aluminum plug (~0.25 in. on a side) was mechanically polished and then chemically polished in Alcoa R5 Bright Dip. Various thin layers of plastic and carbon were applied to the specimens, and a 100-A film of UO_2 was evaporated on these strippable layers. The fissionable material was removed after an irradiation of 2×10^{16} nvt (thermal) by dissolving the plastic layer. Analysis of the sample by gamma-ray spectroscopy verified the presence of recoil products in the aluminum. Direct replicas were formed by evaporating carbon onto the platinum-shadowed aluminum. These replicas were removed with $HgCl_2$, which attacked the aluminum. The surface appeared to contain many small nodules, and a considerable number of these aligned themselves in a linear fashion that was similar to the previously reported results for thin films. Tracks of this type were also observed in prethinned aluminum foils that were irradiated to the same level. The track widths (a few hundred angstroms) were irregular and discontinuous, as previously reported for the thin films.

Neutron-irradiated copper crystals were etched and studied with replicas and electron microscopy.[37] Small pits were observed after an irradiation of 10^{18} neutrons/cm^2; these pits were interpreted as loops produced by about 10^{14} dislocations/cm^3. All traces of these pits were removed by annealing for 30 min at 400°C.

Simmons and Balluffi[38] have extended their measurements[39] of equilibrium vacancy concentrations at high temperatures to include gold. They are able to compare their results with other experiments in gold, and have determined a volume expansion of 0.45 ± 0.10 atomic volume per vacancy.

The number of atoms ejected from the surface of uranium metal by fission fragments leaving its surface has been measured over a considerable range of neutron doses.[40] The results indicate that the rate at which uranium is returned, by ejection from the collector to the parent uranium surface, becomes equal to the rate of evaporation from that surface when the collected layer is about 10,000 times thinner than the range of fission fragments in uranium. Possible mechanisms for reejection are discussed. Both the present and previously published experiments, when interpreted on this basis, indicate that the number of atoms ejected per escaping fission fragment is of the order of 2000. The exact nature of the surface in all the experiments reviewed did not appear to cause a significant change in this number. This interpretation is believed to be quite different from that given in previously published work of others.

R. S. Barnes[41] has summarized his results on atomic displacements and impurity effects in fissile metals. Grenall's[42] discussion of electron-microscope observations of fast-neutron damage in gold films is accompanied by an explanation developed with Brinkman et al.[43] Makin[44] et al. have studied the formation of dislocation loops in copper during neutron irradiation.

Defects in Other Materials. Fission-recoil tracks in mica have been stabilized by etching in HF before observation in the electron microscope.[45] Sensitivity is also improved by this etching, so that previously unobservable regions of the track are seen. In bulk micas of various types, the track densities vary and indicate that only recoils from the heavy elements present in the mica (e.g., iron and potassium) contribute to the track density. An observed difference in proton-irradiated micas between muscovite ($\sim 8 \times 10^{-8}$/cm^2 per p/cm^2) and synthetic mica ($\sim 4 \times 10^{-9}$/cm^2 per p/cm^2) is explained by the presence of 1.5 wt.% iron in the natural crystal.

Lattice defects produced by fission recoils in natural graphite were identified by studying xenon-gas release.[46] Heating the specimens revealed four peaks in the gas-release curve (not observed in artificial graphite). These four peaks were associated with the recovery of interstitial clusters, single vacancies, combinations of single vacancies, and divacancies, respectively.

Bridge et al.[47] have presented an extensive report on their studies of stored energy and

dimensional changes in fast-neutron-irradiated graphite. Doses up to 10^{21} neutrons/cm^2 and temperatures from 30 to 300°C were used. The first part of the report presents data on the stored energy associated with irradiation-induced defects, the rate of increase of damage as measured by the total stored energy, and the release of stored energy at various temperatures. Results have been obtained on the effect on stored energy of thermal annealing, reirradiation after thermal annealing, and irradiation annealing. These annealing results can be described by a phenomenological modification of the Vand model of thermal annealing in disordered metal films. The second part of the report presents data on the changes in lattice parameter and associated dimensional changes in polycrystalline reactor graphite. Reasonable agreement with the theories of irradiation growth is reported. Reynolds and Simmons[48] have also reported on high-flux neutron damage in graphite. A rather comprehensive picture is presented, together with the data of others that they quote.

Fast-neutron-irradiation-induced expansions in BeO result in volume changes[15] of from 0.57 to 1.7 per cent (various types of BeO) at dosages in the range of 2×10^{20} neutrons/cm^2. This expansion exceeds the expected values, as calculated from lattice-parameter changes, at these doses by about a factor of 2.

Observations of the fractional length changes produced by 2-Mev-electron irradiation of germanium and silicon are also much less than would have been expected from previous results for deuteron and neutron irradiations.[49] The fractional length increase, $\Delta L/L$, is of the order of 10^{-26}/2-Mev electron/cm^2. Assuming simple displacement theory ($E_d = 30$ ev for germanium and 28 ev for silicon) and no annealing results in concentrations of displaced atoms of the order 10^{-3}, with corresponding fractional atomic volume changes per interstitial vacancy of $(f_i + f_v) = 0.008 \pm 0.021$ for germanium and 0.002 ± 0.011 for silicon. Calculations of cluster-size distributions indicate that the volume change per defect is nonlinear; therefore the volume change increases as the cluster size increases.

The variation in conductivity and Hall mobility of n type germanium after neutron bombardment was analyzed in terms of a disordered-region model of lattice damage.[50] The observed changes could be accounted for if the neutron damage resulted in disordered zones about 200 A in diameter. (T. G. Knorr)

Theories of Radiation Effects

Flynn[51] has presented an extensive discussion of effects of vacancies and complexes in noble metals. Resistivity changes that account for lattice relaxations can be calculated by assuming a particular model for the scattering power of the vacancy. The use of this same model yields satisfactory results for formation energies. From these calculations, electron densities near the vacancies can be deduced, and hence interactions among various defects can be calculated by studying the interaction of these electron densities.

Barnes[52] has suggested a simple model for explaining the behavior of point-defect clusters in irradiated metals. This model, where clusters of interstitial atoms compete with the equivalent number of vacancies left in the crystal for subsequent interstitial atoms, is used to discuss the rate of accumulation of the vacancies and the conditions governing the size of the interstitial-atom clusters. Recombination becomes important at an interstitial-cluster size that is dependent upon the relative interaction distances of interstitial atoms with vacancies and dislocation lines. Varley[53] reports on the agglomeration into clusters of interstitial atoms and vacancies generated by fast-neutron irradiation.

Calculations have been made of the number of instances of lattice damage due to irradiation with high-energy particles.[54] The assumption incorporated here was that the atoms responsible for the displacements due to collision may be captured in the lattice sites of the displaced atoms.

Brinkman[55] has added to his theory of the damage produced by fission fragments in metals. The number and spatial distribution of interstitials, vacancies, and displacement spikes are considered, as well as the role these defects have in producing various effects in the metals. A new empirical atomic-interaction potential is proposed. Comparison with experiments shows that this theory gives reasonably accurate predictions of the number of Frenkel defects produced per fission event, the total volume of displacement spikes per fission event, and the average size of these displacement spikes.

Amar[56] has revised previous calculations for the formation energy of a vacancy in copper. The previously reported value was about 1 ev. The present report shows that corrections are necessary to the contributions of the electrostatic self-energy and the Fermi energy of the valence electrons. These changes result in a value of about 2 ev per vacancy.

The equation for the kinetics of vacancy-interstitial annihilation with interstitial trapping at impurities has been solved in closed form.[57] Although the transients are given by rather complex combinations of exponentials, the later part of the decay is simply quadratic. This quadratic decay is governed by the decomposition of the interstitial-impurity complex. The effective activation energy is the sum of the interstitial migration energy and its binding energy to the impurity. The equations for the kinetics of vacancy-interstitial annihilation with di-interstitial formation have been solved on an analog computer for either high or low di-interstitial binding energies.[58] For high energy (low temperature) the decomposition reaction can be negative. Analytical approximations have been found and are shown to be valid in this case. Conventional methods of activation-energy determinations are valid in this region for evaluating the interstitial migration energy. As for low binding energies (high temperature), the di-interstitial concentration can be neglected, and the resulting kinetics is the simple quadratic interstitial-vacancy annihilation, governed by the interstitial-migration energies. For intermediate binding energies no analytical approximations have been found as yet.

Calculations of the mobility of vacancy pairs in ionic crystals indicate an activation energy for migration equal to or greater than that for a single vacancy.[59] These conclusions imply the necessity for a revision of the theories involving color centers at low temperatures. Various potentials were used to represent the closed-shell interactions. These potentials consisted of the modification made to the Born-Mayer potential by Verwey (B-M-V), then by Tosi and Fumi (B-M-T-F), and finally by Dienes (B-M-D). Comparisons with the activation energies for single-vacancy migrations were made in terms of Guccione's calculations (see Table IV-2). Contributions due to coulombic interactions, closed-shell repulsions, and polarization are compared in the report for the two defects. (T. G. Knorr)

Table IV-2 ACTIVATION ENERGIES[59] FOR THE MOTION OF IONS INTO VACANCY PAIRS IN NaCl AND KCl

(The Comparison Values for Motions into Single Vacancies Are in Parentheses; E_f Is the Formation Energy of the Vacancy Pair)

Moving ion	ΔE, ev	Potential	E_f, ev
Na^+ in NaCl	1.46 (0.87)	B-M-V	1.27
Cl^- in NaCl	1.27 (1.11)	B-M-V	1.27
K^+ in KCl	1.30 (1.13)	B-M-V	1.28
Cl^- in KCl	1.15 (1.18)	B-M-V	1.28
Cl^- in KCl	0.91	B-M-T-F	1.24
Cl^- in KCl	0.89 (0.64)	B-M-D	1.19

Surveys on Radiation-Induced Defects

A general survey report[60] on the mechanical properties of irradiated stainless steels has been prepared.

Radiation effects in inorganic solids was the subject of a symposium[61] held at Saclay on Apr. 11 and 12, 1961. Reprints of the papers presented appear in the *Discussions of the Faraday Society*. The proceedings of the 4th International Symposium on the Reactivity of Solids,[62] held in Amsterdam from May 30 through June 4, 1960, are also of general interest. The reprints of the papers presented at the International Conference on Chemical Physics of Nonmetallic Crystals,[63] which was held at Northwestern University from Aug. 28 to 31, 1961, are likewise of some general interest. (T. G. Knorr)

Effects of Radiation on Mechanical Properties

Radiation-induced property changes in structural materials are known to play an important part in the service life of reactor components. Oak Ridge[64] has tested a group of Izod impact specimens that were a part of a materials surveillance program for the pressure vessel of the SM-1 reactor. The specimens were fabricated from ASTM A-212 grade B steel that was used in the vessel. These samples were irradiated in the SM-1 reactor to a 16.4-Mw-year exposure of the SM-1 core. The fast-neutron equivalence of this exposure is not given. The specimens had been positioned at various heights above the center of the reactor core, thus receiving different total exposure to neutrons. The samples in the vicinity of the center line of the core received the largest total flux. The

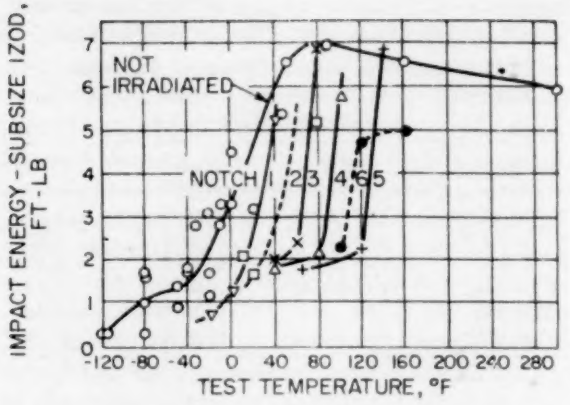

Fig. IV-3 Results of impact energy tests on surveillance specimens of ASTM A-212 grade B steel from SM-1 pressure-vessel material after an exposure of 16.4 Mw-years in the SM-1 core.[64]

increase in brittle-to-ductile transition temperature was greatest for those samples near the center of the core (Fig. IV-3). The effects of increasing total neutron fluxes are shown by the curves, which are numbered consecutively to indicate the flux of 1 > 2 > 3, etc. Studies have been made[65] of the notch ductility of ASTM A-212 grade B carbon-silicon steel for two conditions: (1) synthetic weld-heat-affected materials that correspond to energy inputs of 100,000 and 50,000 joules/in. and (2) unaffected parent-metal plate. This study included tests on materials in both the irradiated and unirradiated conditions. The Charpy V-notch impact specimens were irradiated to about 8.8×10^{18} neutrons/cm^2 at approximately 120°F. The influence of irradiation on the transition temperature is illustrated in Fig. IV-4. The major difference between heat-affected zones appeared to be the ferrite network. The network was discontinuous in the 4B series and continuous in the 2B series. The effect of irradiation on the parent base metal is shown in Fig. IV-5, and the results are summarized in Table IV-3.

The effect of neutron irradiation on the notch ductility of ASTM A-212 grade B for a specialized pressure-vessel application[66] was investigated also. Charpy V-notch impact samples were cut from steel that was formed at 2200°F from 6½-in., aluminum-killed, rolled slab. The material was normalized at 1650°F, spray quenched, and stress relieved for 7 hr at 1125°F. These samples were irradiated in the Oak Ridge Research Reactor for 23 days at approximately 500°F. The fast-neutron dose (>1 Mev), the irradiation temperature, and the increase in brittle-to-ductile transition temperature are shown in Figs. IV-6 and IV-7. The unirradiated control samples were given the same thermal treatment, 23 days at 500°F, as those in the reactor.

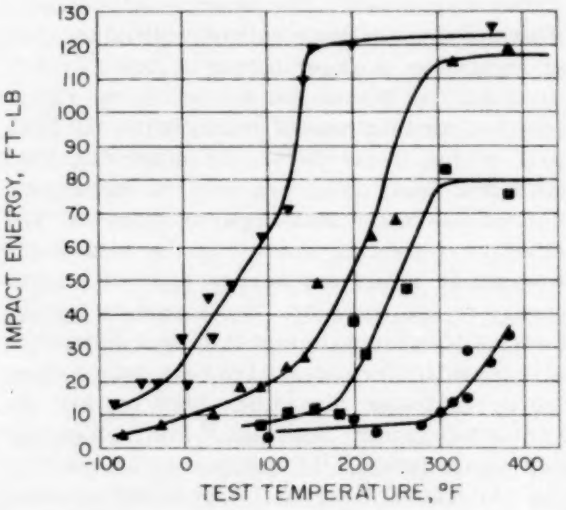

Fig. IV-4 Charpy V-notch impact tests of irradiated, synthetic, heat-affected zones in ASTM A-212 grade B steel.[65] ●, irradiated 2B series. ■, irradiated 4B series. ▲, irradiated 2B series, 100,000 joules/in. ▼, irradiated 4B series, 50,000 joules/in. Flux: 2.2×10^{12} neutrons/(cm^2)(sec) (>1 Mev); dose: 8.8×10^{18} neutrons/cm^2 (>1 Mev); irradiation temperature: ~120°F.

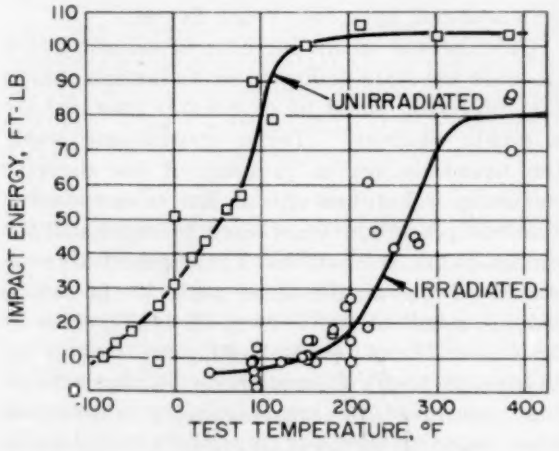

Fig. IV-5 Charpy V-notch impact tests of irradiated ASTM A-212 grade B steel base plate.[65] Flux: 2.2×10^{12} neutrons/(cm^2)(sec)(>1 Mev); dose: 8.8×10^{18} neutrons/cm^2 (>1 Mev); irradiation temperature: ~120°F.

An investigation of the effect of specimen size and rate of loading on the transition temperature of irradiated Conlo I was carried out by the British.[67] Notched specimens that were 2 by $2^3/_4$ by 20 in. and standard Charpy V-notch specimens were irradiated in the Calder Hall reactor at about 156°C. Sulfur dosimeters were used, and total fluxes of 8.8×10^{18} neutrons/cm^2 for the large specimens and 8.1×10^{18} neutrons/cm^2 for the Charpy bars were indicated. Radiation produced an increase in ductile-to-brittle transition temperature of 110°C for the large specimens and 75°C for the standard Charpy, indicating an influence of specimen size. A similar effect of size was not noted for differences in notch ductility produced by a normalizing heat-treatment.

Several nickel-base alloys, including Inconel X, Hastelloy X, and René 41, and type A-286 stainless steel have been investigated by General

Table IV-3 EFFECT OF NEUTRON IRRADIATION AT 90 TO 130°F ON FRACTURE-TRANSITION TEMPERATURE OF ASTM A-212 GRADE B STEEL[65]

[Neutron Dose: 6×10^{18} neutrons/cm^2 (>1 Mev)]

Material	Transition temp., °F		
	10 ft-lb criterion	30 ft-lb criterion	50% of ductile-energy criterion
Series 2B (100,000 joules/in.):			
Unirradiated	20	150	200
Irradiated	295	365	>400
Increase	275	215	>200
Series 4B (50,000 joules/in.):			
Unirradiated	−100	10	90
Irradiated	140	215	270
Increase	240	205	180
Parent plate:			
Unirradiated	−80	−5	60
Irradiated	150	230	270
Increase	230	235	210

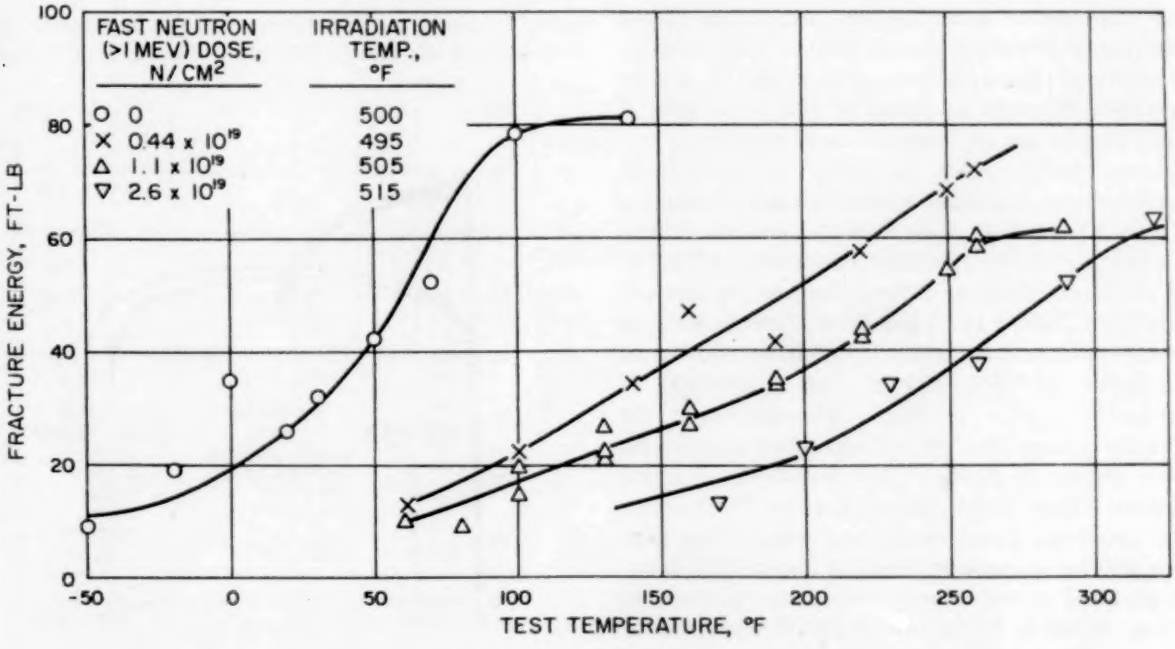

Fig. IV-6 Charpy V-notch impact-specimen fracture energy versus test temperature for various fast-neutron (>1 Mev) doses.[66] Data are for A-212 grade B steel.

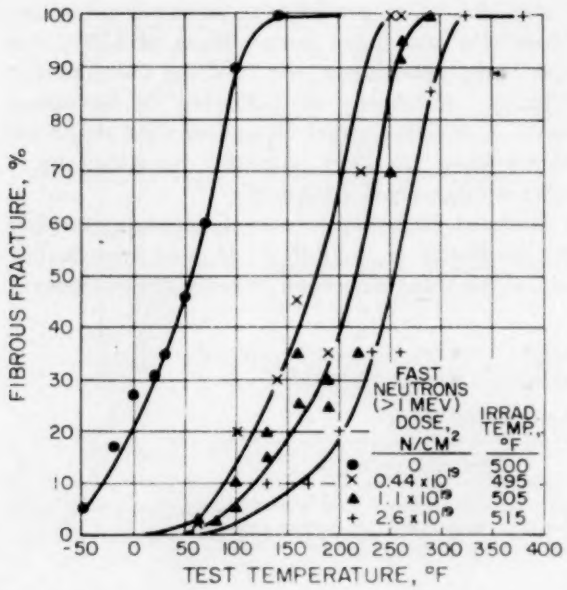

Fig. IV-7 Percentage of fibrous fracture in Charpy V-notch impact specimen versus test temperature for various fast-neutron (>1 Mev) doses.[66] Data are for A-212 grade B steel.

Electric.[68] These materials were irradiated at several elevated temperatures and to total doses ranging from 3×10^{18} to 2×10^{21} neutrons/cm^2. It is reported that the 100-hr rupture strength of Inconel X at 1200°F after irradiation is decreased about 50,000 psi. Type A-286 stainless steel that was irradiated under similar conditions also showed a decrease in 100-hr rupture strength of about 40,000 psi at 1200°F and 20,000 psi at 1000°F. Both materials appeared to be notch sensitive and to exhibit brittle type fracture. Postirradiation annealing (1200°F) did not cause any appreciable change in properties of samples irradiated at 140°F. The results of these stress-rupture studies are given in Tables IV-4 and IV-5. Tensile tests at room temperature after irradiation showed an increase in yield strength but a decrease in ultimate tensile strength. Summaries of the tensile properties before and after irradiation are shown in Tables IV-6 and IV-7. A more recent report from General Electric[22,69] on work in progress gives early data which show that the 100-hr rupture strength of type A-286 stainless steel in the overaged condition is reduced from 93,000 to 81,000 psi at 540°C. Reduction of thermal flux by shielding was used to study the effect of small amounts of boron transmutation on the properties of irradiated type A-286 stainless steel. A limited number of tests conducted at 650°C showed no significant difference between shielded and unshielded test samples.

The influence of B^{10} transmutation products on the creep properties of Inconel during irradiation has been studied at Oak Ridge.[65] When all data were analyzed with respect to B^{10} concentration, the results did not support the concept that the rupture strength of Inconel is impaired by helium that is generated during thermal-neutron bombardment of B^{10}. Results of tests conducted at 1500°F are shown in Table IV-8.

Studies of irradiated Zircaloy-2 have been made at Hanford.[70] Room-temperature burst tests performed on a Zircaloy-2 tube removed from the KER-3 after about two years of service showed that, as a result of the exposure, burst pressure increased from 16,700 to about 18,700 psi, which corresponds to a change from 108,000 to 116,000 psi in hoop stress. The fracture of the control sample initially propagated through the wall by cleavage and progressed along the length by shear, whereas that of the irradiated sample appeared to have propagated by 100 per cent cleavage.

In a nuclear reactor, Zircaloy-2 showed a creep rate of 1 to 2×10^{-7}/hr, whereas a control sample run in standard creep-test apparatus showed a strain rate of 1×10^{-6} to 9×10^{-7}/hr. The strain that occurred during shutdown accounted for about 75 per cent of the

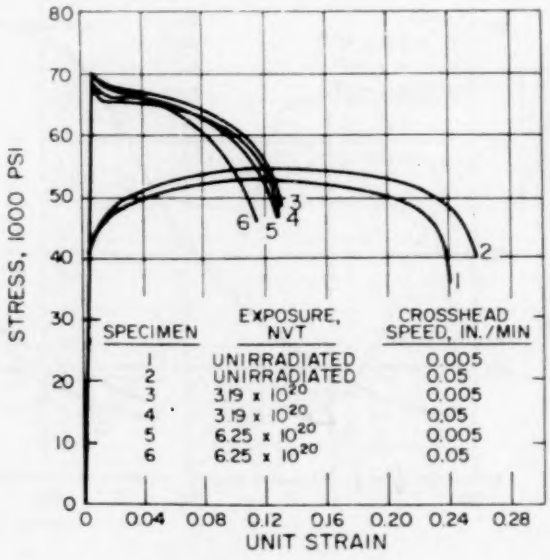
STRESS, 1000 PSI
UNIT STRAIN
SPECIMEN EXPOSURE, NVT CROSSHEAD SPEED, IN./MIN
1 UNIRRADIATED 0.005
2 UNIRRADIATED 0.05
3 3.19 x 10²⁰ 0.005
4 3.19 x 10²⁰ 0.05
5 6.25 x 10²⁰ 0.005
6 6.25 x 10²⁰ 0.05

Fig. IV-8 Typical stress-strain curves[36] for unirradiated and irradiated Zircaloy-2.

Table IV-4 STRESS-RUPTURE MEASUREMENTS[68] OF INCONEL X

Sample No.	Type*	Irradiation conditions: Dosage, neutrons/cm² (≥1 Mev)	Irradiation conditions: Temp., °F	Premeasurement treatment†	Measurement conditions: Temp., °F	Measurement conditions: Stress, 1000 psi	Rupture life, hr	Fracture location	Elongation, %
Heat 436X:									
	C	Nonirradiated			1200	82	98.8	Gauge	12.5
	C	Nonirradiated			1200	82	72.4	Gauge	7.1
	S	Nonirradiated			1200	83	45.8	Fillet	
4B	S	7×10^{20}	140–200	Yes	1200	82	0.06	Fillet	2.0
5B	S	7×10^{20}	140–200	Yes	1200	50	11.2	Fillet	0.7
10B	S	7×10^{20}	140–200	None	1200	60	1.4	Fillet	1.02
21B	S	7×10^{20}	140–200	None	1200	45	2.4	Gauge	1.6
12B	S	7×10^{20}	140–200	None	1200	40	Broke on loading	Fillet	0.03
17B	S	7×10^{20}	140–200	None	1200	35	6.4	Fillet	0.8
30B	S	7×10^{20}	140–200	None	1200	35	12.6	Gauge	1.0
29B	S	7×10^{20}	140–200	None	1200	20	22.3	Fillet	0.86
48B	S	7×10^{20}	140–200	None	1200	15	>900	Gauge	0.95
2	S	3×10^{18}	140–200	Yes	1200	82	0.2	Gauge	
1	S	3×10^{18}	140–200	None	1200	82	0.04	Fillet	
3	S	3×10^{18}	140–200	None	1200	50	104.7	Fillet	
6	N	3×10^{18}	140–200	None	1200	36	129.1	Notch	
7	N	3×10^{18}	140–200	None	1200	31	432.8	Notch	
Heat 8376:									
	S	Nonirradiated			1500	17.5	138	Gauge	
	S	Nonirradiated			1350	45	91	Gauge	
	S	Nonirradiated			1200	70	50	Gauge	
	S	Nonirradiated			1100	85	142	Gauge	
	S	Nonirradiated			1200	75	61.6	Gauge	2.66
	S	Nonirradiated			1200	70	50	Gauge	
	N	Nonirradiated			1200	70	106	Notch	
32F	S	3×10^{18}	1200	None	1200	82	0.05		
33F	S	3×10^{18}	1200	None	1200	30	69.6	Fillet	
10G	C	3×10^{18}	1200	None	1200	82	Broke on loading	Notch	
8G	C	3×10^{18}	1200	None	1200	40	1.03	Notch	
Heat 436X:									
7B	S	7×10^{20}	140–200	Yes	1000	80	41.1	Fillet	1.3
38B	S	7×10^{20}	140–200	Yes	1000	80	4.2	Fillet	1.5
11B	S	7×10^{20}	140–200	None	1000	70	1.7	Fillet	1.02
15B	S	2×10^{19}	1110	None	1110	60	0.2	Gauge	0.95
44B	S	2×10^{19}	1110	None	1110	30	60.5	Gauge	0.68
9B	S	2×10^{19}	1110	None	1000	70	0.07	Fillet	0.6
37B	S	2×10^{19}	1110	None	1000	60	1.9	Fillet	0.98
22B	S	2×10^{19}	1030	None	1000	80	0.6	Gauge	0.76
35B	S	2×10^{19}	1030	None	1000	70	3.2	Gauge	0.98
6C	C	2×10^{19}	600	None	1000	50	63.8	Notch	2.20
8	C	3×10^{18}	140–200	None	1000	60	200.3	Notch	
Heat 8376:									
9G	C	3×10^{18}	1200	None	1000	40	331.1	Notch	

*S = smooth; N = notched; C = combination.

†Premeasurement treatment consisted of 24 hr of exposure at the measurement temperature.

Table IV-5 STRESS-RUPTURE MEASUREMENTS[68] OF A-286 STAINLESS STEEL

Sample No.	Type*	Irradiation conditions: Dosage, neutrons/cm² (≥1 Mev)	Irradiation conditions: Temp., °F	Premeasurement treatment†	Measurement conditions: Temp., °F	Measurement conditions: Stress, 1000 psi	Rupture life, hr	Fracture location	Elongation, %
Heat B12878:									
	S	Nonirradiated			1200	65	20.75	Gauge	
	S	Nonirradiated			1200	65	21.3	Gauge	
	C	Nonirradiated			1200	65	26.3	Gauge	11.6
10A	S	7×10^{20}	140–200	Yes	1200	30	74	Fillet	2.5
12A	S	7×10^{20}	140–200	Yes	1200	30	978	Gauge	
23A	S	7×10^{20}	140–200	Yes	1200	50	93.8	Gauge	0.7
24A	S	7×10^{20}	140–200	Yes	1200	45	28.6	Gauge	1.6
25A	S	7×10^{20}	140–200	None	1200	50	36.9	Fillet	1.0
6D	S	$\sim 2 \times 10^{19}$	1110	None	1200	60	0.1	Gauge	0.9
18	S	3×10^{18}	140–200	Yes	1200	65	0.27	Fillet	
16A	S	3×10^{18}	140–200	Yes	1200	61	1.8	Fillet	
27A	S	3×10^{18}	140–200	Yes	1200	65	1.2	Gauge	
19	S	3×10^{18}	140–200	None	1200	65	1.7	Fillet	
11	C	$\sim 2 \times 10^{19}$	600	None	1200	25	0.1	Notch	0.85
17	C	$\sim 2 \times 10^{19}$	600	None	1200	20	0.02	Notch	0.45
13	C	3×10^{18}	140–200	Yes	1200	41	0.3	Notch	
14	C	3×10^{18}	140–200	Yes	1200	25	38.1	Notch	
15	C	3×10^{18}	140–200	Yes	1200	20	20.4	Notch	
27	N	3×10^{18}	140–200	Yes	1200	19	731	Notch	
Heat C2527:									
	C	Nonirradiated			1200	77	2.1	Gauge	8.2
	C	Nonirradiated			1200	65	65.7	Gauge	0.5
	C	Nonirradiated			1200	65	36.8	Gauge	6.2
	S	Nonirradiated			1200	65	62.0	Gauge	7.65
34L	S	3×10^{18}	1200	None	1200	60	0.06	Fillet	
32L	S	3×10^{18}	1200	None	1200	30	1.95	Fillet	
56L	C	3×10^{18}	1200	None	1200	60	0.3	Notch	
55L	C	3×10^{18}	1200	None	1200	20	0.74	Notch	
54L	C	3×10^{18}	1200	None	1200	10	1226		
Heat B12878:									
	S	Nonirradiated			1000	90	236.1	Gauge	
	N	Nonirradiated			1000	90	414.7	Notch	
25	S	7×10^{20}	140–200	None	1000	80	289.9	Fillet	1.3
26A	S	7×10^{20}	140–200	Yes	1000	80	56.1	Gauge	1.5
10D	S	2×10^{19}	1030	None	1000	80	52.1	Gauge	0.8
8D	S	2×10^{19}	1030	None	1000	70	8.1	Fillet	0.7
4D	S	2×10^{19}	1030	None	1000	65	144.9	Fillet	0.44
12D	S	2×10^{19}	1030	None	1000	60	19.1	Fillet	0.56
2D	S	2×10^{19}	1110	None	1100	65	0.3	Gauge	4.6
21	S	3×10^{18}	140–200	None	1000	90	132.6	Fillet	
13A	S	3×10^{18}	140–200	Yes	1000	90	71.1	Gauge	
9	C	2×10^{19}	600	None	1000	65	1.1	Notch	1.3
12	C	2×10^{19}	600	None	1000	75	33.2	Notch	1.0
10	C	2×10^{19}	600	None	1000	70	19.8	Notch	0.1
31	N	3×10^{18}	140–200	None	1000	73	72.6	Notch	

*S = smooth; N = notched; C = combination.

†Premeasurement treatment consisted of 24 hr of exposure at the measurement temperature.

Table IV-6 TENSILE PROPERTIES[68] OF INCONEL X, HEAT 436X

Sample type	Irradiation conditions: Dosage, neutrons/cm² (≥1 Mev)	Irradiation conditions: Temp., °F	Premeasurement treatment	Measurement temp., °F	Strength, 1000 psi: Yield (0.2% offset)	Strength, 1000 psi: Ultimate tensile	Elongation in 1 in., %	Reduction of area, %
Smooth	Nonirradiated		None	70	114.0	168.5	25.5	35.0
Smooth	Nonirradiated		None	70	113.8	169.5	21.0	34.7
Smooth	Nonirradiated		None	800	95.0	146.8	19.0	31.4
Smooth	Nonirradiated		None	800	91.0	145.5	20.0	27.3
Smooth	Nonirradiated		None	1000	88.0	146.2	18.5	29.8
Smooth	Nonirradiated		None	1000	95.0	148.3	21.0	29.8
Smooth	Nonirradiated		None	1200	86.8	131.0	21.5	13.5
Smooth	Nonirradiated		None	1200	103.2	136.5	15.7	12.0
Notched	Nonirradiated		None	70		200		
(K_t = 3.4)	Nonirradiated		None	800		130		
(K_t = 3.4)	Nonirradiated		None	1000		140		
(K_t = 3.4)	Nonirradiated		None	1200		128		
Smooth	2×10^{20}	140–200	None	70	157.4	162.3	6.4	29.8
Smooth	2×10^{20}	140–200	24 hr at 800°F	800		146.3	12.0	15.7
Smooth	2×10^{20}	140–200	24 hr at 800°F	800		147.1	5.0	13.2
Smooth	2×10^{20}	140–200	24 hr at 800°F	800		144.5	4.0	14.3
Smooth	2×10^{20}	140–200	None	1000	130.9	137.9	Nil	8
Smooth	2×10^{20}	140–200	None	1000	130.9	137.5	Nil	6.6
Smooth	2×10^{20}	140–200	24 hr at 1000°F	1000		127.5	2.0	7.4
Smooth	2×10^{20}	140–200	None	1200	101.7	105.9	Nil	2.5
Smooth	2×10^{20}	140–200	24 hr at 1200°F	1200	113.2	113.2	Nil	2.5
Notched	2×10^{20}	140–200	None	1200		79.6		
Notched	2×10^{20}	140–200	24 hr at 1200°F	1200		80.6		

Table IV-7 TENSILE PROPERTIES[68] OF A-286 STAINLESS STEEL, HEAT B12878

Sample type	Irradiation conditions: Dosage, neutrons/cm² (≥1 Mev)	Irradiation conditions: Temp., °F	Premeasurement treatment	Measurement temp., °F	Strength, 1000 psi: Yield (0.2% offset)	Strength, 1000 psi: Ultimate tensile	Elongation in 1 in., %	Reduction of area, %
Smooth	Nonirradiated		None	70	134.0	164.7	24	53.8
Smooth	Nonirradiated		None	70	113.0	163.2	23.5	53.8
Smooth	Nonirradiated		None	800	107.8	143.6	14.5	46.3
Smooth	Nonirradiated		None	800	103.6	144.0	12.5	40.5
Smooth	Nonirradiated		None	1000	108.8	136.0	9.0	13.9
Smooth	Nonirradiated		None	1000	106.0	136.0	12.0	17.2
Smooth	Nonirradiated		None	1200	103.6	111.0	8.0	12.4
Smooth	Nonirradiated		None	1200	101.0	108.5	4.0	6.6
Notched	Nonirradiated		None	70		228.2		
(K_t = 3.4)	Nonirradiated		None	800		202.2		
(K_t = 3.4)	Nonirradiated		None	1000		191.0		
(K_t = 3.4)	Nonirradiated		None	1200		179.0		
Smooth	2×10^{20}	140–200	None	70	139.8	148.3	6.3	11.9
Smooth	2×10^{20}	140–200	24 hr at 1000°F	1000	111.0	130.0	6.3	10.7
Smooth	2×10^{20}	140–200	None	1200	91.1	111.0	2.5	2.5
Smooth	2×10^{20}	140–200	24 hr at 1200°F	1200	115.7	115.7	2.0	5.0
Notched	2×10^{20}	140–200	None	1200		75.5		

Table IV-8 EFFECT OF NEUTRON BOMBARDMENT ON THE STRESS-RUPTURE CHARACTERISTICS OF "BORON-ADJUSTED" HEATS OF INCONEL TESTED AT 1500°F IN AIR[65]

Material	Boron content	Specimen	Stress, psi	Time to rupture, hr
0B	<10 ppm, natural B	29-8	4500	252
		29-3	3700	666
2B	20 ppm, natural B	29-5	4500	151
		29-9	4000	123
10B	100 ppm, natural B	29-2	4500	98
		29-6	3750	186
6B11	60 ppm, 98% B^{11}	29-1	3500	339
		29-7	3000	684
6B10	60 ppm, 95% B^{10}	29-4	3250	372
		29-10	2600	360

total creep strain observed. Other studies conducted by Hanford[36] included irradiation of Zircaloy-2 samples to 3.19 and 6.25×10^{20} neutrons/cm^2. Room-temperature tensile tests made on irradiated Zircaloy-2 at two strain rates, 0.005 and 0.05 in./min crosshead speeds, showed considerable loss of uniform plastic strain with neutron exposure. Uniform elongation was essentially zero at 1×10^{20} neutrons/cm^2. The data are shown in Table IV-9 and Fig. IV-8.

The French report[71] that sintered aluminum powder (SAP) showed an increase in hardness of about 4 and 5 per cent after exposure to 2×10^{18} and 1×10^{19} neutrons/cm^2, respectively. The ultimate tensile strength showed no change at room temperature after irradiation of 4×10^{18} neutrons/cm^2. The elongation, however, was decreased about 8 per cent.

Several summaries of irradiation effects in structural materials have been issued. One contains 85 references and an annotated bibliography that abstracts an additional 450 articles.[72] Savannah River[60,73] has issued summaries of irradiation effects in plain-carbon and low-alloy steels and stainless steels. These cover quite well the data generated as of Dec. 30, 1961. (F. R. Shober)

Selected Mechanical Properties of Cladding and Structural Materials

Creep Rupture of SAP Alloys

A program to determine the effect of long-time exposure (to 20,000 hr) on the creep-rupture strength of three SAP alloys, designated as M-583, SAP 895, and M-257, is being conducted at Battelle.[74] Preliminary tests from 1 to 1000 hr at 700, 800, and 900°F have been completed. The tests in progress will be continued in order to establish the short-time (to 1000 hr) stress-rupture properties of the SAP 895 and M-257 alloys. Because of a great deal of scatter in results, testing of the M-583 alloy has been discontinued.

Strength of Nickel-Base Alloys

A report by General Electric[75] presents, in graphical form, design data on Inconel X plate,

Table IV-9 CHANGE IN MECHANICAL PROPERTIES AND SMALL RATE EFFECT AS A FUNCTION OF EXPOSURE[36]

No. of specimens tested	Exposure, nvt (thermal)	Strain rate, in./min	Strength, 1000 psi: Yield (0.2% offset)	Strength, 1000 psi: Ultimate tensile	Elastic modulus, 10^6 psi	Total elongation, %
2	Unirradiated	0.05	$\frac{44.0}{42.5} = 1.04$	$\frac{55}{54} = 1.02$	$\frac{13.9}{16.6} = 0.84$	$\frac{26.9}{26.6} = 1.01$
2	Unirradiated	0.005				
1	6.95×10^{19}	0.05	$\frac{64.7}{60.1} = 1.08$	$\frac{66.4}{65.2} = 1.01$	$\frac{14.5}{13.8} = 1.05$	$\frac{24}{24} = 1.00$
4	6.95×10^{19}	0.005				
2	3.19×10^{20}	0.05	$\frac{70.5}{67.5} = 1.04$	$\frac{70.5}{68} = 1.03$	$\frac{13.1}{13.3} = 0.99$	$\frac{11.9}{13.1} = 0.91$
2	3.19×10^{20}	0.005				
2	6.25×10^{20}	0.05	$\frac{71.4}{68.6} = 1.04$	$\frac{71.4}{68.6} = 1.04$	$\frac{12.9}{13.3} = 0.97$	$\frac{11.6}{12.6} = 0.92$
2	6.25×10^{20}	0.005				

forged bar, and sheet; Hastelloy X sheet; and 19-9 DL sheet. Included are tensile, stress-rupture, and creep data and, to a limited extent, notch data in rupture.

The short-time stress-rupture properties of Hastelloy X were determined by General Atomic.[76] Figure IV-9 shows a plot of the experimental data obtained. The slopes of the plots shown increase with increasing temperature in the range 1200 to 1600°F. This trend is reversed between 1600 and 1700°F due to the onset of recrystallization. Between 1800 and 2000°F the slope again increases with temperature, but at 2100°F the trend is reversed for reasons unknown.

The strain-fatigue behavior of INOR-8 at 1300 and 1500°F is being evaluated by Oak Ridge.[32] The test results are shown in Fig. IV-10 with a plot of Coffin's equation:

$$N_f^{1/2}\,\epsilon_p = 1/2\,\overline{\epsilon}_f$$

where N_f is the number of cycles to failure, ϵ_p is the plastic-strain range, and $\overline{\epsilon}_f$ is the true fracture ductility. The tensile ductility at $N_f = 1/4$ was used as the intercept for these curves.

Further strain-fatigue tests, both mechanical and thermal, on tubular specimens from another heat of material are being conducted.

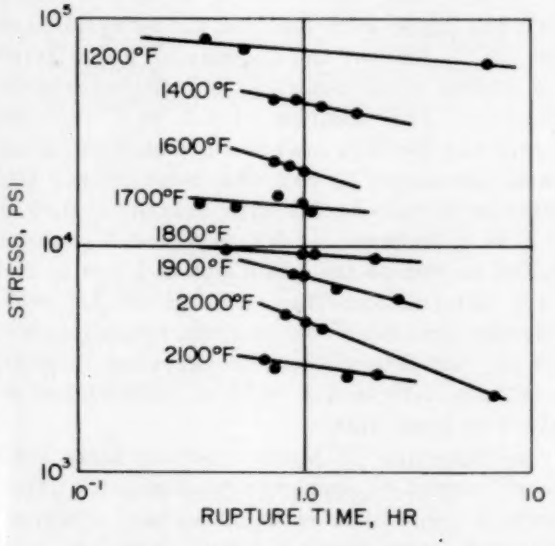

Fig. IV-9 Short-time stress-rupture properties of Hastelloy X in a helium atmosphere.[76]

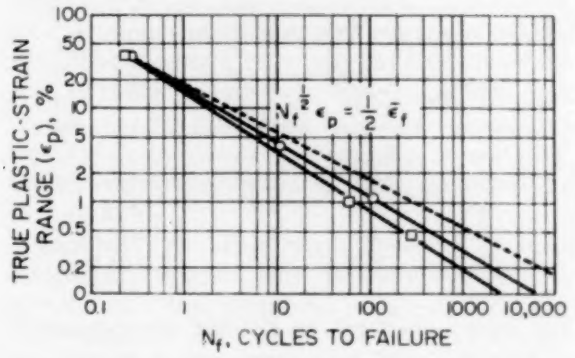

Fig. IV-10 Strain-fatigue curves[32] for INOR-8. ○, heat SP-25, 1300°F; □, heat SP-25, 1500°F, 40 cycles/hr.

Properties of Refractory Alloys

An extensive report covering research on tantalum-, tungsten-, and niobium-base alloys has been published by Union Carbide.[77] Two categories of properties that pertain to selected refractory-alloy systems are presented. A part of the report deals with alloys that were screened as to their usefulness as high-temperature structural materials. Measurements of hot hardness and oxidation resistance of arc-cast specimens delineated compositional areas within the tungsten-tantalum-niobium ternary systems in which alloys exhibited high hardness at 2900°F and improved oxidation resistance at 2190°F.

The second area reported deals with mechanical properties of tungsten or niobium at low and intermediate temperatures. The low-temperature yield properties of tungsten were studied (compression tests). Static strain aging of tungsten at 400 to 600°C was attributed to hydrogen. Dynamic strain aging of niobium-oxygen alloys occurred at 300 to 400°C, whereas the addition of titanium, zirconium, and vanadium to niobium was found to shift the strain-aging region to 700 to 800°C.

Bartlett and Schmidt[78] have reported the results of elevated-temperature tensile tests for the niobium–1 wt.% zirconium alloy. The material tested was about 10 per cent recrystallized prior to testing. The results as given in Table IV-10 show very rapid decreases in strength between 2000 and 2500°F. The falloff in strength between 2500 and 3000°F is much less rapid.

A study of tungsten- and molybdenum-base alloys for use at temperatures up to 2400°F

Table IV-10 TENSILE PROPERTIES OF NIOBIUM–1 WT.% ZIRCONIUM ALLOYS[78]

Temp., °F	Strength, 1000 psi		Elongation, %
	Yield	Ultimate	
RT	35.4	48.1	15
2000	20.7	22.8	14
2500	6.6	8.4	>48
2700	4.8	6.0	>44
3000	2.1	3.2	>41

has been completed by Climax Molybdenum.[79] In general, good high-temperature tensile and creep strengths were displayed by the following alloys: molybdenum–1.25 wt.% titanium–0.3 wt.% zirconium–0.15 wt.% carbon, molybdenum–25 wt.% tungsten–0.1 wt.% zirconium–0.03 wt.% carbon, and molybdenum–1.5 wt.% niobium–0.5 wt.% titanium–0.3 wt.% zirconium–0.3 wt.% carbon. Typical strength values are shown in Table IV-11.

Strengths of binary alloys of tungsten with 10, 30, or 50 wt.% molybdenum were below those of the better molybdenum-base alloys at 2400°F and below. It is postulated that the beneficial effects of tungsten-rich refractory alloys would be realized at higher test temperatures.

The results of studies on tungsten-nickel-iron alloys have been reported by Armour.[80] At 90 wt.% tungsten, highest room-temperature ductility occurred at nickel-iron ratios of 7 to 3 and 6 to 4. Impact tests conducted on V-notched 95 wt.% tungsten–3 wt.% nickel–2 wt.% iron specimens showed a marked increase in impact resistance between 250 and 350°F. Tensile data for ternary tungsten-nickel-iron alloys revealed a pronounced peak in elongation at about 750°F. The stress-rupture life at 1600°F increased as the iron level was raised; a 100-hr strength of 11,000 psi was noted for the 90 wt.% tungsten–4 wt.% nickel–6 wt.% iron alloy and a strength of about 9000 psi for the 90 wt.% tungsten–6 wt.% nickel–4 wt.% iron alloy.

Table IV-11 TENSILE STRENGTH OF MOLYBDENUM-BASE ALLOYS IN RECRYSTALLIZED CONDITION[79]

Composition	Temp., °F	Tensile strength, psi
Mo–1.25 Ti–0.3 Zr	1800	67,400
	2400	57,100
Mo–25 W–0.1 Zr–0.03 C	1800	45,300
	2400	26,900
Mo–1.5 Nb–0.5 Ti–0.3 Zr–0.3 C	1800	53,700
	2400	42,100

The addition of oxides of aluminum, magnesium, thorium, titanium, and zirconium as dispersion strengtheners failed to improve the long-time strength properties of the tungsten-nickel-iron base alloys. Additions of boron produced slight improvements in the 1600 and 2000°F stress-rupture properties. The additions of carbon, $CbAl_3$, TiAl, and several carbides proved to be detrimental to long-time elevated-temperature strength.

An addition-alloy system that contained 90 wt.% tungsten–2 wt.% molybdenum–0.5 wt.% ruthenium with a wide range of nickel-iron ratios was investigated. Alloys that contained 3 wt.% iron were exceptionally strong and ductile at room temperature, and they had 100-hr stress-rupture values of 12,000 to 14,000 psi at 1600°F. (J. A. DeMastry)

Selected Metallurgical Aspects of Cladding and Structural Materials

Aluminum Alloys

In an effort to eliminate the coarse-grained structure that results when aluminum alloys that are plated with aluminum are recrystallized at 500°C, Belyaev and Gol'shtein[81] investigated the effects of various alloying additions as grain refiners. The addition of 0.2 wt.% titanium prevented the formation of coarse-grained structure above 15 per cent deformation. The addition of 0.05 to 0.5 wt.% beryllium, 0.05 to 0.2 wt.% niobium, or 0.1 to 0.5 wt.% gallium failed to reduce the grain size at 1.5 to 15 per cent deformation. The addition of 0.2 wt.% rhenium prevented coarse-grain formation until 15 per cent deformation was exceeded. Smaller additions (0.05 to 0.1 wt.%) of rhenium had no effect on grain size.

Investigators at North Carolina State College[82] report on studies to determine the presence of cubic nitrides in 13 ternary systems. Ternary nitrides with a lattice of the $L'l_2$ type were observed in the following systems: cobalt-zinc-nitrogen, nickel-aluminum-nitrogen, and

nickel-zinc-nitrogen. In addition, γ' iron nitride dissolves appreciable amounts of aluminum and zinc so that the homogeneity range of this phase is extended into the ternary systems. Two cubic nitrides were found in the nickel-zinc-nitrogen system.

Specific Heat of INOR-8

The specific heat of annealed INOR-8 has been determined by direct calorimetric measurements at the University of Tennessee.[32] The value was observed to increase uniformly from 0.409 joule/(g)(°C) at 60°C to 0.483 joule/(g)(°C) at 540°C. At 550°C an anomalous rise of about 20 per cent in the specific heat was observed, reaching a maximum value of 0.586 joule/(g)(°C) at 610°C. Above this temperature the specific heat decreased to 0.578 joule/(g)(°C) at 700°C. The phenomenon has been attributed to an ordering reaction. The values for the specific heat are presented in Table IV-12.

Metallurgy of Refractory Alloys

The proceedings of a symposium on niobium metallurgy held at Bolton Landing, New York,[83] has been published. Thirty-three papers, which present a critical comparison of niobium with other materials for missile, aircraft, and nuclear applications, are included. The following topics are given special attention: fabrication, mechanical properties, general metallurgy, oxidation, and corrosion.

Single crystals of $NbZn_2$ were examined by the Naval Research Laboratory[84] using Weissenberg and precision methods. The unit cell was found to be hexagonal with Lave symmetry of $D6h$, with $a_0 = 5.05$ A and $c_0 = 16.32$ A. Examination of the structure factors for the most intense reflections showed that the observed structure factors were smaller in magnitude than the corresponding calculated values. Of particular interest is the unusually short Zn-Zn distance, the shortest observed being a Zn_{II}-Zn_{II} distance of 2.45 A.

Russian[85] workers have presented a constitutional diagram for ruthenium-chromium alloys with the following points of interest: Two liquid-phase reactions exist; they are liq + Ru $\rightleftharpoons$ σ at 1600°C and liq $\rightleftharpoons$ Cr + σ at 1470°C. At lower temperatures the chromium-base solid solution and the σ phase form Cr_3Ru. A two-phase region, σ + Ru, is found between the σ phase and the ruthenium-base solid solution. The solubility of chromium in ruthenium does not exceed 30 wt.% chromium and does not vary with temperature. In the ruthenium phase the hardness decreases from 970 to ≈350 kg/cm^2 as the composition is changed from 90 to 70 wt.% ruthenium.

Structure of Zirconium Alloys

The results of a preliminary investigation made at the University of Florida[86] indicate that twinning in a polycrystalline zirconium alloy that contains a small tin addition is highly dependent upon grain orientation. Twins appeared to form primarily in grains with basal planes nearly normal to the stress axis in tensile tests in which the strain rate was varied by a factor of 10^4. Slip was apparently the predominant deformation mode in grains, with basal planes nearly parallel to the stress axis. Slip and twinning in this polycrystalline mate-

Table IV-12 SPECIFIC HEAT[32] OF INOR-8

Temp., °C	C_p, joule/(g)(°C)	Temp., °C	C_p, joule/(g)(°C)	Temp., °C	C_p, joule/(g)(°C)
60	0.4090	320	0.4592	550	0.4922
80	0.4152	340	0.4616	560	0.5060
100	0.4207	360	0.4641	570	0.5226
120	0.4257	380	0.4666	580	0.5422
140	0.4303	400	0.4688	590	0.5637
160	0.4340	420	0.4710	600	0.5808
180	0.4370	440	0.4730	610	0.5858
200	0.4403	460	0.4749	620	0.5848
220	0.4439	480	0.4766	640	0.5825
240	0.4475	500	0.4781	660	0.5808
260	0.4510	520	0.4794	680	0.5792
280	0.4539	530	0.4805	700	0.5778
300	0.4566	540	0.4833		

rial appear to be cooperative deformation mechanisms rather than competitive. The most prevalent type of twin in this test was deduced to be the $\{10\bar{1}2\}$.

The solubility of oxygen in alpha zirconium in the temperature region 400 to 800°C was investigated by workers at the University of Stockholm,[87] utilizing X-ray techniques. The solubility, which is independent of temperature, was found to be 28.6 at.% $ZrO_{0.40}$. The length of the c axis increases with increasing oxygen content over the entire solubility range, whereas that of the a axis passes through a maximum at the composition $ZrO_{0.25}$. Two phases exist in the solubility range: ZrO_{0+x}, with randomly distributed oxygen atoms, and Zr_3O_{1+y}, with partly ordered oxygen atoms. The oxygen atoms are completely ordered (Zr_3O) at the limiting composition ($ZrO_{0.33}$).

(J. A. DeMastry)

Diffusion Studies

In the investigation of diffusion barriers for refractory metals being conducted at Manufacturing Laboratories,[88] which has been discussed in previous reviews in this series, screening tests at 1700°C have been continued, and similar tests at 1800°C have been initiated. On the basis of tests thus far, the 15 base-barrier metal combinations listed in Table IV-13 have been selected as promising. The arbitrary criteria being used in the studies pertain to the extent of interdiffusion between the base and barrier metals, the minimum melting point of the base-barrier alloy system, and the oxidation resistance of the barrier metal in conjunction with the extent of interdiffusion between the barrier metal and chromium, a potential protective-coating material. In future work the screening studies at 1700 and 1800°C will be completed, tungsten-base combinations will be evaluated at 1900 or 2000°C, and further investigations of interdiffusion in barrier-coating combinations will be conducted. Also, interdiffusion rates for selected combinations will be determined by measuring the growth kinetics of intermediate phases.

Table IV-13 TENTATIVE LIST OF 15 OPTIMUM BASE-BARRIER METAL COMBINATIONS[88]

Tungsten base	Molybdenum base	Tantalum base	Niobium base
W-Re	Mo-W	Ta-W	Nb-W
W-Ru	Mo-Re	Ta-Re	Nb-Re
W-Ir	Mo-V	Ta-Os	Nb-Os
W-Rh		Ta-Ru	Nb-Zr

Some information on the rate of diffusion and the diffusion zones formed in the niobium-silicon system is contained in a translation[89] of a Russian article on silicon-diffusion coatings for niobium. In this investigation the structure and phase composition of niobium that had been saturated with solid-phase silicon for 30 min to 15 hr at temperatures of 1100 to 1300°C were determined. Metallographic examinations and X-ray spectrum analyses of the local chemical compositions were conducted, and parameters for the diffusion of silicon into niobium were calculated. The phases observed were $NbSi_2$, Nb_5Si_3, and Nb_4Si. Diffusion processes that occurred in the grain boundaries of metals are discussed in an English translation of a Russian book.[90] In addition, this book includes interesting information on autoradiographic and radiographic techniques that are applicable to study of the distribution and diffusion of elements in metals, on the chemical inhomogeneity of alloys, and on the structure, thermodynamics, and properties of grain boundaries.

An investigation to determine the diffusion coefficients of niobium in pressed-and-sintered UO_2 pellets is in progress at Oak Ridge.[33] The experiments are being conducted by heat-treating a Nb^{95}-UO_2 couple, removing thin sections of measured thickness, and counting the Nb^{95} activity in each section. Results thus far indicate that, at 1500°C, the bulk diffusion coefficient of niobium in UO_2 is about four orders of magnitude larger than the reported value for diffusion of uranium in UO_2. The interdiffusion between graphite and type 304L stainless steel is also being studied at Oak Ridge.[65] A 0.030-in.-thick carburization zone was observed after 1000 hr at 1300°F using a contact pressure of 2000 psi; this result is reasonable, based on other data. $Cr_{23}C_6$ was determined to be the principal carbide on the stainless-steel side of the diffusion couples, whereas Cr_7C_3 was predominant at the graphite-metal interface. Neither Fe_3C nor Cr_3C_2 was detected.

A cursory study[91] of interdiffusion in a plutonium-nickel couple was conducted at Mound Laboratory. It was found that little diffusion

had occurred after 92 days at 100°C; no additional information could be obtained from the sample because the diffusion zone was too narrow. The observed low rate of diffusion seems reasonable because of the low temperature of the experiment and the formation of compounds in this system during diffusion, which would decrease the diffusion rate.

(D. C. Carmichael)

Ceramic Technology

Sintering studies[33] on CaF_2 are being continued at Oak Ridge. In a recent experiment, two crystals of CaF_2 were sintered in contact until slight adhesion developed. The crystals were then separated, and the interface of one crystal was etched. Etching revealed a massive concentration of dislocations within the area of the interface, or the area of incipient neck formation. This observation seemed to indicate generation of dislocations within the neck area, or flow of existing dislocations into the area. The observers postulated a plastic-flow mechanism to explain the mobility of the dislocations but did not exclude the possibility of other mechanisms.

Storms and associates[92] report precise lattice-parameter measurements on $NbC_{0.993}$. The composition of the material studied was niobium, 87.00 wt.%; total carbon, 13.04 wt.%; and free carbon, 1.87 wt.%. It was exposed to nickel-filtered copper X rays for 16 hr at 25°C. The structure was found to be the NaCl type, and the lattice parameter a_0 was 4.47095 ± 0.00009 A at 25°C. The niobium-carbon distance was 2.2355 A, and the calculated theoretical density was 7.79 g/cm^3.

The compatibility of various ceramic materials with selected metals is being explored at Oak Ridge.[64] Couples were made of the following systems: Al_2O_3-rhenium; BeO-rhenium; ThO_2-rhenium; UO_2-rhenium; MgO-molybdenum; zirconium-molybdenum; pyrolytic graphite–molybdenum; pyrolytic graphite–tantalum; and UO_2-tantalum. These systems were heated at 1400°C in argon for a minimum of 100 hr. Reaction of unspecified extent was reported between MgO and molybdenum and between pyrolitic graphite and molybdenum. No evidences of reaction were seen in the other systems.

A somewhat similar experiment is described in the Russian literature.[19] In this work couples were heated in a vacuum for up to 5 hr, and interfacial areas were examined metallographically. Reactants and temperatures, together with the character of the reaction or reaction products, are shown in Table IV-14.

Electron-microscope studies of the fracture surfaces of Al_2O_3 have been reported by scientists at Alfred University.[93] The material was hot-pressed Al_2O_3 that had an average crystal size of about 20 μ. Specimens were fractured at low and at high temperatures, and their surfaces were examined to determine, if possible, the mode of failure. At temperatures below 1200°C, both transgranular and intergranular fractures were observed. In the range of 1200°C, the strengths of the specimens decreased rapidly; above 1200°C fracture was predominantly intergranular. It thus appeared that, in the range of 1200°C, the strengths of intercrystalline and

Table IV-14 REACTIONS BETWEEN METALS AND CERAMICS[19]

Oxide or carbide	Metal	Temp. of onset of reaction, °C	Character of reaction or reaction product
BeO	Nb	1700	Alloy appearing to be a NbBe composition
BeO	Mo	1700	Molybdenum-beryllium
BeO	W	1800	Volatile tungsten oxide, no new phases
MgO	Nb	1900	Diffuse new phase
MgO	Mo, W	2000–2100	Not given
ZrO_2(CaO)	Nb	2000	Diffuse new phase
ZrO_2(CaO)	Mo	2000	Not given
ZrO_2(CaO)	W	1900	Porous interface, volatile tungsten oxide
ZrC	Mo	2000	New phase
HfC	Mo	2000	Diffuse new phase
NbC	Mo	1800	Solid-solution niobium-carbon or molybdenum carbon, or niobium-molybdenum alloy
TaC	Mo	2100	Not given

rial appear to be cooperative deformation mechanisms rather than competitive. The most prevalent type of twin in this test was deduced to be the $\{10\bar{1}2\}$.

The solubility of oxygen in alpha zirconium in the temperature region 400 to 800°C was investigated by workers at the University of Stockholm,[87] utilizing X-ray techniques. The solubility, which is independent of temperature, was found to be 28.6 at.% $ZrO_{0.40}$. The length of the c axis increases with increasing oxygen content over the entire solubility range, whereas that of the a axis passes through a maximum at the composition $ZrO_{0.25}$. Two phases exist in the solubility range: ZrO_{0+x}, with randomly distributed oxygen atoms, and Zr_3O_{1+y}, with partly ordered oxygen atoms. The oxygen atoms are completely ordered (Zr_3O) at the limiting composition ($ZrO_{0.33}$).

(J. A. DeMastry)

Diffusion Studies

In the investigation of diffusion barriers for refractory metals being conducted at Manufacturing Laboratories,[88] which has been discussed in previous reviews in this series, screening tests at 1700°C have been continued, and similar tests at 1800°C have been initiated. On the basis of tests thus far, the 15 base-barrier metal combinations listed in Table IV-13 have been selected as promising. The arbitrary criteria being used in the studies pertain to the extent of interdiffusion between the base and barrier metals, the minimum melting point of the base-barrier alloy system, and the oxidation resistance of the barrier metal in conjunction with the extent of interdiffusion between the barrier metal and chromium, a potential protective-coating material. In future work the screening studies at 1700 and 1800°C will be completed, tungsten-base combinations will be evaluated at 1900 or 2000°C, and further investigations of interdiffusion in barrier-coating combinations will be conducted. Also, interdiffusion rates for selected combinations will be determined by measuring the growth kinetics of intermediate phases.

Table IV-13 TENTATIVE LIST OF 15 OPTIMUM BASE-BARRIER METAL COMBINATIONS[88]

Tungsten base	Molybdenum base	Tantalum base	Niobium base
W-Re	Mo-W	Ta-W	Nb-W
W-Ru	Mo-Re	Ta-Re	Nb-Re
W-Ir	Mo-V	Ta-Os	Nb-Os
W-Rh		Ta-Ru	Nb-Zr

Some information on the rate of diffusion and the diffusion zones formed in the niobium-silicon system is contained in a translation[89] of a Russian article on silicon-diffusion coatings for niobium. In this investigation the structure and phase composition of niobium that had been saturated with solid-phase silicon for 30 min to 15 hr at temperatures of 1100 to 1300°C were determined. Metallographic examinations and X-ray spectrum analyses of the local chemical compositions were conducted, and parameters for the diffusion of silicon into niobium were calculated. The phases observed were $NbSi_2$, Nb_2Si_3, and Nb_4Si. Diffusion processes that occurred in the grain boundaries of metals are discussed in an English translation of a Russian book.[90] In addition, this book includes interesting information on autoradiographic and radiographic techniques that are applicable to study of the distribution and diffusion of elements in metals, on the chemical inhomogeneity of alloys, and on the structure, thermodynamics, and properties of grain boundaries.

An investigation to determine the diffusion coefficients of niobium in pressed-and-sintered UO_2 pellets is in progress at Oak Ridge.[33] The experiments are being conducted by heat-treating a Nb^{95}-UO_2 couple, removing thin sections of measured thickness, and counting the Nb^{95} activity in each section. Results thus far indicate that, at 1500°C, the bulk diffusion coefficient of niobium in UO_2 is about four orders of magnitude larger than the reported value for diffusion of uranium in UO_2. The interdiffusion between graphite and type 304L stainless steel is also being studied at Oak Ridge.[65] A 0.030-in.-thick carburization zone was observed after 1000 hr at 1300°F using a contact pressure of 2000 psi; this result is reasonable, based on other data. $Cr_{23}C_6$ was determined to be the principal carbide on the stainless-steel side of the diffusion couples, whereas Cr_7C_3 was predominant at the graphite-metal interface. Neither Fe_3C nor Cr_3C_2 was detected.

A cursory study[91] of interdiffusion in a plutonium-nickel couple was conducted at Mound Laboratory. It was found that little diffusion

had occurred after 92 days at 100°C; no additional information could be obtained from the sample because the diffusion zone was too narrow. The observed low rate of diffusion seems reasonable because of the low temperature of the experiment and the formation of compounds in this system during diffusion, which would decrease the diffusion rate.

(D. C. Carmichael)

Ceramic Technology

Sintering studies[33] on CaF_2 are being continued at Oak Ridge. In a recent experiment, two crystals of CaF_2 were sintered in contact until slight adhesion developed. The crystals were then separated, and the interface of one crystal was etched. Etching revealed a massive concentration of dislocations within the area of the interface, or the area of incipient neck formation. This observation seemed to indicate generation of dislocations within the neck area, or flow of existing dislocations into the area. The observers postulated a plastic-flow mechanism to explain the mobility of the dislocations but did not exclude the possibility of other mechanisms.

Storms and associates[92] report precise lattice-parameter measurements on $NbC_{0.993}$. The composition of the material studied was niobium, 87.00 wt.%; total carbon, 13.04 wt.%; and free carbon, 1.87 wt.%. It was exposed to nickel-filtered copper X rays for 16 hr at 25°C. The structure was found to be the NaCl type, and the lattice parameter a_0 was 4.47095 ± 0.00009 A at 25°C. The niobium-carbon distance was 2.2355 A, and the calculated theoretical density was 7.79 g/cm^3.

The compatibility of various ceramic materials with selected metals is being explored at Oak Ridge.[64] Couples were made of the following systems: Al_2O_3-rhenium; BeO-rhenium; ThO_2-rhenium; UO_2-rhenium; MgO-molybdenum; zirconium-molybdenum; pyrolytic graphite–molybdenum; pyrolytic graphite–tantalum; and UO_2-tantalum. These systems were heated at 1400°C in argon for a minimum of 100 hr. Reaction of unspecified extent was reported between MgO and molybdenum and between pyrolitic graphite and molybdenum. No evidences of reaction were seen in the other systems.

A somewhat similar experiment is described in the Russian literature.[19] In this work couples were heated in a vacuum for up to 5 hr, and interfacial areas were examined metallographically. Reactants and temperatures, together with the character of the reaction or reaction products, are shown in Table IV-14.

Electron-microscope studies of the fracture surfaces of Al_2O_3 have been reported by scientists at Alfred University.[93] The material was hot-pressed Al_2O_3 that had an average crystal size of about 20 μ. Specimens were fractured at low and at high temperatures, and their surfaces were examined to determine, if possible, the mode of failure. At temperatures below 1200°C, both transgranular and intergranular fractures were observed. In the range of 1200°C, the strengths of the specimens decreased rapidly; above 1200°C fracture was predominantly intergranular. It thus appeared that, in the range of 1200°C, the strengths of intercrystalline and

Table IV-14 REACTIONS BETWEEN METALS AND CERAMICS[19]

Oxide or carbide	Metal	Temp. of onset of reaction, °C	Character of reaction or reaction product
BeO	Nb	1700	Alloy appearing to be a NbBe composition
BeO	Mo	1700	Molybdenum-beryllium
BeO	W	1800	Volatile tungsten oxide, no new phases
MgO	Nb	1900	Diffuse new phase
MgO	Mo, W	2000–2100	Not given
ZrO_2(CaO)	Nb	2000	Diffuse new phase
ZrO_2(CaO)	Mo	2000	Not given
ZrO_2(CaO)	W	1900	Porous interface, volatile tungsten oxide
ZrC	Mo	2000	New phase
HfC	Mo	2000	Diffuse new phase
NbC	Mo	1800	Solid-solution niobium-carbon or molybdenum carbon, or niobium-molybdenum alloy
TaC	Mo	2100	Not given

intracrystalline bonds were approximately equal. The authors called this temperature the equicohesive temperature. They concluded that, at temperatures below 1200°C, the grain boundaries were stronger than the crystals themselves and that the opposite was the case at temperatures exceeding 1200°C.

Continued research on BeO-foamed ceramics was reported by workers at General Electric.[22] The foamed structure is caused by reaction of H_3PO_4 with BeO. Since phosphates are generally undesirable in refractories, means were sought to reduce the phosphate content of the foamed shapes. It was learned that sintering the pieces in hydrogen at 1370°C yields a phosphate-free composition. It was also learned that shrinkage of a foamed casting in the mold could be minimized by adding dead-burned BeO to the active UOX-grade* BeO customarily used. The most uniform body containing the finest pore structure consisted of 60 wt.% dead-burned and 40 wt.% UOX-grade BeO. The density of this body was 0.99 g/cm^3, and the pore size ranged from 0.01 to 0.15 cm.

Further studies of the effects of ultrasonic activation on various chemical and ceramic processes have been reported by Aeroprojects, Inc.[34] It was found that activation of a magnesium-zinc melt promotes the reduction of U_3O_8. Also, the rate of solution of high-fired ThO_2-UO_2 in HNO_3 was increased by 250 per cent through ultrasonic activation.

(A. K. Smalley)

References

1. H. H. Klepfer et al., The Effect of Heat Treatment on the Corrosion Resistance and Corrosion Hydrogen Embrittlement of Some Zr-Nb Binary Alloys, Report GEAP-3729, General Electric Co., Vallecitos Atomic Laboratory, May 22, 1961.
2. Westinghouse Electric Corp., Bettis Atomic Power Laboratory, Bettis Technical Review. Reactor Technology, USAEC Report WAPD-BT-24, December 1961.
3. M. K. Millhollen et al., Hydriding in Purposely Defected Zircaloy-Clad Fuel Rods, USAEC Report HW-65465, Hanford Atomic Products Operation, August 1961.
4. L. S. Rubenstein et al., Effect of Five Impurities on the High-Temperature Water and Steam Corrosion Resistance of Zircaloy-2, *Corrosion*, 18(2): 45t–54t (February 1962).
5. S. J. Gregg et al., Reaction of Zirconium with Carbon Dioxide at 550–750°C, *Corrosion*, 17: 575t–578t (December 1961).
6. M. I. Sturtridge, Investigation of Corrosion Problems in NRU Orifice Sections, Canadian Report CRE-1048, August 1961.
7. Hanford Atomic Products Operation, Reactor Fuels Research and Development Operation Monthly Report, December 1961, USAEC Report HW-72142A, Jan. 15, 1962. (Classified)
8. C. N. Spalaris et al., Design, Fabrication, and Irradiation of Superheat Fuel Element SH-4B in VBWR, USAEC Report GEAP-3796, General Electric Co., Atomic Power Equipment Dept., Sept. 1, 1961.
9. M. C. Rowland and W. R. Smith, Sr., Precipitation-Hardening Stainless Steels in Water-Cooled Reactors, *Nuclear Eng.*, 7(68): 14–22 (January 1962).
10. J. H. DeVan, Catastrophic Oxidation of High-Temperature Alloys, USAEC Report ORNL-TM-51, Oak Ridge National Laboratory, Nov. 10, 1961.
11. G. R. Vavasour (Ed.), Proceedings of the Tripartite Conference on Transport of Materials in Pressurized-Water Reactors, Chalk River, February 28 and March 1, 1961, Canadian Report AECL-1265, June 1961.
12. V. V. Gerasimov and A. I. Gromova, Investigation of the Corrosive and Electrochemical Behavior of 12XM Steel in Water at High Temperature (translated by M. J. Weinreich from a publication of the State Committee of the Council of Ministers of the USSR on the Utilization of Atomic Energy, Moscow, 1960).
13. J. McGrew et al., Autoclave Testing of Monel, Nickel, and Inconel, Report MND-E-2655, Martin Co., Nuclear Div., October 1961.
14. Aerojet-General Nucleonics, The Army Gas-Cooled Reactor Systems Program, Semiannual Progress Report for July 1 through December 31, 1961, USAEC Report IDO-28581, Feb. 28, 1962.
15. General Electric Co., Flight Propulsion Laboratory Dept., High-Temperature Materials and Reactor Component Development Programs, Volume I. Materials, USAEC Report GEMP-106A, Feb. 28, 1962.
16. A. Draycott and R. W. Hubery, Oxidation of 1% Cr, 0.5% Mo Steel in Carbon Dioxide, Australian Report AAEC/E-71, June 1961.
17. R. E. Pawel et al., "Break-Away" Phenomena in the Oxidation of Columbium Single Crystals, in *Columbium Metallurgy*, pp. 667–684, Interscience Publishers, New York, 1961.
18. B. A. Wilcox and F. H. Beck, The Effect of Concurrent Stressing on the Air Oxidation of Tantalum, Report WADD-TR-60-839, The Ohio State University, April 1961.
19. G. V. Samsonov et al., The Reaction of Certain Oxides and Carbides with Refractory Metals at

*Brush Beryllium Company.

High Temperatures, Report FTD-TT-61-74 [translated from *Ogneupory*, (7): 335–338 (1961)].

20. H. A. Fisch et al., The High-Temperature Steam Corrosion of Columbium-Vanadium Alloys, in *Columbium Metallurgy*, pp. 597–613, Interscience Publishers, New York, 1961.
21. W. D. Klopp et al., The Hot Water Corrosion Resistance of Columbium and Columbium Alloys, in *Columbium Metallurgy*, pp. 685–718, Interscience Publishers, New York, 1961.
22. General Electric Co., Flight Propulsion Laboratory Dept., High-Temperature Materials Program Progress Report No. 7, Part A, USAEC Report GEMP-7A, Jan. 15, 1962.
23. General Electric Co., Flight Propulsion Laboratory Dept., Summary of High-Temperature Materials Work Performed in FY 61, Part A, May 1, 1961–June 30, 1961, USAEC Report GEMP-103A, December 1961.
24. J. W. Clark, The Ignition of Columbium and Selected Alloys, in *Columbium Metallurgy*, pp. 615–647, Interscience Publishers, New York, 1961.
25. C. A. Krier, Coatings for the Protection of Refractory Metals from Oxidation, Report DMIC-162, Battelle Memorial Institute, Defense Metals Information Center, Nov. 24, 1961.
26. W. D. Klopp, Review of Recent Developments on Oxidation-Resistant Coatings for Refractory Metals, Report DMIC Newsletter, Battelle Memorial Institute, Defense Metals Information Center, Feb. 2, 1962.
27. E. S. Bartlett, The Protection of Metals at High Temperatures, SAE preprint 511C of paper presented at a meeting of the Society of Automotive Engineers, Apr. 3, 1962.
28. Denver Research Institute, unpublished data.
29. T. L. Mackay, Oxidation of Zirconium and Zirconium Alloys in Liquid Sodium, USAEC Report NAA-SR-6674, Atomics International, Feb. 15, 1962.
30. J. H. Reynolds (Ed.), Nuclear Engineering Department Progress Report, May 1–August 31, 1961, USAEC Report BNL-696, Brookhaven National Laboratory, January 1962.
31. W. L. McCullough, Stress-Corrosion Properties of 19-9 DL Alloy in Lithium Hydride, USAEC Report APEX-674, General Electric Co., Flight Propulsion Laboratory Dept., June 26, 1961. (Classified)
32. Oak Ridge National Laboratory, Molten-Salt Reactor Program Progress Report for Period from March 1 to August 31, 1961, USAEC Report ORNL-3215, Jan. 19, 1962.
33. Oak Ridge National Laboratory, Feb. 13, 1962, unpublished data.
34. Argonne National Laboratory, Chemical Engineering Division Summary Report for July, August, September, 1961, USAEC Report ANL-6413.
35. R. C. Liimatainen et al., Studies of Metal-Water Reactions at High Temperatures II. TREAT Experiments, Status Report on Results with Aluminum, Stainless Steel-304, Uranium, and Zircaloy-2, USAEC Report ANL-6250, Argonne National Laboratory, January 1962.
36. Hanford Atomic Products Operation, Fuels Development Operation Quarterly Progress Report, October, November, December, 1960, USAEC Report HW-70355, Jan. 13, 1961. (Classified)
37. E. W. Young, Jr., Etching of Irradiated Copper, *J. Appl. Phys.*, 33: 749–750 (February 1962).
38. R. O. Simmons and R. W. Balluffi, Measurements of Equilibrium Concentrations of Lattice Vacancies in Gold, *Phys. Rev.*, 125(3): 862–872 (Feb. 1, 1962).
39. R. O. Simmons and R. W. Balluffi, Measurements of the Equilibrium Concentration of Lattice Vacancies in Silver Near the Melting Point, *Phys. Rev.*, 119: 600 (1960).
40. M. D. Rogers and J. Adam, Ejection of Uranium by Fission Fragments, British Report AERE-R-3908, December 1961.
41. R. S. Barnes, Atomic Displacement and Impurity Effects in Fissile Metals, British Report AERE-R-3821, September 1961.
42. A. Grenall, Electron Microscope Observations of Fast Neutron Damage in Gold Films, *J. Nuclear Materials*, 4(3): 329–331 (August–September 1961).
43. J. A. Brinkman et al., An Interpretation of Electron Microscope Observations in Neutron Irradiated Copper and Gold, *J. Nuclear Materials*, 4(3): 332–333 (August–September 1961).
44. M. J. Makin et al., The Formation of Dislocation Loops in Copper During Neutron Irradiation, *Phil. Mag.*, 7(74): 285 (February 1962).
45. P. B. Brice and R. M. Walker, Electron Microscope Observations of Etched Tracks from Spallation Recoils in Mica, *Phys. Rev. Letters*, 8(5): 217–219 (Mar. 1, 1962).
46. S. Ichiba, The Study of Lattice Defects in Graphite by the Emanation of Fission Product Rare Gas, *J. At. Energy Soc. Japan*, 3: 763–766 (October 1961).
47. H. Bridge et al., Stored Energy and Dimensional Changes in Reactor Graphite, in *Proceedings of the 5th Carbon Conference, University of Buffalo, 1961*, pp. 285–312, Pergamon Press, 1962.
48. W. N. Reynolds and J. N. W. Simmons, The Effect of High Flux Neutron Irradiation on the Physical Properties of Graphite, British Report AERE-R-3871, November 1961; also in *Proceedings of the 5th Carbon Conference, University of Buffalo, 1961*, Pergamon Press, 1962.
49. F. L. Vook, Low Temperature Length Change Measurements of Electron-Irradiated Germanium and Silicon, *Phys. Rev.*, 125(3): 855–861 (Feb. 1, 1962).

50. J. W. Cleland and J. H. Crawford, Jr., Radiation-Induced Disorder in Semiconductors, in *Proceedings of the International Conference on Semiconductor Physics*, Prague (1960), Publishing House of the Czechoslovak Academy of Sciences, 1961.
51. C. P. Flynn, Vacancies and Complexes in the Noble Metals, *Phys. Rev.*, 125(3): 881–895 (Feb. 1, 1962).
52. R. S. Barnes, The Behavior of Point Defect Clusters in Irradiated Metals, *Phil. Mag.*, 6(72): 1487–1492 (December 1961).
53. J. H. O. Varley, The Agglomeration into Clusters of Interstitial Atoms and Vacancies Generated by Fast Neutron Irradiation, *Phil Mag.*, 7(74): 301 (February 1962).
54. G. Nemeth, Calculation of the Replacement Effect in the Statistical Theory of Lattice Damage, *Nuovo Cimento*, (10) 21: 764–772 (Sept. 1, 1961).
55. J. A. Brinkman, Fission Damage in Metals, USAEC Report NAA-SR-6642, Atomics International, Mar. 1, 1962.
56. H. Amar, Energy of Formation of a Vacancy in Copper, *J. Appl. Phys.*, 33: 666–668 (February 1962).
57. A. C. Damask and G. J. Dienes, Kinetics of Vacancy-Interstitial Annihilation: I. Impurity-Interstitial Trapping, *Phys. Rev.*, 125: 444–446 (Jan. 15, 1962).
58. G. J. Dienes and A. C. Damask, Kinetics of Vacancy-Interstitial Annihilation: II. Di-Interstitial Formation, *Phys. Rev.*, 125: 447–450 (Jan. 15, 1962).
59. K. Tharmalingam and A. B. Lidiard, Mobility of Vacancy Pairs in Ionic Crystals, *Phil. Mag.*, 6(69): 1157–1162 (September 1961).
60. R. E. Schreiber, Mechanical Properties of Irradiated Stainless Steels. A Compilation of Data in the Literature, USAEC Report DP-579, Savannah River Laboratory, September 1961.
61. Radiation Effects in Inorganic Solids, *Discussions Faraday Soc.*, No. 31 (1961).
62. *Reactivity of Solids*, Elsevier Publishing Co., 1961.
63. Supplement to the *Journal of Applied Physics*, *J. Appl. Phys.*, 33: 251–518 (January 1962).
64. Oak Ridge National Laboratory, Army Reactors Program Progress Report, USAEC Report ORNL-3231, Feb. 14, 1962.
65. Oak Ridge National Laboratory, Gas-Cooled Reactor Program Quarterly Progress Report for Period Ending September 30, 1961, USAEC Report ORNL-3210, Feb. 5, 1962.
66. V. O. Haynes and W. C. Thurber, Determination of the Effect of Neutron Irradiation on the Nil-Ductility–Transition Temperature for Type A-212, Grade B, Steel Used in the N. S. *Savannah* Pressure Vessel, USAEC Report ORNL-TM-132, Oak Ridge National Laboratory, Mar. 21, 1962.
67. P. R. Hames et al., The Effects of Neutron Irradiation on the Ductile-Brittle Transition Temperature of Steels and Its Relevance to Reactor Pressure Vessels, *Steels for Reactor Pressure Circuits Symposium, Special Report No. 69*, pp. 297–327, Iron and Steel Institute, 1961.
68. C. G. Collins et al., Radiation Effects on the Stress Rupture Properties of Inconel-X and A-286, USAEC Report APEX-676, General Electric Co., Flight Propulsion Laboratory Dept., December 1961.
69. General Electric Co., Flight Propulsion Laboratory Dept., High-Temperature Materials Program Progress Report No. 9, Part A, USAEC Report GEMP-9A, Mar. 30, 1962.
70. Hanford Atomic Products Operation, January 1962. (Unpublished)
71. K. E. Mann and M. B. Boudouresques, Sinter Aluminium as Cladding Material for Fuel Element, French Report CEA-1993, 1961.
72. F. R. Shober, The Effect of Nuclear Radiation on Structural Metals, Report REIC-20 (DMIC-166), Battelle Memorial Institute, Radiation Effects Information Center, Sept. 15, 1961.
73. R. E. Schreiber, Mechanical Properties of Irradiated Plain Carbon and Alloy Steels, USAEC Report DP-581, Savannah River Laboratory, October 1961.
74. S. W. Porembka, Progress on USAEC/AECL Cooperative Program, Quarterly Report for Period December 1961–February 1962, USAEC Report BMI-X-193, Battelle Memorial Institute, Mar. 1, 1962.
75. M. A. Pugacz, Mechanical Properties and Welded Characteristics of Inconel X, Hastelloy X, and 19-9DL, Report APEX-683, General Electric Co., Flight Propulsion Laboratory Dept., December 1961. (Classified)
76. General Atomic Div., General Dynamics Corp., Maritime Gas-Cooled Reactor Program Quarterly Progress Report for the Period Ending December 31, 1960, USAEC Report GA-1954.
77. C. R. McKinsey et al., Investigation of Tungsten-Tantalum-Columbium-Base Alloys, Report ASD-TR-61-3, Union Carbide Metals Co., March 1961.
78. E. S. Bartlett and F. F. Schmidt, Review of Recent Developments in the Technology of Columbium and Tantalum, Report DMIC-Memo-130, Battelle Memorial Institute, Defense Metals Information Center, Oct. 10, 1961.
79. M. Semchyshen and R. Q. Barr, Extrusion and Mechanical Properties of Some Molybdenum- and Tungsten-Base Alloys, Report ASD-TR-61-193, Climax Molybdenum Co., Mar. 15, 1961.
80. F. C. Holtz, Illinois Institute of Technology, Armour Research Foundation, Oct. 1, 1960, unpublished data.
81. A. P. Belyaev and R. M. Gol'shtein, Effect of Ti, Be, Ga, Re, and Nb Additions on Grain Size of Aluminum, *Metalloved. i Termichesk. Obrabotka Metal.*, (7): 37–38 (July 1961).

82. H. H. Stadelmaier and T. S. Yun, Nitrogen Alloys of the T-Metal Manganese, Iron, Cobalt, and and Nickel with Magnesium, Aluminum, Zinc, and Cadmium, *Z. Metallk.*, 52: 477–480 (July 1961).
83. D. L. Douglass and F. W. Kinz (Eds.), *Columbium Metallurgy*, Vol. 10, Metallurgical Society Conferences, Interscience Publishers, New York, N. Y., 1961.
84. C. L. Vold, The Crystal Structure of $NbZn_2$, *Acta Cryst.*, 14: 1289–1290 (December 1961).
85. E. M. Savitskii et al., Constitution Diagram of Ru-Cr Alloys, *Zhur. Neorg. Khim.*, 6: 1960–1962 (August 1961).
86. University of Florida Engineering and Industrial Experiment Station, An Evaluation of the Role of Deformation Twinning in the Plastic Deformation of Zircaloy-2, USAEC Report TID-14185, September 1961.
87. B. Holmberg and T. Dagerhamn, X-ray Studies on Solid Solutions of Oxygen in α-Zirconium, *Acta Chem. Scand.*, 15: 919–925 (1961).
88. Manufacturing Labs., Inc., Investigation of Diffusion Barriers for Refractory Metals, Progress Report No. 8, July 15, 1961–October 15, 1961, Report NP-11060, Oct. 30, 1961.
89. P. M. Arzhanyi et al., An Investigation of the Structure and Phase Composition of a Silicon Diffusion Coating for Niobium, Report NP-tr-789 [translated from *Issled. Zharoproch. Splavam, Akad. Nauk S.S.S.R., Inst. Met. im. A.A. Baikova*, 6: 201–205 (1960)].
90. S. Z. Bokshtein et al., Investigation of the Structure of Metals by Radioactive Isotope Methods, USAEC Translation AEC-tr-4505 [translated from a publication of the State Publishing House of the Ministry of Defense Industry (1959)].
91. J. F. Eichelberger, Mound Laboratory Progress Report [on Research] for August 1961, USAEC Report MLM-1118, Mound Laboratory, Dec. 8, 1961.
92. E. K. Storms et al., Crystallographic Data for Niobium Monocarbide, USAEC Report TID-6757, Los Alamos Scientific Laboratory, 1960.
93. D. Tunison and V. Burdick, The Fracture Analysis of Alumina Using the Electron Microscope, Report NP-11270, Alfred University, Nov. 30, 1961.
94. Aeroprojects, Inc., Applications of Ultrasonic Energy, Progress Report No. 22, covering period from June 1, 1960, to July 31, 1960, USAEC Report NYO-2576, August 1960.

Section V

Reactor Materials

Special Fabrication Techniques

Melting and Casting

The thermodynamics of the cold-mold, consumable-electrode, arc-melting process is being investigated by the Bureau of Mines.[1] Initial tests have been concerned with the effects of various coolant flow rates on crucible damage. Results indicate that, with a crucible of reasonable thickness, there was no increase in effective cooling when the coolant flow was increased from 3 to 15 gal/min. Vacuum, consumable-electrode melting is also being investigated as a method of preparing refractory alloys that contain molybdenum, niobium, and tungsten. Another study[2] concerned with preparation of the F-48 alloy has shown that no increase in the interstitials, oxygen and nitrogen, can be attributed to the consumable-electrode melting process.

Wah Chang[3] has been utilizing consumable-electrode melting as a technique for the preparation of tungsten–3 wt.% molybdenum alloys. During these studies various melting rates, crucible sizes, and electrode-preparation techniques have been employed. The results to date have shown that the electrode diameter should not exceed one-half that of the crucible, or there must be at least 1 in. side-wall clearance, and that straight polarity yields better quality ingots than does reverse polarity. It was also noted that a stirring coil must be employed to stabilize the arc. A melting rate of 2 lb/min at 7500 amp and 31 volts was obtained when melting a 2-in.-diameter electrode in a $4\frac{1}{2}$- to 5-in.-diameter crucible.

An electron-beam-melting study[1] on hafnium metal is continuing at the Bureau of Mines. This work has shown that purity levels comparable with those exhibited by material produced by the iodide process can be attained by electron-beam melting. During melting the metallic impurities and hydrogen are removed during the first few minutes, and carbon, nitrogen, and oxygen are decreased in this order at a slower rate. It was found that oxygen removal is a function of the energy input and that a minimum of 100 ppm oxygen is attained when buttons are held molten for up to 4 hr.

The continued interest in the refractory compounds is reflected in work reported concerning the preparation of HfC, USi_2, and UC. Work is reported[4] on UC which concerns the preparation of small castings utilizing skull-melting techniques for consolidation of UC pellets. As reported in similar work of this nature, it was found imperative to obtain a homogeneous skull with a composition approximating that desired in the cast product. The carbide work reported by the Bureau of Mines[1] was concerned primarily with stoichiometric HfC, although alloys that contain up to 15.7 wt.% carbon have been prepared. It was interesting to note that the high-carbon-content material was amenable to sawing, filing, and drilling.

Of interest to the reviewer were the vacuum-induction melts of U_3Si_2 prepared by Atomics International.[5] In the preparation of these melts, all the graphite crucibles, molds, and accessories that contacted the molten materials were coated with a slurry of either Y_2O_3 or ZrO_2. During melting it was found that the extreme fluidity of the material made it difficult to retain in the bottom-pour crucibles. All the castings that were produced were brittle and, although essentially U_3Si_2, contained trace amounts of gamma uranium and USi.

Studies of plutonium melting[6] reviewed during the past quarter were concerned with the use of boron nitride as a crucible and mold material and with electron-beam melting of master alloy buttons of plutonium and refractory metals. Boron nitride exhibited no reaction with the

plutonium when used as a mold material, but proved entirely unsatisfactory as a crucible. Analyses showed 5000 to 20,000 ppm boron in the material that melted in the boron nitride crucible. (E. L. Foster)

Fabrication and Heat-Treatment

Fabrication and heat-treatment studies reviewed during the immediate past have been concerned primarily with the refractory alloys of molybdenum, niobium, tantalum, and tungsten. Of particular interest among these was a report[7] by Harvey Aluminum concerning its experiences and the techniques employed in fabricating 309 billets of 60 different compositions. This is a very complete report which includes a typical extrusion schedule such as given below:

1. Warm the billet and then coat with glass powder.
2. Heat, by induction, to temperature under an argon atmosphere. A typical 3-in.-diameter billet is heated to 3200°F in 23 min using 18 kw of power.
3. Extrude using dies which have a 90° entrance angle and which have been flame sprayed with zirconium oxide (Rokide).
4. Cool slowly in an insulating blanket.

Also included are results of recrystallization and forgeability studies conducted at another site. These studies were concentrated on the molybdenum–0.5 wt.% tungsten–0.08 wt.% zirconium–0.02 wt.% carbon and the molybdenum–25 wt.% tungsten–0.1 wt.% zirconium–0.02 wt.% carbon.

The Defense Metals Information Center has recently issued a relatively complete state-of-the-art memorandum[8] concerning the forging of refractory alloys. Included are techniques of billet preparation and photographs of some of the shapes that can be produced from these alloys by forging. There are 35 references in this paper which should serve as a good reference for those contemplating or engaged in work in this area.

Other literature reviewed has included fabrication studies concerning 3Z1, TZM, F-48, tantalum, and Zircaloy-2 alloys. The work concerning the 3Z1 alloy[9] was directed primarily toward determining the mechanical properties of this material. However, while obtaining test specimens, it was determined that (1) an 1800°F forging temperature was superior to a 1950°F temperature, (2) the material could be rolled at 1450, 1550, or 1650°F, and (3) cold rolling was feasible if proper annealing temperatures were employed. The work reported[3,10] on the TZM and F-48 alloys was of a preliminary nature. For instance, it was reported that the as-cast and extruded TZM billets exhibited wide differences in microstructure over the length of the extrusion; the wrought and extruded billets exhibited a more uniform, fine-grained microstructure.

Los Alamos reported[11] the successful fabrication of closed-end tantalum containers that were approximately 9 in. long, 0.375 in. in inside diameter, and 0.020 to 0.030 in. in wall thickness. Disks of tantalum were impacted to form cups, which were then ironed in stages to form the tubes. Pressures of 30 to 40 tons were used for impacting, and 600 to 3000 lb of draw pressure was used for the ironing operations. The results from work in progress at Argonne[12] concerning the preparation of Zircaloy-2 tubing indicate that, when the Zircaloy is extruded in a copper jacket, the two metals react to form Zr_2Cu and Cu_3N at the interface. These reactions apparently enhance the fabricating characteristics of the material.

Among the more unconventional fabrication techniques is the application of ultrasonics as an aid in drawing. Significant decreases in the required drawing forces were noted when ultrasonic activation of the dies was utilized.[13] The mechanism is attributed to either an increase in plasticity in the metal or a decrease in friction at the metal-to-die interface.

Hydrostatic extrusion studies with various fluid media showed that a decrease in extrusion pressure was possible when fatty acids were used as the lubricant at room temperature. At elevated temperature these acids break down, and an increase in pressure is required. Ethanol, water, and kerosene tend to aid extrusion at elevated temperatures. Optimum extrusion conditions were obtained with mixtures of oils and kerosene.[14] (E. L. Foster)

Cladding

Rolling and Swaging

Primary interest this quarter was in roll bonding of fuel elements. Work is continuing on

the cladding and densification of UO_2 by swaging, but the results are not significantly different from those previously reviewed.

Beaver[15] was granted a U. S. patent on a technique for the roll cladding of thorium with zirconium. He describes a method for improving the core-to-cladding bond achieved during hot rolling. This is done by inserting a thorium-zirconium alloy foil between the core and cladding before rolling.

Lingafelter[16] has investigated the tandem rolling of stainless-steel-clad UO_2 fuel rods as a high-rate production technique. The rods were loaded with UO_2 powder to 65 to 70 per cent of theoretical density by a modified vibratory-packing technique referred to as "jet loading." The samples were then fed from a hopper, apparently cold, through tandem rolls. Coarse fractions of powder yielded a final density of 88 to 89 per cent of theoretical. Cross-sectional dimensional control was no problem, but some bowing was noted in the finished rods. It was estimated that production rates of 350,000 ft of rods per month could be achieved in a large range of diameters. (H. D. Hanes)

Diffusion Bonding

On the basis of investigations that show embrittlement to be a problem in welding niobium or tantalum, the Bureau of Mines is conducting a study[1] of diffusion bonding of each of these metals using a thin, dissimilar-metal layer as a bonding agent between the components. The specimens to be joined are heated for 4 to 7 hr at a high temperature in either an electron-beam furnace or a direct-resistance heating chamber. A low, unspecified interfacial pressure is used. It is reported that two tantalum rods with an intermediate layer of titanium were bonded by maintaining the temperature just below the melting point of titanium. Complete bonding in a niobium-alloy specimen was not obtained due to a slight physical mismatching at the interface, which apparently is very critical in this technique. (D. C. Carmichael)

Coextrusion

The multitemperature coextrusion technique has been employed by workers at Nuclear Metals[17] for the fabrication of stainless-steel-clad UO_2 fuel elements and irradiation specimens. The process, based upon some conventional as well as novel hot-extrusion techniques, involves the coextrusion of UO_2 at 1875°C within the stainless-steel cladding at 760°C, the temperatures at which their relative stiffnesses are sufficiently similar. The coextrusion of a low-carbon-steel can is required over the cladding to prevent it from melting and to exert a relatively high, approximately isostatic, pressure on the ceramic core. Two rods that were destructively examined had an average bulk density of 97.5 per cent of theoretical, with an average deviation of about 0.3 per cent of theoretical, and an oxygen-to-uranium ratio of 2.02. In the as-extruded condition, the average diameter was 410 mils, with an average deviation of 4 mils and a maximum deviation of 8 mils. A program to investigate this process of fabrication in terms of economics and irradiation performance is now being conducted.[18] The cost study is being performed to determine coextrusion process costs to produce stainless-steel-clad UO_2 fuel elements where a high-speed, high-capacity extrusion press and production techniques are used. The cost, per kilogram, of a large quantity of fuel will be determined. Hot-coextruded, stainless-steel-clad UO_2 fuel rods are now being tested in-pile at Vallecitos in the Vallecitos Boiling-Water Reactor.

(C. B. Boyer)

Canning

A recent French patent[19] describes a canning operation that provides for a continuous snug fit between can and fuel slug under the reactor operating conditions. This particular fuel element would be used in a heterogeneous reactor with a pressurized coolant, which causes some plastic deformation in the canning material to maintain the snug fit. The fuel elements are manufactured by introducing a number of slightly convex, concave, or tapered slugs into a tube. The tubes are capped and heated while subjecting them to a high gas pressure.

Progress in vibratory-compaction studies[20] at Hanford has led to the achievement of theoretical densities of 88 per cent with porous, fused UO_2 (95 per cent particle density). This gives a compaction efficiency of 93 per cent, which is the highest thus far reproducibly attained. Shattering of porous agglomerates during the high-intensity vibration is believed to be a possible explanation for this improved vibrational-compaction result.

Vibratory-compaction studies at Oak Ridge[21] have been made to determine the particle-size distributions that would yield high bulk densities. In this work a ThO_2–3.4 wt.% UO_2 mixture was used in three particle-size fractions: −10 +16 mesh, −70 +100 mesh, and −200 mesh. A NAVCO BH 1.25-in. pneumatic vibrator with an air pressure of 90 psi and a vibration time of 10 min was used. The vibrated bulk densities that were obtained ranged from 67 to 89 per cent of theoretical (see Table V-1).

Although mixtures that contain three size fractions give higher densities than a two-fraction system, they have the disadvantage of requiring a medium-size fraction that is difficult and expensive to obtain. In a series of tests employing two size fractions, −10 +16 mesh and −200 mesh particles were vibratorily compacted to determine the maximum bulk density obtainable with this two-component-size mixture. The results are shown in Fig. V-1, and indicate a maximum density of about 8.75 g/cm^3 at a mixture composition of 70 wt.% −10 +16 mesh and 30 wt.% −200 mesh.

Table V-1 BULK DENSITIES OBTAINED BY VIBRATORY COMPACTION* OF ThO_2–3.4 WT.% UO_2 MIXTURES OF VARIOUS PARTICLE-SIZE DISTRIBUTIONS[21]

Mixture	Particle-size distribution, wt.% of indicated particle-size fraction			Vibrated bulk densities, g/cm^3
	−10 +16 mesh	−70 +100 mesh	−200 mesh	
1	100			6.77
2	90		10	7.42
3	75	15	10	8.32
4	75		25	8.59†
5	70	10	20	8.66
6	70		30	8.74‡
7	65		35	8.68‡
8	60	30	10	8.64
9	60	25	15	8.69
10	60	20	20	8.90
11	62.5	17.5	20	8.88
12	60	15	25	8.85
13	58	15	27	8.84
14	62.5	10	27.5	8.22
15	60		40	8.62‡
16	55	30	15	8.89
17	55	25	20	8.94
18	55	17.5	27.5	8.89
19	55	10	35	8.58
20	55		45	8.55
21	50	30	20	8.84
22	50	25	25	8.73
23	50		50	8.22
24	45	45	10	8.32
25	45	30	25	8.74
26	45	15	40	8.44
27	45		55	8.19
28			100	6.72

*All mixtures were vibrated in a NAVCO BH 1¼-in. pneumatic vibrator with an air pressure of approximately 90 psi; length of vibration run was 10 min; material vibrated was fused ThO_2–3.4 wt.% UO_2; the rod was type 304 stainless steel, 19 in. long, 0.5 in. in outside diameter, and 0.035 in. in wall thickness.

†Average of three vibration runs.

‡Average of two vibration runs.

Particle-size distributions that contained four, five, and seven size fractions have been studied by other investigators, and they report densities in excess of 90 per cent of theoretical. Compaction studies at Oak Ridge are continuing, and the effect of the impact thrust on compaction efficiency is being studied. Preliminary results show that a small density increase can be achieved by increasing the thrust.

Studies at Hanford[22] concerning the vibratory compaction of UO_2-PuO_2 fuel mixtures have continued. One of the problems associated with vibrating this system is in maintaining the desired longitudinal distribution of PuO_2 in the long tubes. Evaluation of the uniformity of PuO_2 in a fuel rod is rather difficult, but some indication of the PuO_2 distribution can be determined from the ratio of fine-to-coarse particles of UO_2, since the PuO_2 is blended with UO_2 fines before being loaded into the fuel tube.

Two tubes were compacted while being incrementally loaded with UO_2 fines and then with coarse-plus-medium sizes. After loading, the tubes were cut into 6-in. lengths, and the contained UO_2 was resieved. Longitudinal distribution of the uniformly added fines varied from 18.5 to 26 per cent in the first tube. For the second tube the fines varied from 20 to 24.8 per cent along the length of the rod. Longitudinal density variations for the two tubes were 81 to 87 and 82.2 to 88.5 per cent, respectively.

Vibratory compaction of fused UO_2 into 9.5-ft-long Zircaloy-4 fuel tubes at Savannah River[23] has yielded bulk densities of 85 per cent of theoretical. The particle-size fractions used for the UO_2 mixture were 52 wt.% −5 +10 mesh, 28 wt.% −40 + 80 mesh, and 20 wt.% −325 mesh. The tubes measured 2.06 in. in outside diameter, 0.250 in. in wall thickness (containing the UO_2), and 0.030 in. in cladding thickness.

A major problem in the fabrication of the long tubes is the maintenance of uniform longi-

tudinal fuel thickness during loading of the UO_2 powders. A loading device is being used to fit into the tube annulus to maintain the 0.250-in. dimension during loading. This spacing device has reduced the maximum wall-thickness variations from 0.150 to 0.016 in.

Fabrication of six 18-in.-long tubular fuel elements (1.750-in. outside diameter by 0.500-in. inside diameter) for KER irradiation testing

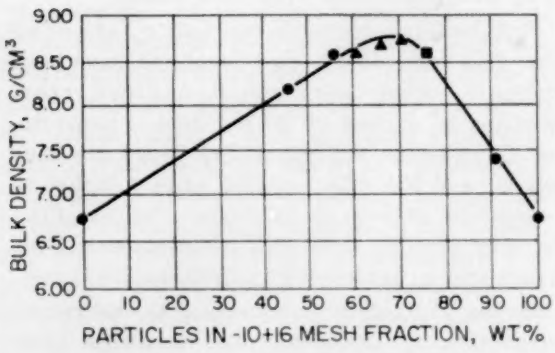

Fig. V-1 Effect of particle-size distribution on the vibratory-compacted density of two-particle-size (−10 +16 and −200 mesh) ThO_2−3.4 wt.% UO_2 material.[21] ●, single vibration run. ▲, average of two vibration runs. ■, average of three vibration runs.

has been accomplished at Hanford[24] by vibratory compaction. Maximum UO_2 density of 88.1 per cent of theoretical was obtained, and this was found to be highly dependent on fuel quality. Careful selection of the coarse-fraction material resulted in the highest densities. The particle-size fractions for the optimum mixture were 50 wt.% −6 +10 mesh, 12.5 wt.% −10 +20 mesh, 17.5 wt.% −35 +60 mesh, and 20 wt.% −200 mesh. Previous studies using similar particle-size fractions yielded densities in excess of 90 per cent of theoretical. This would indicate that cladding geometry might also affect density, and studies to determine this effect are being made.

Several methods of loading the 18-in.-long tubes and coupling the cladding to the shaker were investigated. Highest densities were obtained by incremental loading. A special fixture was used to couple the fuel tube to the shaker. This consisted of a cap to position the fuel tube, connected by four 0.125-in. rods to a pedestal that was coupled to the shaker table.

(E. G. Smith)

Electroplating

Studies at the Bureau of Standards[25] showed that water films are adsorbed on uranium surfaces during descaling, cleaning, or plating treatments, which result in black films that prevent good coating adherence. Uranium dioxide was identified in X-ray diffraction patterns from copper-plated uranium surfaces. Hot-dip coatings were unsatisfactory because they did not completely wet or cover the uranium surface. A predip in a fused mixture of lithium, potassium, and stannous chloride improved the wettability of tin and gallium. Adhesion was unsatisfactory, however, presumably because an oxide film had not been completely removed by the flux. Zinc that had been electrodeposited in an anhydrous lithium chloride–zinc chloride–ethyl alcohol bath was too porous to protect the uranium during short-term storage tests. Good protection was obtained with a composite of zinc (2 mils) and aluminum (2 mils) deposited in nonaqueous solutions, but heating at 500°C caused the formation of a brittle diffusion alloy. Earlier studies at Battelle,[26] which showed a procedure for depositing pore-free and adherent aluminum in an ether-hydride bath, were confirmed. Heating (200°C) in a hydrogen atmosphere, however, caused a large volume change when the uranium was converted to UH_3. This volume change caused detachment of the coating. Investigators at the Bureau of Standards conclude that organic type solvent electroplating baths offer the best approach for a hydrogen-impermeable, protective cladding. In view of independent studies at Battelle,[27] Atomics International,[28] and Hanford, there appears to be no need for development of organic plating solutions, as claimed by the Bureau of Standards. Pore-free, adherent nickel plate has been deposited on uranium by reproducible procedures with no evidence of the harmful black oxide or hydrate films encountered at the Bureau of Standards.

(W. H. Safranek)

Nonelectrolytic Chemical-Plating Techniques

For this review it is convenient to discuss first the deposition of various materials in massive form and then to consider the formation of coatings on both metallic and nonmetallic substrates by nonelectrolytic chemical plating.

High-purity molybdenum,[29] prepared by hydrogen reduction of sublimed $MoCl_5$, was consolidated and further purified by electron-beam

melting. Tungsten was obtained by reduction of distilled WCl_6 with sodium, magnesium, or hydrogen.[30] The WCl_6 was prepared by direct chlorination of tungsten scrap or by the treatment of WO_3 with carbon and chlorine. Tungsten[31a] also was prepared by direct pyrolysis of WCl_6. In a continuing study, factors influencing the nature of tungsten deposited by hydrogen reduction of WF_6 were investigated.[32,33] The deposits contained 23 to 60 ppm of total metallic impurities, the major impurity being silicon (12 to 28 ppm). Knoop microhardness values ranged from 402 to 512. No correlation could be detected between the WF_6-to-hydrogen ratio and purity, grain size, or microhardness.

The use of chemical-vapor deposition as a means of fabricating components of pyrolytic graphite is being actively pursued. Although it is difficult to adjust conditions to permit deposition of shapes to final dimensions, particularly for small parts, numerous tests have shown that the as-deposited surface is more resistant to rocket exhausts than is a machined surface.[34] Deposition rates for pyrolytic graphite range from 2 to 20 mils/hr at deposition temperatures of 1900 to 2400°C; hydrocarbon gases are used as source materials.[31a] Property data for pyrolytic graphite have been published.[35,36] Preparation of "alloys" of refractory elements with pyrolytic graphite has been described.[31a,37] Additions of up to 2 wt.% of boron, chromium, manganese, molybdenum, niobium, silicon, tantalum, titanium, tungsten, and zirconium were successfully incorporated singly into the pyrolytic-graphite structure. Plating atmospheres contained hydrogen, hydrocarbon (methane, propane, benzene), and alloy sources (volatilized halides, carbonyls, organometallics).

Pyrolytically deposited carbides of hafnium, niobium, tantalum, and zirconium were studied.[31a] Redesign of deposition equipment, to provide for increased total specimen surface area and decreased cross-sectional flow of the coating atmosphere, yielded more uniform deposits and permitted more efficient use of source materials. Pyrolytic boron nitride[31a] holds much promise as a construction material for use in critical environments.

An attempt to coat a graded tungsten-BeO rocket-nozzle insert with tungsten by hydrogen reduction of WF_6 was unsuccessful[37] owing to reaction of the coating atmosphere with BeO.

Conditions for laying down pyrolytic-carbon coatings on various substrates are well established. Important process variables include substrate temperature, concentration or partial pressure of the carbon-source gas, and gas dynamics over the substrate.[31b] The deposition rate of carbon from C_3H_8 at 2000°C is twice that from CH_4 under similar conditions. Useful property data for pyrolytic-carbon coatings are now available. Data from various sources indicate that the degree of preferred crystal orientation in the coating may influence its adherence on the substrate. Modification of pyrolytic-carbon-deposition conditions so as to minimize and maximize, respectively, the degree of preferred orientation had little effect on the adherence of carbon on UO_2-ZrO_2 and polished Vycor test specimens.[38] The deposition of coatings that consisted of alloys of refractory elements in pyrolytic graphite was investigated.[31a,39] Graphite substrates used were in the form of thin disks, tubes, and massive shapes with blind holes. A pyrolytic process was developed for producing high-density, single-phase, impervious coatings of HfC, NbC, and TaC, intimately bonded to graphite substrates.[39]

Addition of CO to the $AlCl_3$-CO_2-H_2 coating atmosphere yields more uniform Al_2O_3 coatings and minimizes the formation of fluffy deposits.[40] Results of this addition include a linear dependence of deposition rate on $AlCl_3$ flow rate, a reduction in deposition rate with increasing CO concentration, less influence of $AlCl_3$ flow rate on deposition rate with increasing CO content, an increase in substrate coverage with increasing CO concentration, and an increase in deposition rate with increasing specimen temperature. Minimum coating temperature was 1230°C with CO, compared with 1130°C without it.

Boride diffusion coatings are used to increase the surface hardness of nickel and the refractory metals molybdenum, niobium, rhenium, tantalum, and tungsten.[41,42] An adherent 1-mil coating of chromium was deposited on the interior of a stainless-steel tube by pyrolysis of chromium dicumene vapors at 540°C. Silicide diffusion coatings, which are used to protect refractory-metal substrates against high-temperature oxidation, are the subject of numerous continuing investigations.[43] Proprietary alloy pack-cementation processes for coating molybdenum and molybdenum-base alloys,[31c,45] employ pack mixtures that contain halide en-

ergizers, silicon, alloying elements, and an inert diluent (Al_2O_3). Processing cycles of 4 to 24 hr at temperatures in the range 925 to above 1100°C are required. Coatings formed in two 6-hr cycles are superior to those formed in one 12-hr cycle. A statistical study of the results of one process[31c] shows that the temperature of processing and the number of cycles employed exert by far the greatest influence on reliability. In another investigation,[44] the heating rate in the coating cycle has been found to have an important influence on the ratio of coating deposition to coating diffusion. Correlation of the ratio of carrier compound to substrate surface area, coating thickness, and unit area weight-gain parameters with specimen life has been obtained for a 5-hr process cycle. Pack-formed diffusion coatings for niobium and its alloys include silicon-chromium-titanium,[31d] silicon-chromium-aluminum,[45] and silicon-chromium-boron.[45] Chromium can also be added subsequent to siliciding. For vanadium-base alloys, silicide diffusion coatings are formed in 16 hr under static argon at 1200°C, with a pack mixture that contains NaF as an activator and −325-mesh solar-grade silicon.[46,47] Metal-bonded/metal-modified oxide-ceramic coatings are formed on tungsten sheet in a fluoride (NaF, KF)-activated vacuum-pack process, followed by conversion of surface-layer elements to oxides by treatment in an atmosphere of water-vapor-saturated hydrogen.[48] Alloying elements include silicon, titanium, yttrium, zirconium, and codeposited boron-tungsten, singly and in combination. Protection of tungsten at 1370°C for 36 hr under cyclic conditions has been achieved. (E. M. Sherwood)

Ceramic Coatings

Research by the TAPCO Division of Thompson Ramo Wooldridge Inc.,[49] on coatings for titanium-containing tungsten sheet, showed that alloying the surface with a combination of zirconium, yttrium, and silicon and subsequent oxidizing produced coatings that protected the tungsten in air for 10 to 20 hr at 2800°F and for 2.5 hr at 3200°F. The specimens could be cycled to room temperature without destroying the protective qualities.

Sperry[50] has completed a literature review and a laboratory evaluation of ceramic-metal seals. This work indicates that glass migration and sintering of the molybdenum powder used in the seals are important in bond development. Stronger bonds resulted with decreased alumina content in alumina porcelain-metal seals.

In a patent[51] recently assigned to the U. S. Atomic Energy Commission, a method for coating graphite with niobium carbide is described. The method includes obtaining physical contact between niobium and graphite, degassing at 1400°C, heating to 2200 to 2400°C while outgassing, and thereafter carburizing the niobium.

The coating-to-substrate bond and cohesive strength of flame-sprayed oxide coatings have been examined at Illinois Institute of Technology.[52] The bond strength was found to range from 700 to 1520 psi for suitably prepared specimens. A 1-mil subcoat of a nickel-chromium alloy was found to promote adhesion. The average cohesive strength of some zirconia coatings was about 2600 psi.

The development and evaluation of plate type uranium dioxide fuel elements made by using plasma-jet spraying techniques are being investigated by American-Standard.[53] Adherent UO_2 films that are 0.03 to 0.10 in. thick have been deposited on stainless-steel or Zircaloy-2 substrates. Coatings that have 87 per cent of theoretical density and an oxygen-to-uranium ratio of nearly 2.00 have been deposited with an efficiency of about 40 per cent. It was found necessary to keep the coating temperature below 870°C and the substrate below 450°C during deposition to assure soundness of the composite. Fabrication costs using plasma-jet spraying were estimated at $100/kg of uranium.

(B. W. King)

Welding and Brazing

Reports covering many investigations related to the joining of zirconium and its alloys were received during this period. The welding characteristics of a high-strength zirconium alloy designated 3Z1 (zirconium−1.25 wt.% aluminum−1 wt.% tin−1 wt.% molybdenum) were determined by Atomics International.[9] This alloy can be welded readily by use of the inert-gas tungsten-arc process and has properties comparable with those of unwelded base metal after annealing. The annealing treatment used on weldments of this alloy was done in vacuum at 1450 to 1500°F for 2 hr, followed by furnace cooling. In the as-welded condition, the weld

metal exhibits much poorer ductility than the base metal or annealed weld metal. Both tensile elongation and bend ductility in the weld area are poor in the as-welded condition. However, there appear to be no problems related to welding if the alloy is given the previously mentioned anneal after welding.

In another Hanford study[54] it was found that high-frequency resistance welding could be used to apply spacer ribs to the Zircaloy-2 cladding of a UO_2 fuel element. Welding was accomplished on both straight and spirally wound ribs positioned on tubes up to 8 ft long. The welding was done with a 60-kw, 450-kc high-frequency welding unit. One of the major advantages of this type of joining for this application is that it essentially eliminates crevices that may be sites for corrosion damage in ribs attached by other joining techniques.

Canadian experience with the zirconium-beryllium brazing alloys has been presented in a series of monthly reports that have just become available.[55] These reports contain considerable tabulated information on the properties of these brazing alloys. The interested reader is referred to the reports for details.

Another technique[56] of brazing Zircaloy-2 has been developed at Knolls. This technique, which is termed "eutectic brazing," has been used to join Zircaloy to both stainless steel and Inconel. A brazing filler metal is not used in this technique. Instead, formation of a eutectic liquid occurs by a diffusion-controlled reaction. In the case of Zircaloy-to-stainless steel brazes, the eutectic is formed at about 980°C. The braze alloys formed in this technique have reasonable strength, but low ductility. In addition, the alloys have good corrosion resistance in pressurized water.

Battelle[57] is continuing work on the joining of sintered aluminum powder alloy M-583 by friction-bonding techniques. The use of external heating has been found to promote different types of bonding as would be expected, whereas joints have been produced which had 50 per cent of the ultimate strength of the unwelded base alloy.

The Defense Metals Information Center recently issued a report on methods of evaluating welded joints.[58] Although this report is not directly concerned with nuclear applications, it could serve as a handbook for anyone interested in the welding area. (R. E. Monroe)

Explosive Forming

A program has been conducted at National Northern[59] to determine the processes for explosive welding of materials that are quite difficult to weld by conventional techniques. Aluminum, nickel alloys, and plain steels have previously been successfully explosively welded. However, the materials involved in this study were AISI 4340 steel, B120VCA titanium, 6A1-4V titanium, molybdenum–0.5 wt.% titanium, and type 310 stainless steel.

The major portion of the preliminary work under this program was concerned with the explosive welding of AISI 4340 steel to itself. The parameters studied during this initial investigation included surface preparation (as received, degreased, various degrees of roughness), spacing between sheets (0 to 20 mils parallel, angled to 10°), explosive forces applied (10,000 to 400,000 psi, obtained by various combinations of charge and standoff), initiating directions (top and end, see Fig. V-2), and transfer media (water, rubber, chipboard, plastics, etc.).

The end initiation (Fig. V-2*b*) produced an orifice type of compression–escape of the gases (air) between the sheet materials. However, the quantities of explosive required to generate pressures equal to those obtained by top initiation were so great that the material fractured.

The transfer medium used during this testing was primarily water. However, it was found that the gaseous products of detonation moved the water away from the specimen, permitting the hot gases to contact the materials being welded. Burning and distortion of the sheets resulted. A buffer, a medium other than water which would protect the sheet and not move during application of the pressure, was therefore incorporated. Tests were conducted with rubber, other sheet metals, chipboard, and plastics as the buffer. Chipboard was selected as the most suitable material, since it can be readily varied and controlled.

The results of these initial tests indicated that controlled conditions were required for welding with explosives and that these conditions must be established for each type of material. However, even for a given material these conditions will vary with physical properties and thickness.

The welding of the AISI 4340 steel to itself was conducted with 3- by 3- by 0.030-in. specimens. The conditions that were found to produce the best results with this material were as follows:

Explosive	Trona 509, aluminized RDX-TNT composition
Explosive geometry	2 in. in diameter by $\frac{5}{8}$ in. high
Explosive weight	98 g, top initiation (for 3- by 3-in. pieces) 35 g, top initiation (for 1- by 3-in. pieces)
Etchant	Aqua regia—cupric chloride solution on the surface to be welded, for 2 min
Medium and standoff	Chipboard, 1 in. thick between explosive and metal; water surrounding the sides and top of explosive charge
Clearance between metal sheets	Metal sheet placed on top of another metal sheet; average clearance 5 mils

Metallographic examination of the welds produced in this manner revealed that the periphery of the overlapped surfaces was welded, whereas the central portion was merely in intimate contact. A thin white layer that varied in thickness up to 0.002 in. and appeared martensitic in structure was found in the weld interface. Bend tests were conducted in which the 3- by 3-in. specimens were bent 180° flat with no separation. A hardness survey run on the weld interface showed that the interface was considerably harder than the parent material, confirming previous findings with other explosively welded materials.

Tensile shear tests were conducted on 4-in.-long strips that were $\frac{1}{2}$ in. wide with a $\frac{1}{2}$-in. overlap and 1 in. wide with a 1-in. overlap. All these specimens ruptured in the region adjoining the overlap and not at the welded joints, which suggested that the welds were stronger than the parent metal. The region adjoining the overlap was probably weakened during explosive welding due to a visible thinning of the sheet in that area. These specimens showed ultimate tensile strengths of around 80,000 psi. However, since the material was thinned in the area of the rupture and since the calculations for these strength values were based on a 0.030-in.-thick material, a more accurate value for the ultimate tensile strength would be about 100,000 psi, which is the original parent-material strength.

The explosive welding tests with the 6A1-4V titanium material were conducted with 3- by 3- by 0.020-in. specimens. The test conditions found to be optimum for welding this material to itself were as follows:

Explosive	Trona 506, aluminized RDX-TNT composition
Explosive geometry	1 in. in diameter by 2 in. high
Explosive weight	64 g, top initiation (for 3- by 3-in. pieces) 24 g, top initiation (for 1- by 3-in. pieces)

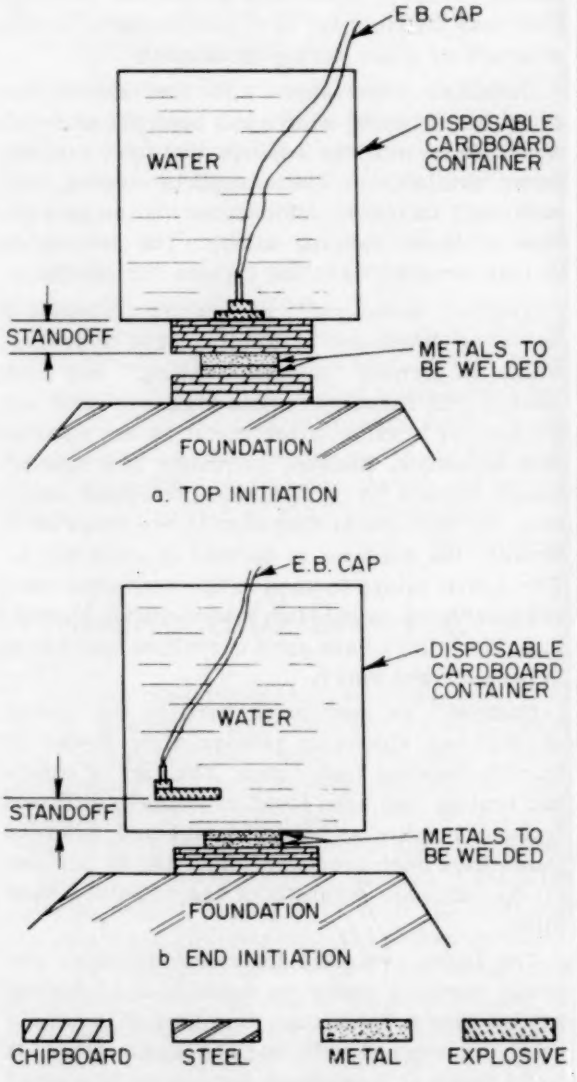

Fig. V-2 Setups for explosive welding.[59]

Etchant	Concentrated HCl on surfaces to be welded, for 2 min
Temperature	Material heated to 300°F prior to test
Medium and standoff	Water; ½ in. between explosive base and metal
Clearance between metal sheets	Metal sheet placed on top of another metal sheet; average clearance 5 mils

The metallographic examination of the welded specimens again revealed that only peripheral welding had occurred, the central portion being merely in intimate contact. A fairly uniform thin white layer of between 0.0002 and 0.0003 in. was found at the weld interface. Bend tests were conducted with these welded specimens in which they were bent 180° flat with no evidence of separation between the sheets. A microhardness survey through the welded area showed the interface to be considerably harder than the base metal.

Tensile shear tests were conducted on 1-in.-wide by 15-in.-long strips with a 1-in. overlap. Again the specimens ruptured in the area adjoining the overlap and not at the welded joint. Visual examination of the specimens revealed that the thickness of the material in this area was reduced about 10 per cent. The results of these tests, based on a 0.020-in.-thick specimen, showed an ultimate tensile strength of 114,000 psi. However, by taking into account the thinning, the tensile strengths would be higher.

Explosive welding tests were conducted with 3- by 3-in. specimens of 0.020-in.-thick molybdenum–0.5 wt.% titanium to 0.025-in.-thick type 310 stainless steel. The optimum conditions for welding this combination of materials were found to be as follows:

Explosive	Trona 509, aluminized RDX-TNT composition
Explosive geometry	2 in. in diameter by 1 in. high
Explosive weight	100 g, top initiation
Etchant	Aqua regia–cupric chloride on the surfaces to be welded, for 2 min
Medium and standoff	Chipboard and a 0.020-in. sheet of steel, totaling 1 in.
Clearance between metal sheets	Averaged 0.005 in.
Temperature	300°F

Metallographic examinations and hardness surveys were not conducted with these specimens. However, they could be bent 180° without separation.

No successful welds were made with the molybdenum–0.5 wt.% titanium to molybdenum–0.5 wt.% titanium combination. When explosive welding was attempted, many veinlike cracks resulted, even at 600°F.

In the tests that were conducted with the hot-rolled, annealed, all-beta B120VCA titanium, only slight success of edge bonding was achieved on a few specimens.

The results of these tests showed that good welds could be produced by explosively welding AISI 4340 steel to itself, 6A1-4V titanium to itself, and molybdenum–0.5 wt.% titanium to type 310 stainless steel. These materials were all in the 0.020- to 0.040-in. thickness range and in the annealed condition. All the welds produced were lap type welds and were as strong as the parent material. Also, in each case, the weld interface was considerably harder than the parent material.

A study on the high-energy-impact forming of UO_2 is being conducted by use of a Bridgman anvil ultrahigh-pressure technique.[24] Micronized UO_2 and Shippingport Pressurized-Water Reactor (PWR) core 1 type UO_2 have been consistently compacted during this study to a density of 99 per cent of theoretical at 500,000 psi and 1100 and 1200°C in stainless-steel capsules that have porous end caps to allow for the escape of evolved gases. A slight excess of oxygen is necessary to obtain a density of 99 per cent of theoretical. This technique was used to prepare high-energy-impact-formed UO_2 for vibrational-compaction studies and for fabrication of a fuel capsule for irradiation in the Engineering Test Reactor. The average particle density of this material was 10.90 g/cm^3 (99.4 per cent of theoretical), whereas the oxygen-to-uranium ratio, after hydrogen reduction at 500°C, was 2.0057.

Minus 200-mesh fused UO_2 and sintered UO_2 were compacted at 1200°C and 500,000 psi in sealed capsules in the Dynapak machine to bulk densities of 99.5 and 99.0 per cent of theoretical, respectively. Electron micrographs of these compacted materials indicate a greater plasticity for the fused UO_2 than for the sintered UO_2. This cannot be explained by oxygen-to-uranium ratios, since both samples were nearly stoichiometric after compaction, being 2.0018

for the fused UO_2 and 2.0046 for the sintered UO_2. Minus 200-mesh sintered UO_2 compacted in a porous capsule under similar conditions had an oxygen-to-uranium ratio of 2.0223.

Three-inch-long by 1.75-in.-diameter stainless-steel capsules that contained micronized UO_2 were compacted at 1000 and 1200°C by high-energy impact in unsealed capsules. The densities attained were 91.5 per cent of theoretical at 1000°C and 96.8 per cent of theoretical at 1200°C. The oxygen-to-uranium ratios for these specimens were 2.0425 and 2.0426, respectively. Additional tests at 1300°C and similar pressure conditions were conducted with micronized and PWR core 1 type UO_2. The densities and oxygen-to-uranium ratios obtained with these powders were 91.7 and 90.9 and 2.0069 and 2.0151 per cent of theoretical, respectively. A decrease in plasticity of the UO_2 caused by the evolution of excess oxygen at 1300°C probably resulted in this decrease in density.

Micronized UO_2 specimens were compacted at various temperatures between 900 and 1200°C in sealed, stainless-steel capsules in the Dynapak machine and analyzed for oxygen-to-uranium ratio. It was found, as expected, that the oxygen-to-uranium ratio decreased with increasing temperature.

A study[57] is presently being conducted at Battelle to determine the feasibility of employing explosive techniques for achieving a mechanical or metallurgical bond between type 410 stainless steel and Zircaloy-2. Initial studies using $2\frac{1}{2}$- by $2\frac{1}{2}$-in. flat-plate assemblies were conducted for the purpose of determining the optimum surface preparation and charge density required to produce a sound bond. The results of this initial testing were used as a basis for conducting a series of experiments using tubular components approximating the required joint configuration. Joint design, transfer medium, and charge configuration and density have been varied during this testing in an effort to determine the optimum conditions required to achieve metallurgical bonding.

During the test period covered by this report, four types of joint designs have been prepared for investigation. The first type of joint consisted of 8, 10, and 12° tapered circumferential grooves machined into the inside diameter of the stainless steel. Each tapered groove was approximately $\frac{1}{2}$ in. long and $\frac{1}{4}$ in. deep. The purpose of these specimens was to ascertain which, if any, of the three tapers would be most conducive to producing surface jetting. The second design consisted of a grooved joint, similar to that previously used, in which a 0.005-in. type 304 stainless-steel sleeve was inserted in the gap between the type 410 stainless steel and Zircaloy-2. The insert was incorporated into this joint with the idea that, on impacting, both the stainless-steel sleeve and the Zircaloy-2 would be forced into the grooves in the inside diameter of the type 410 stainless steel. It was intended that the deformation experienced by the stainless-steel sleeve and Zircaloy-2 would perhaps be sufficient to rupture their oxide films and to promote metallurgical bonding. The third type of joint consisted simply of machining 0.005- and 0.010-in. clearances between the type 410 stainless-steel and Zircaloy-2 members. This design modification was intended to permit the Zircaloy-2 to attain a sufficient velocity to produce surface jetting when it impinged against the stainless steel. The fourth type of joint design consisted of a straight joint with a 0.020-in. clearance between the stainless steel and Zircaloy-2 and in which the thickness of the Zircaloy-2 member was reduced to 0.030 in. in one case, 0.045 in. in the second, and 0.060 in. in the third. In all cases the outside surface of the Zircaloy-2 was machined to a 300-μin. rms surface finish, whereas the inside surface of the stainless steel was machined to a 1500-μin. rms surface finish in the first three types of joints and to a 500-μin. rms surface finish in the fourth type of joint.

Specimens of each of the four types of joints have been tested using air as the transfer medium, a $\frac{3}{4}$-in. standoff distance, and a 35-g charge. The results of these tests showed that a limited amount of bonding had occurred; however, the bonds produced were quite weak. It appears from these results that, perhaps by using a greater clearance between the Zircaloy-2 and type 410 stainless-steel members and by improving the coupling of the charge energy to the specimen, a good bond can be achieved.

(C. C. Simons)

Nondestructive Testing

Ultrasonic Techniques

A British patent[60] describes a method of inspecting welds in tubular sections by using a reflector to scan the section. The transducer is

nonrotatable, and its axis remains fixed with respect to the tube, which eliminates problems associated with twisting the transducer cables. The unit is said to be useful in inspecting a weld joint with a plane that is oblique to the axis of the tubular body.

At Harwell[61] the British have conducted work similar to that being done at Armour with the image-converter tube although, instead of pulse methods, the British use continuous waves. For through-transmission techniques the British claim that the lower defect limit on detectability appears to be about one wavelength. Defects about one wavelength across can produce diffraction effects that result in an increased transmission signal. (D. Ensminger)

Magnetic, Eddy-Current, and Other Techniques

A nondestructive testing device[62] has been designed to give an approximate indication of the air-gap length between $\frac{1}{4}$-in.-thick steel reinforcing bands used to strengthen a large steel pressure vessel. When a magnet is placed on the near side of a band, some magnetic flux passes across the air space on the far side into an adjacent band or shell plate. A change in the air-gap length varies this flux, which in turn affects the main flux passing through the test zone. The change in the main flux is then shown as a change in the external field strength between the magnetic poles on a moving-magnet magnetometer. Under proper conditions the tester reads average gap directly from 0 to 0.060 in. within 20 per cent.

A semiautomatic carbon-coating thickness gauge[38] has been developed for carbon-coated fuel wafers. Since the fuel wafers are composed of nonconducting materials with pyrolytic-carbon coatings, the electrical resistance between two points on the same face of a wafer should vary directly as the distance between them and inversely as the thickness of the coating. The gauge, based on the measurement of this resistance, indicates the thickness of the carbon coating on any particular type of wafer directly on the front-panel meter with a precision of 1 μin.

A sensitive magnetic test[38] has been developed for the determination of the amount of ferromagnetic iron contamination present in fuel powders. The Fuel Powder Tramp Gage has a useful detection range from 4 to 3500 ppm of ferromagnetic iron content with a precision of ±3 per cent at the two-sigma level when a five-grain sample of fuel powder is used. Residual magnetic field is used as the measuring parameter, and detection is accomplished by a sensitive gauss meter.

The pulsed-field reflection system[12] is being used to check the bond quality of pins of plutonium alloy enclosed in jackets made from a variety of materials and bonded with sodium. The resolution of this system is good enough to provide a very sensitive test for voids in the bond layer. The bond quality of nine jacketed pins has been checked prior to irradiation of the pins. Six were found to be well bonded. Nonbond areas in the other three ranged from 10 to 30 per cent of the total pin area.

Feasibility studies[63] have been made to determine capabilities and limitations of several nondestructive testing methods for the core B fuel element of the Enrico Fermi Fast Breeder Reactor. An eddy-current technique is capable of measuring the fuel-plate cladding thickness with an accuracy of ±0.001 in. Another eddy-current device will measure coolant-channel spacing between fuel plates with an accuracy of 0.005 in. This technique utilizes the leaf spring and coil device discussed in previous work. A radiographic technique can be used to detect UO_2 concentration inhomogeneities in excess of the specified ±5 per cent tolerance. (C. L. Seale)

References

1. Bureau of Mines, Quarterly Metallurgical Progress Report No. 13, October 1, 1961, to December 31, 1961, USAEC Report USBM-U-887.
2. J. B. Guernsey, The Development of Optimum Manufacturing Methods for Columbium Alloy Sheet, Report ASD-TR-7-784 (V), Crucible Steel Co. of America, Mar. 15, 1961.
3. Wah Chang Corp., Tungsten Extrusion Program, Second Interim Technical Report, April 10, 1961–August 24, 1961, Report NP-11044, 1961.
4. United Nuclear Corp., Nuclear Fuel Research: Fuel Cycle Development Program Quarterly Progress Report, July 1 to September 30, 1961, USAEC Report NYO-2695, Nov. 22, 1961.
5. N. H. Katz and M. H. Binstock, Vacuum Induction Melting and Casting of Uranium-Silicon Alloys, USAEC Report NAA-SR-6226, Atomics International, Mar. 15, 1962.
6. Hanford Atomic Products Operation, Plutonium Metallurgy Operation Quarterly Progress Report,

April, May, June 1961, USAEC Report HW-70312, July 14, 1961. (Classified)

7. R. W. Tombaugh et al., Development of Optimum Methods for the Primary Working of Refractory Metals, Report WADD-TR-60-418(Pt. II), Harvey Aluminum, June 1961.
8. H. J. Henning and F. W. Boulger, Notes on the Forging of Refractory Metals, Report DMIC-Memo-143, Battelle Memorial Institute, Defense Metals Information Center, Dec. 21, 1961.
9. R. K. Wagner, Fabrication and Welding Characteristics of High Strength Zirconium Alloy 3Z1, USAEC Report NAA-SR-6431, Atomics International, Dec. 15, 1961.
10. P. A. Santoli, Molybdenum Alloy Extrusion Development Program, Report ASD-TR-7-785, Allegheny Ludlum Steel Corp., October 1961.
11. R. S. Kirby et al., Fabrication of Tantalum Capsules by Impact Extrusion and Ironing, USAEC Report LA-2591, Los Alamos Scientific Laboratory, January 1961.
12. Argonne National Laboratory, Reactor Development Program Progress Report, January 1962, USAEC Report ANL-6509, Feb. 15, 1962.
13. W. B. Tarpley and H. Kartluke, Ultrasonic Tube Drawing: Niobium, Zircaloy-2, and Copper, USAEC Report NYO-10008, Aeroprojects, Inc., December 1961.
14. B. I. Beresnev et al., Characteristics of Extruding Metal by High-Pressure Liquid at Elevated Temperatures, Report NP-tr-755 [translated from *Fiz. Metal. i Metalloved.*, 11: 115–122 (1961)].
15. R. J. Beaver, Zirconium-Cladding of Thorium, U. S. Patent 3,009,242 (to USAEC), Nov. 21, 1961.
16. J. W. Lingafelter, Fabrication of Fuel Rods by Tandem Rolling, USAEC Report GEAP-3775, General Electric Co., Atomic Power Equipment Dept., July 1961.
17. J. G. Hunt et al., Hot Extrusion of UO_2 Fuel Elements. Fundamental and Applied Research and Development in Metallurgy. Final Report for Period July 1, 1960, Through June 30, 1961, USAEC Report NMI-1245, Nuclear Metals, Inc., Oct. 31, 1961.
18. J. G. Hunt and P. Loewenstein, Development of Hot-Extruded Uranium Monocarbide and Dioxide. Fundamental and Applied Research and Development in Metallurgy, Quarterly Report for July 1–September 30, 1961, Nuclear Metals, Inc., Nov. 29, 1961. (Classified)
19. Slug Canning, French Patent 1,244,632, Sept. 19, 1960.
20. Hanford Atomic Products Operation, January 1962. (Unpublished)
21. Oak Ridge National Laboratory, Maritime Reactor Program Annual Progress Report for Period Ending November 30, 1961, USAEC Report ORNL-3238, Mar. 9, 1962.
22. F. W. Albaugh, Reactor and Fuels Research and Development Operation Monthly Report, December 1961, USAEC Report HW-72142A, Hanford Atomic Products Operation, Jan. 15, 1962. (Classified)
23. R. R. Hood and L. Isakoff (Comps.), Heavy Water Moderated Power Reactors Progress Report, November 1961, USAEC Report DP-685, E. I. du Pont de Nemours & Co., December 1961.
24. Hanford Atomic Products Operation, Fuels Development Operation, Quarterly Progress Report, October, November, December 1960, USAEC Report HW-70355, Jan. 13, 1961. (Classified)
25. D. E. Couch and A. M. Brown, Coatings for Uranium, USAEC Report SCR-307, National Bureau of Standards, December 1961.
26. J. G. Beach and C. L. Faust, Electroclad Aluminium on Uranium, *J. Electrochem. Soc.*, 106: 654 (1959).
27. J. G. Beach et al., Electroplated Metals on Uranium, USAEC Report BMI-912(Del.), Battelle Memorial Institute, May 7, 1954.
28. M. H. Binstock, Fuel Element Development for Piqua OMR, USAEC Report NAA-SR-5119, Atomics International, June 30, 1960.
29. N. W. Kirschenbaum et al., Research on the Production of Ultrapure Molybdenum, Final Report, Alloyd Electronics Corp., Jan. 15, 1962.
30. P. C. Good and F. E. Block, Preparation of Tungsten by Reduction of Tungsten Hexafluoride, *U. S. Bur. Mines, Rept. Invest. No. 5861*, 1961.
31. Papers presented at National Symposium on Ceramics and Composites, Coatings, and Solid Bodies, Society of Aerospace Materials and Process Engineers, Dayton, Ohio, Nov. 14–15, 1962.
    a. R. G. Bourdeau, Pyrolytic Deposition of Materials.
    b. J. D. Batchelor, Processing and Properties of Pyrolytic Graphite Coatings.
    c. R. Wachtell, Protective Coatings for Molybdenum.
    d. R. A. Jefferys and J. D. Gadd, Protective Coatings for Columbium.
32. Department of the Interior, Rolla Metallurgical Research Center, Vapor Deposition of Tungsten and the Effect of Process Variables, Monthly Report of Progress No. 3, January 1962.
33. Department of the Interior, Rolla Metallurgical Research Center, Vapor Deposition of Tungsten and the Effect of Process Variables, Monthly Report of Progress No. 4, February 1962.
34. D. L. Shipp, Fabrication of Pyrolytic Graphite Rocket Nozzle Components, Final Report, General Electric Co., Flight Propulsion Laboratory Dept., Dec. 30, 1961.
35. J. Pappis and S. L. Blum, Properties of Pyrolytic Graphite, *J. Am. Ceram. Soc.*, 44: 592–597 (Dec. 1, 1961).
36. A. R. Gardner, Beat the Heat with Pyrolytic Graphite, *Prod. Eng.*, 33: 72–75 (Jan. 2, 1962).
37. R. Francis, Development of Pyrolytic Refractory Materials for Solid Fuel Rocket Motor Applica-

tions, Quarterly Status Report No. 1, Arthur D. Little Co., Oct. 10, 1961.

38. Westinghouse Electric Co., Bettis Atomic Power Laboratory, Pressurized Water Reactor (PWR) Project Technical Progress Report, for the Period October 24, 1961, to December 23, 1961, USAEC Report WAPD-MRP-95.
39. High Temperature Materials, Inc., Pyrolytic Carbide Development Program, Final Report, March 15, 1960, Through September 30, 1961.
40. E. A. Aitken and R. E. Latta, The Use of Carbon Monoxide in the Vapor Coating of Ceramics with Al_2O_3, preprint of paper presented at Pacific Coast Regional Meeting of the American Ceramic Society, San Francisco, Calif., October 1961.
41. M. L. Rutkovskii et al., Kinetics of the Boriding of Nickel, *Fiz. Metal. i Metalloved.*, 12: 217–222 (February 1961) (in Russian).
42. A. N. Minkevich, Boride Diffusion Layers, *Metalloved. i Termichesk. Obrabotka Metal.*, pp. 9–15 (August 1961) (in Russian).
43. C. A. Krier, Coatings for the Protection of Refractory Metals from Oxidation, Report DMIC-162, Battelle Memorial Institute, Defense Metals Information Center, Nov. 24, 1961.
44. G. J. Dormer et al., Development of a Cementation Coating Process for High-Temperature Protection of Molybdenum, Quarterly Progress Report No. 3 (Sept. 10–Dec. 10, 1961), Report PF62-2, Pfaudler Co., Jan. 10, 1962.
45. W. L. Aves et al., Diffusion Coating Process for Columbium-Base Alloys, Aeronautical Systems Division Technical Report (Aug. 15–Nov. 15, 1961), Chance Vought Corp., November 1961.
46. F. C. Holtz, High-Temperature Oxidation Protective Coatings for Vanadium-Base Alloys, Bimonthly Report No. 3, October 12–December 11, 1961, Report ARF-2227-3, Illinois Institute of Technology, Armour Research Foundation, Jan. 8, 1962.
47. F. C. Holtz, High-Temperature Oxidation Protective Coatings for Vanadium-Base Alloys, Bimonthly Report No. 4, December 12, 1961–February 11, 1962, Report ARF-2227-4, Illinois Institute of Technology, Armour Research Foundation, Mar. 7, 1962.
48. H. J. Nolting, Oxidation-Resistant, High-Temperature Protective Coatings for Tungsten, Third Quarterly Report for Nov. 1, 1961, to Jan. 31, 1962, TAPCO Div. of Thompson Ramo Wooldridge, Inc., Jan. 31, 1962.
49. H. J. Nolting and R. H. Burgess, Oxidation-Resistant High-Temperature Protective Coatings for Tungsten, Second Quarterly Progress Report for Aug. 1 to Oct. 31, 1961, Report NP-11069, TAPCO Div. of Thompson Ramo Wooldridge, Inc., Nov. 15, 1961.
50. S. S. Cole, Jr., et al., Metal-to-Ceramic Seal Technology Study, Final Technical Report, Report RADC-TR-60-236, Sperry Gyroscope Co., October 1960.
51. J. S. Kane et al., Method for Coating Graphite with Niobium Carbide, U. S. Patent 3,017,286 (to USAEC), Jan. 16, 1962.
52. J. L. Bliton and H. L. Rechter, Determination of Physical Properties of Flame-Sprayed Ceramic Coatings, *Am. Ceram. Soc. Bull.*, 40(11): 683–688 (November 1961).
53. N. E. Weare et al., Development of Clad Ceramic Fuel Plates by Spray-Coating Techniques, Quarterly Technical Progress Report, April–June 1961, USAEC Report ATL-A-121, Advanced Technology Laboratories, Div. of American-Standard, June 1961.
54. L. R. Vancott, High Frequency Resistance Welding of Spacer Ribs to Zircaloy-2-Clad UO_2 Fuel Components, USAEC Report HW-67679, Hanford Atomic Products Operation, October 1961.
55. J. A. Green et al., Zircaloy Brazing Program, Progress Report Nos. 8 Through 18, Reports NP-11010 Through NP-11019, June 24, 1960, Through Apr. 27, 1961.
56. W. A. Owczarski, Eutectic Brazing of Zircaloy-2 to Type 304 Stainless Steel, *Welding J. (N. Y.)*, 41(2): 78s–83s (February 1962).
57. S. W. Porembka, Progress on USAEC/AECL Cooperative Program. Quarterly Report for Period December 1961–February 1962, USAEC Report BMI-X-193, Battelle Memorial Institute, Mar. 1, 1962.
58. M. D. Randall et al., Methods of Evaluating Welded Joints, Report DMIC-165, Battelle Memorial Institute, Defense Metals Information Center, Dec. 28, 1961.
59. V. Philipchuk, Explosive Welding, Report ASD-TR-61-124, American Potash & Chemical Corp., National Northern Div., May 1961.
60. R. F. Hanstock et al., Improvements in or Relating to Ultrasonic Inspection Apparatus, British Patent 883,173, Nov. 22, 1961.
61. R. S. Sharpe et al., Atomic Energy Research Establishment, Harwell, 1961. (Unpublished)
62. J. W. Walley, A Magnetic Tester for the Measurement of Interlayer Air-Gaps Between Steel Reinforcing Bands in Pressure Vessels, *Metallurgia*, 64(384): 165–175 (October 1961).
63. R. V. McClung, Feasibility Studies–Nondestructive Testing of the Enrico Fermi Reactor Core B Fuel Element, USAEC Report ORNL-3221, Oak Ridge National Laboratory, Jan. 11, 1962.

LEGAL NOTICE

This document was prepared under the sponsorship of the U. S. Atomic Energy Commission. Neither the United States, nor the Commission, nor any person acting on behalf of the Commission:

A. Makes any warranty or representation, expressed or implied, with respect to the accuracy, completeness, or usefulness of the information contained in this report, or that the use of any information, apparatus, method, or process disclosed in this report may not infringe privately owned rights; or

B. Assumes any liabilities with respect to the use of, or for damages resulting from the use of any information, apparatus, method, or process disclosed in this report.

As used in the above, "person acting on behalf of the Commission" includes any employee or contractor of the Commission, or employee of such contractor, to the extent that such employee or contractor of the Commission, or employee of such contractor prepares, disseminates, or provides access to, any information pursuant to his employment or contract with the Commission, or his employment with such contractor.

NUCLEAR SCIENCE ABSTRACTS

The U. S. Atomic Energy Commission, Division of Technical Information, publishes *Nuclear Science Abstracts (NSA)*, a semimonthly journal containing abstracts of the literature of nuclear science and engineering.

NSA covers (1) research reports of the U. S. Atomic Energy Commission and its contractors; (2) research reports of government agencies, universities, and industrial research organizations on a world-wide basis; and (3) translations, patents, books, and articles appearing in technical and scientific journals.

Complete indexes covering subject, author, source, and report number are included in each issue. These are cumulated quarterly, semiannually, and annually providing a detailed and convenient key to the literature.

Availability of *NSA*

SALE *NSA* is available on subscription from the Superintendent of Documents, U. S. Government Printing Office, Washington 25, D. C., at $22.00 per year for the semimonthly abstract issues and $15.00 per year for the four cumulated-index issues. Subscriptions are postpaid within the United States, Canada, Mexico, and all Central and South American countries, except Argentina, Brazil, British and French Guiana, Surinam, and British Honduras. Subscribers in these Central and South American countries, and in all other countries throughout the world, should remit $27.50 per year for subscriptions to semimonthly abstract issues and $17.50 per year for the four cumulated-index issues.

EXCHANGE *NSA* is also available on an exchange basis to universities, research institutions, industrial firms, and publishers of scientific information. Inquiries should be directed to the Division of Technical Information Extension, U. S. Atomic Energy Commission, P. O. Box 62, Oak Ridge, Tennessee.